Functional analyses of microtubule and centrosome-associated proteins in *Dictyostelium discoideum*

Matthias Samereier

Published online at the
Institutional Repository of the University of Potsdam:
URL http://opus.kobv.de/ubp/volltexte/2011/5283/
URN urn:nbn:de:kobv:517-opus-52835
http://nbn-resolving.de/urn:nbn:de:kobv:517-opus-52835

Institut für Biochemie und Biologie
Abteilung Zellbiologie

Functional analyses of microtubule and centrosome-associated proteins in *Dictyostelium discoideum*

-Dissertation-

zur Erlangung des Doktorgrades der Naturwissenschaften
(Dr. rer. nat.)

Vorgelegt der Mathematisch-Naturwissenschaftlichen Fakultät der Universität Potsdam
von
Matthias Samereier

März 2011

Ehrenwörtliche Versicherung

Hiermit versichere ich, dass ich die vorliegende Arbeit selbständig und ohne unerlaubte Hilfe angefertigt habe. Andere als die in der Dissertation angegebenen Hilfsmittel wurden nicht benutzt. Die Dissertartion wurde in der dieser oder einer ähnlichen Form noch bei keiner anderen Hochschule eingereicht.

Matthias Samereier

Potsdam, März 2011

Teile dieser Arbeit wurden bereits veröffentlicht:

Samereier, M., Baumann, O., Meyer, I. and Gräf, R. (2011). Analysis of Dictyostelium TACC reveals differential interactions with CP224 and unusual dynamics of Dictyostelium microtubules. Cell Mol Life Sci. **68**(2): 275-287.

Samereier, M., Meyer, I., Koonce, M. P. and Gräf, R. (2010). Live cell-imaging techniques for analyses of microtubules in Dictyostelium. Methods Cell Biol. **97**: 341-357.

Schulz, I., Baumann, O., Samereier, M., Zoglmeier, C. and Graf, R. (2009a). Dictyostelium Sun1 is a dynamic membrane protein of both nuclear membranes and required for centrosomal association with clustered centromeres." Eur J Cell Biol **88**(11): 621-38.

Schulz, I., Erle, A., Graf, R., Kruger, A., Lohmeier, H., Putzler, S., Samereier, M. and Weidenthaler, S. (2009b). "Identification and cell cycle-dependent localization of nine novel, genuine centrosomal components in Dictyostelium discoideum." Cell Motil Cytoskeleton **66**(11): 915-28.

Supplementary material available on CD

All movies are provided in .avi format. Shown are maximum intensity projections.

Mov. 1: FRAP of centrosomal GFP-CP224 during interphase
Mov. 2: FRAP of centrosomal GFP-CP224 in TACC-RNAi cell during interphase
Mov. 3: FRAP of spindle pole GFP-CP224 during mitosis
Mov. 4: FRAP of spindle pole GFP-CP224 in TACC-RNAi cell during mitosis
Mov. 5: FRAP of centrosomal GFP-α-tubulin during interphase
Mov. 6: FRAP of centrosomal GFP-α-tubulin in TACC-RNAi cell during interphase
Mov. 7: FRAP of spindle pole GFP-α-tubulin during mitosis
Mov. 8: FRAP of spindle pole GFP-α-tubulin in TACC-RNAi cell during mitosis
Mov. 9: Typical microtubule dynamics that can be observed in a GFP-α-tubulin expressing *Dictyostelium* cell during interphase
Mov. 10: Microtubule dynamics that can be observed in cells co-expressing mFRP-α-tubulin and GFP-TACCdom
Mov. 11: FRAP of microtubules in the cell periphery of GFP-α-tubulin expressing cells
Mov. 12: Time series of a mitotic cell co-expressing GFP-Cenp68 and cherry-histone 2B
Mov. 13: Second time series of a mitotic cell co-expressing GFP-Cenp68 and cherry-histone 2B
Mov. 14: Time series of a mitotic cell co-expressing GFP-Mad1 and cherry-histone 2B
Mov. 15: Early prophase in a GFP-α-tubulin expressing *Dictyostelium* cell
Mov. 16: Late mitotic stages in a GFP-TACC expressing cell
Mov. 17: FRAP of GFP-Cenp68 in late mitosis
Mov. 18: FRAP of GFP-Cenp68 in early mitosis
Mov. 19: Rapid recovery of GFP-Cenp68 in a FRAP experiment during interphase
Mov. 20: Slow recovery of GFP-Cenp68 in a FRAP experiment during interphase

The CD contains a digital copy of this work in high resolution.

Table of contents

Summary

Understanding the role of microtubule-associated proteins is the key to understand the complex mechanisms regulating microtubule dynamics. This study employs the model system *Dictyostelium discoideum* to elucidate the role of the microtubule-associated protein TACC (Transforming acidic coiled-coil) in promoting microtubule growth and stability. *Dictyostelium* TACC was localized at the centrosome throughout the entire cell cycle. The protein was also detected at microtubule plus ends, however, unexpectedly only during interphase but not during mitosis. The same cell cycle-dependent localization pattern was observed for CP224, the *Dictyostelium* XMAP215 homologue. These ubiquitous MAPs have been found to interact with TACC proteins directly and are known to act as microtubule polymerases and nucleators. This work shows for the first time *in vivo* that both a TACC and XMAP215 family protein can differentially localize to microtubule plus ends during interphase and mitosis. RNAi knockdown mutants revealed that TACC promotes microtubule growth during interphase and is essential for proper formation of astral microtubules in mitosis. In many organisms, impaired microtubule stability upon TACC depletion was explained by the failure to efficiently recruit the TACC-binding XMAP215 protein to centrosomes or spindle poles. By contrast, fluorescence recovery after photobleaching (FRAP) analyses conducted in this study demonstrate that in *Dictyostelium* recruitment of CP224 to centrosomes or spindle poles is not perturbed in the absence of TACC. Instead, CP224 could no longer be detected at the tips of microtubules in TACC mutant cells. This finding demonstrates for the first time *in vivo* that a TACC protein is essential for the association of an XMAP215 protein with microtubule plus ends. The GFP-TACC strains generated in this work also turned out to be a valuable tool to study the unusual microtubule dynamics in *Dictyostelium*. Here, microtubules exhibit a high degree of lateral bending movements but, in contrast most other organisms, they do not obviously undergo any growth or shrinkage events during interphase. Despite of that they are affected by microtubule-depolymerizing drugs such as thiabendazole or nocodazol which are thought to act solely on dynamic microtubules. Employing 5D-fluorescence live cell microscopy and FRAP analyses this study suggests *Dictyostelium* microtubules to be dynamic only in the periphery, while they are stable at the centrosome.

In the recent years, the identification of yet unknown components of the *Dictyostelium* centrosome has made tremendous progress. A proteomic approach previously conducted by our group disclosed several uncharacterized candidate proteins, which remained to be verified

as genuine centrosomal components. The second part of this study focuses on the investigation of three such candidate proteins, Cenp68, CP103 and the putative spindle assembly checkpoint protein Mad1. While a GFP-CP103 fusion protein could clearly be localized to isolated centrosomes that are free of microtubules, Cenp68 and Mad1 were found to associate with the centromeres and kinetochores, respectively. The investigation of Cenp68 included the generation of a polyclonal anti-Cenp68 antibody, the screening for interacting proteins and the generation of knockout mutants which, however, did not display any obvious phenotype. Yet, Cenp68 has turned out as a very useful marker to study centromere dynamics during the entire cell cycle. During mitosis, GFP-Mad1 localization strongly resembled the behavior of other Mad1 proteins, suggesting the existence of a yet uncharacterized spindle assembly checkpoint in *Dictyostelium*.

Zusammenfassung

Die Kenntnis der Funktion von Mikrotubuli-assoziierenden Proteinen (MAPs) ist von grundlegender Bedeutung für das Verständnis der Mikrotubuli-Dynamik und deren Regulation. Im Rahmen dieser Arbeit wurde die Rolle des Mikrotubuli-assoziierenden Proteins TACC (Transforming acidic coiled-coil), welches in vielen Organismen an der Stabilisierung und dem Wachstum von Mikrotubuli beteiligt ist, im Modellorganismus *Dictyostelium discoideum* untersucht.

Das *Dictyostelium* TACC Protein konnte während des gesamten Zellzyklus am Centrosom nachgewiesen werden. Darüber hinaus wurde es an den Mikrotubuli-Plus-Enden vorgefunden, überraschenderweise jedoch ausschließlich während der Interphase. Die gleiche Zellzyklus-abhängige Lokalisation wurde für CP224 beobachtet, einem Homologen der XMAP215 Proteine in *Dictyostelium*. Diese ubiquitären MAPs sind konservierte, direkte Interaktionspartner der TACC Proteine und spielen eine zentrale Rolle bei der Nukleation und der Polymerisation von Mikrotubuli. Durch diese Arbeit konnte erstmals *in vivo* gezeigt werden, dass TACC und XMAP215 Proteine während der Interphase und Mitose unterschiedlich stark mit Mikrotubuli-Plus-Enden assoziiert sein können.

Durch Untersuchungen an Knockdown-Mutanten wurde ersichtlich, dass *Dictyostelium* TACC eine Rolle beim Mikrotubuli-Wachstum während der Interphase spielt und über weite Strecken der Mitose essentiell für die Ausbildung von astralen Mikrotubuli ist. In anderen Organismen konnte als Ursache instabiler Mikrotubuli in TACC Mutanten häufig unzureichendes Rekrutieren des jeweiligen XMAP215 Proteins an das Centrosom ausgemacht werden. Um entsprechende Auswirkungen auf die Lokalisation von CP224 durch den Knockdown von TACC in *Dictyostelium* zu untersuchen, wurden Fluorescence Recovery after Photobleaching (FRAP) Experimente durchgeführt. Diese ergaben, dass CP224 auch in Abwesenheit von TACC in vollem Umfang an die Centrosomen und Spindelpole rekrutiert wird. Anders als im Wildtyp, konnte in TACC Mutanten allerdings kein CP224 an den Mikrotubuli-Plus-Enden nachgewiesen werden. Somit konnte erstmals *in vivo* gezeigt werden, dass ein TACC Protein essentiell für die Assoziation eines XMAP215 Proteins mit den Mikrotubuli-Plus-Enden ist.

Im Laufe der genannten Experimente stellte sich heraus, dass sich die GFP-TACC Stämme aufgrund ihrer markierten Plus-Enden sehr gut für Untersuchungen zur ungewöhnlichen Mikrotubuli-Dynamik in *Dictyostelium* eignen. Zwar weisen Mikrotubuli hier über die gesamte Länge ausgeprägte Krümmungs- und Seitwärtsbewegungen auf, es können jedoch im Vergleich zu anderen Organismen während der Interphase kaum Wachstums- oder

Verkürzungsvorgänge beobachtet werden. Dennoch können *Dictyostelium* Mikrotubuli unter Verwendung von Agenzien wie Thiabendazol oder Nocodazol, welche ausschließlich auf dynamische Mikrotubuli wirken, signifikant verkürzt werden. Durch FRAP Experimente und Einsatz von 5D Fluoreszenz-Mikroskopie an lebenden Zellen konnte in dieser Arbeit erstmalig nachgewiesen werden, dass *Dictyostelium* Mikrotubuli nur in der Zellperipherie, nicht aber im pericentrosomalen Bereich dynamisch sind.

Die Identifikation bislang unbekannter Bestandteile des *Dictyostelium* Centrosoms erfuhr in den vergangenen Jahren große Fortschritte. Ein von unserer Gruppe durchgeführter Proteomics-Ansatz brachte eine Vielzahl potentiell centrosomaler Proteine zu Tage, von welchen bereits viele am Centrosom nachgewiesen werden konnten. Der zweite Teil dieser Arbeit befasst sich mit der Charakterisierung dreier noch unbekannter Proteine aus dem Proteomics-Ansatz, Cenp68, CP103 und dem *Dictyostelium* Homologen des Spindle Assembly Checkpunkt Proteins Mad1. Hierbei zeigte sich, dass lediglich CP103 Bestandteil isolierter, Mikrotubuli-freier Centrosomen ist, während Cenp68 an die Centromere und Mad1 an die Kinetochoren lokalisieren. Die Charakterisierung von Cenp68 umfasste außerdem die Herstellung eines polyklonalen anti-Cenp68 Antikörpers, das Suchen nach Interaktionspartnern und die Erzeugung eines Cenp68 Knockout-Stammes. Letzterer wies jedoch keinen offensichtlichen Phänotyp auf. Das Verhalten des *Dictyostelium* Mad1 Proteins während der Mitose stimmte in großen Teilen mit dem anderer Mad1 Proteine überein, was auf die Existenz eines bislang unerforschten Spindle Assembly Chekpunkts in *Dictyostelium* hinweisen könnte.

1 Introduction

1.1 *Dictyostelium discoideum* as model organism

The amoeboid organism *Dictyostelium discoideum* is a haploid eukaryote that lives solitarily in the forest soil. Taxonomically it was first described as a primitive fungus, but today's molecular approaches revealed that *Dictyostelium* branched off the animal lineage prior to fungi but after the divergence of plants (Eichinger *et al*., 2005). *Dictyostelium* feeds on a wide range of bacteria and the vegetative form multiplies by equal mitotic division. Under adverse conditions such as starvation, the amoebae undergo the transition from a single-celled organism to a multi-cellular fruiting-body. Once prey is no longer available, individual cells in the population start to emit pulses of cAMP, which can be detected by nearby amoebae. This causes them to crawl towards the source, while releasing pulses of cAMP themselves. In this way, up to 10^5 amoebae can aggregate. During development, *Dictyostelium* cells can differentiate into two cell types, spore cells and stalk cells, which build up a fruiting body. While stalk cells eventually die, spore cells can hatch and re-enter the life cycle once they are under favourable conditions. This enables the population to endure periods of starvation and contributes to its spatial expansion.

Dictyostelium is widely used in laboratories as model organism to study processes like chemotaxis, cell motility, signal transduction, phagocytosis, morphogenesis, development and cell type differentiation. This is a consequence of a multitude of beneficial properties and advantages *Dictyostelium* offers compared to other eukaryotic systems. *Dictyostelium* is easy and cheap to cultivate. It can be grown on lawns of bacteria, typically *Klebsiella aerogenes*, or axenically in tissue flasks and shaking culture. No gassing is required for cultivation. Due to its relatively short generation time of 8 h in liquid media, large quantities of cells can quickly be obtained. Spores formed in response to starvation can easily be harvested and stored for decades. Also, a lot of biochemical, molecular genetic and cell biological techniques have been successfully established for *Dictyostelium*. These include protein-protein interaction studies, restriction enzyme-mediated integration (REMI), specific inhibition of gene expression by RNA interference and the expression of fluorescent fusion proteins for live cell and fixed cell microscopy (Kuspa and Loomis, 1992; Martens *et al*., 2002; Eichinger *et al*., 2005; Koch *et al*., 2006). Another aspect that greatly facilitates molecular genomic approaches is the haploidy of *Dictyostelium's* genome, which renders the generation of knockout mutants quite efficient (Kuspa *et al*., 1995). Furthermore, the completion of the *Dictyostelium* genome sequencing project in 2005 has provided researchers

with a powerful tool for proteomic studies (Eichinger *et al*., 2005). The genome project along with a rich source for information on many aspects of *Dictyostelium* is available at www.dictybase.org. A feature that notably contributed to *Dictyostelium's* popularity as model organism is its similarity to mammalian phagocytic cells. The basic strategy of mammalian innate immune response, phagocytosis, was invented in primitive eukaryotic cells and since then did not change fundamentally throughout evolution (Cosson and Soldati, 2008). Hence, *Dictyostelium* can be regarded as a primitive macrophage that shares properties like chemotaxis and phagocytosis and exhibits basic similarities on molecular level. Accordingly, *Dictyostelium* was established as host system for a variety of human pathogens like *Legionella pneumophila* or *Pseudomonas aeruginosa* (Ma *et al*., 2001; Cosson *et al*., 2002). Since the major part of this work focuses on the characterization of centrosomal proteins such as TACC (Transforming acidic coiled-coil protein) and CP224 (Centrosomal protein 224), it finally has to be mentioned that within the last decade, *Dictyostelium* has become a useful model for centrosome research. One of the main reasons for that was the establishment of a purification protocol for microtubule-free *Dictyostelium* centrosomes, which greatly facilitated proteomic and biochemical approaches (Gräf *et al*., 1998). This also gave rise to the generation of a good set of antibodies directed against centrosomal proteins, providing researchers with great tools for the further investigation of this organelle (Gräf *et al*., 1999).

1.2 The *Dictyostelium* centrosome

In most organisms the centrosome represents the largest non-membranous protein complex of the cell. It occupies crucial roles in a variety of important cellular processes. Undoubtedly, its most prominent task is its function as a nucleator and organizer of the microtubule cytoskeleton in most eukaryotic cell types apart from higher plants. For this reason, it is also termed the microtubule organizing center of the cell (MTOC). Accordingly, the centrosome is involved in many microtubule-dependent processes, such as cell polarization, organelle positioning, vesicle trafficking and maintenance of cell architecture (Schatten, 2008). Moreover, besides their central role in interphase microtubule organization, centrosomes constitute the mitotic spindle poles from which astral and spindle microtubules emanate. Although centrosome function in microtubule organization and spindle formation appears universal, the structural composition of MTOCs can vary fundamentally between different organisms. Most animal centrosomes consist of two orthogonally arranged centrioles, each made up of nine interconnected triplet microtubules. A pair of centrioles is surrounded by pericentriolar material (PCM), which contains the microtubule nucleating γ-tubulin

complexes. While the PCM of animal centrosomes contains large γ-tubulin ring complexes (γ-TuRCs) as well as the smaller γ-TuSCs, lower eukaryotes, such as *Dictyostelium* appear to possess only γ-TuSCs (Daunderer and Gräf 2002, Raynaud-Messina and Merdes 2007). Unlike animal centrosomes, the *Dictyostelium* centrosome does not consist of centrioles but instead is made up of a box-shaped, three layered core structure surrounded by an amorphous corona (Moens, 1976; Omura and Fukui, 1985) (Fig. 1A). The corona is the functional equivalent of the animal PCM and harbors electron-dense nodules that are thought to represent the sites of microtubule nucleation (Euteneuer *et al*., 1998). Further difference between the two types of centrosomes lies is their mode of duplication. While centrioles of animal centrosomes duplicate in synchrony with S phase, the *Dictyostelium* centrosome replicates in early mitosis (Ueda *et al*., 1999) (Fig. 1B).

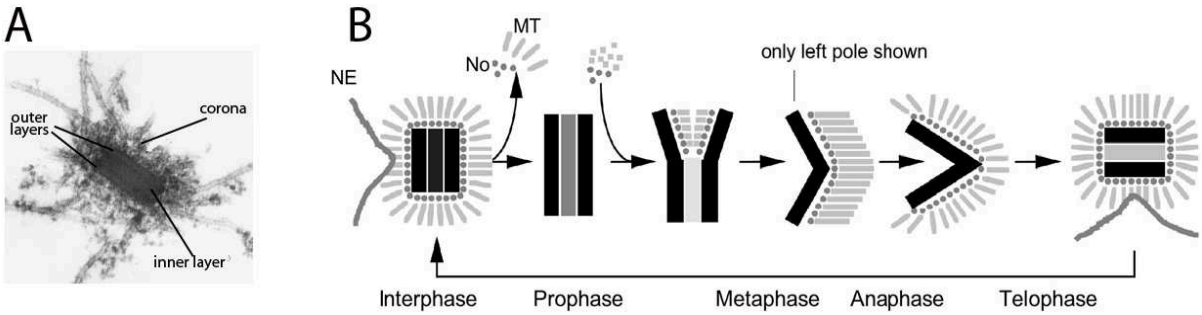

Fig. 1 Structural composition and mode of duplication of the *Dictyostelium* centrosome
(**A**) Electron microscopic image of a single interphase *Dictyostelium* centrosome. Subcentrosomal structures are indicated. Modified from Ueda *et al.* (1999). (**B**) The centrosome cycle in *Dictyostelium*. Used abbreviations comprise NE (nuclear envelope), No (electron-dense nodule) and MT (microtubule). Modified from Gräf *et al.* (2000).

During this process, in prophase, the central core structure enlarges and the microtubule nucleating corona is shed off. Consequently, unlike in animal mitotic cells, the interphase microtubule network is entirely lost. Afterwards, the central layer of the centrosomal core structure disassembles and the outer layers peel apart and insert into the nuclear envelope to function as the spindle poles of a closed mitosis (Kitanishi-Yumura and Fukui, 1987; Ueda *et al*., 1999). Microtubules nucleated from the nuclear side of the former outer layers provide the driving forces to push the spindle poles apart, while astral microtubules are not nucleated until metaphase. As metaphase progresses, the spindle poles start to fold back onto themselves to finally restore the three layered core structure after the inner layer has reassembled in telophase. Astral microtubules grow continuously longer as mitosis progresses, but usually do not reach their normal interphase length until M-Phase has ended. During telophase the

centrosome eventually exits the nuclear envelope and, like animal centrosomes, stays tightly associated with the nucleus throughout the successive cell cycle.

Revealing the molecular composition of centrosomes has long been a difficult task, since proteomic and molecular genetic approaches are usually complicated by the low copy number of centrosomal proteins on mRNA and protein levels. In 2003, however, Andersen *et al.* were very successful in identifying a considerable number of centrosomal proteins in human KE-37 cells (Andersen *et al*., 2003). According to Andersen's work, mammalian centrosomes are estimated to consist of approximately 120 different proteins, with over 70 of them known. After the completion of the *Dictyostelium* genome project and the establishment of an improved centrosome isolation protocol (Eichinger *et al*., 2005; Schulz *et al*., 2006), a similar approach was successfully carried out for *Dictyostelium* centrosomes (Reinders *et al*., 2006). Combined with data from further studies, 28 of the estimated 100 centrosomal proteins in *Dictyostelium* are now known (Kalt and Schliwa, 1993; Gräf *et al*., 2004; Reinders *et al*., 2006; Schulz *et al*., 2009b). Beyond that, several proteins that were identified in the proteomic approach remain, which have not yet been verified as genuine centrosomal components. It was part of this work to test three such candidate proteins in this respect, Cenp68 (centromeric protein 68, DDB0233901), Mad1 (mitotic arrest deficient 1, DDB0304834) and CP103 (centrosomal protein 103, DDB0304837). Since Cenp68 and Mad1 were found to localize to centromeres and kinetochores, respectively, these structures will be briefly introduced below (section 1.7).

1.3 Microtubule dynamics in *Dictyostelium*

Microtubules are one of the three major constituents of the cytoskeleton. Except from polarized epithelial cells, neurons or higher plant cells, the most common pattern of microtubule arrangement within the cell is a radial array of microtubules emanating from the centrosome. Microtubules form hollow cylinders of an outer diameter of 25 nm and consist of 13 parallelly arranged tubulin protofilaments, assembled by head-to-tail association of α- and β-tubulin heterodimers. Within a protofilament, the 8 nm long tubulin heterodimers are uniformly oriented, which confers intrinsic polarity to microtubules. In a radial microtubule array, the terminal α-tubulin subunit adjacent to the centrosome is termed the microtubule minus end and the exposed β-tubulin subunit facing towards the cell cortex is known as the microtubule plus end. While microtubule minus ends are frequently capped and anchored to the MTOC, microtubule plus ends are usually dynamic and stochastically switch between states of growth and shrinkage. The rapid transitions between these two states are known as

"catastrophe" and "rescue", respectively. This behavior was termed dynamic instability (Mitchison and Kirschner, 1984). Dynamic instability enables microtubules to explore the interior of the cell and to find and bind specific structures. Despite its importance the complex mechanisms underlying this dynamic behavior are not yet fully understood. However, a variety of exciting models aiming to explain this phenomenon are available today (Mitchison and Kirschner, 1984; Chretien *et al*., 1999; Rice *et al*., 2008; Howard and Hyman, 2009). *In vivo*, dynamic instability has to be tightly regulated, which is mostly achieved by a set of proteins termed microtubule-associated proteins (MAPs) (Van der Vaart *et al*., 2009). These adjust the dynamic behavior of individual microtubules as appropriate for their respective functions.

Compared to the microtubule cytoskeleton of many other cell types, the one of *Dictyostelium* differs markedly in some points. During interphase, a comparably low number of 30 - 70 microtubules emanate radially from the centrosome, covering most of the cell interior and providing tracks for a large volume of intracellular transport (Kimble *et al*., 2000; Ma *et al*., 2001). Association of the minus end with the centrosome is absolutely vital for microtubule stability in *Dictyostelium*. If minus ends get exposed, either artificially by laser ablation or during prophase upon dissociation of the corona, microtubules are rapidly depolymerized (Koonce and Khodjakov, 2002; Rehberg *et al*., 2005). *Dictyostelium* interphase microtubules exhibit a high degree of flexibility and extensive bending and meandering movements (Neujahr *et al*., 1998; Kimble *et al*., 2000). Apart from that, they seem to be rather stable. *In vivo* observations of GFP-α-tubulin did not reveal noticeable changes in individual microtubule length during interphase, indicating much less dynamics than in mammalian cells (Koonce and Khodjakov, 2002). Yet, these observations were hampered by the lack of suitable microtubule plus end marker proteins, without which reliable tracking of individual microtubule ends is usually impossible at the spatial and temporal resolution provided by the available microscopic systems. Consequently, the growth of astral and kinetochore microtubules during mitosis were the only clearly visible microtubule growth events in *Dictyostelium*. However, evidence for a certain degree of dynamics during interphase came from experiments with microtubule depolymerizing drugs such as nocodazole or thiabendazole (TBZ). These drugs are thought to bind tubulin dimers and prevent them from polymerization. Consequently, stable, non-dynamic microtubules should not be affected by treatment with such drugs, whereas microtubules exhibiting tubulin turnover should shorten. In other eukaryotic systems these drugs usually cause complete microtubule depolymerization. As expected, the impact of TBZ or nocodazol on *Dictyostelium* interphase

microtubules was less pronounced than on dynamic astral or kinetochore microtubules (Rubino *et al*., 1982; Kitanishi *et al*., 1984; Kalt and Schliwa, 1996). Interestingly, however, *Dictyostelium* interphase microtubules were also clearly affected by TBZ treatment, albeit to a lesser extent than microtubules in other organisms (Gräf *et al*., 2003). This contradictory behavior of *Dictyostelium* microtubules, which lack obvious dynamic instability but at the same time exhibit basic tubulin turnover as indicated by the *s*ensitivity to nocodazole, was addressed in this work by combined 5D fluorescence live cell imaging and FRAP analysis.

1.4 The microtubule plus end complex

The dynamic microtubule plus ends play important roles in processes like centrosome positioning, directional cell movement, nuclear migration and spindle orientation (Euteneuer and Schliwa, 1992; Koonce *et al*., 1999; Akhmanova and Hoogenraad, 2005; Honnappa *et al*., 2006). To fulfil this complex set of tasks, microtubule tips require tight regulation of their dynamics. For the most part, this is mediated by a varying subset of MAPs forming the so-called microtubule plus end complex. This complex surfs at microtubule tips and influences their polymerization properties, thereby controlling microtubule growth, shrinkage and stabilization in a cell cycle-dependent manner. Furthermore, this complex specifically binds to target sites such as kinetochores or cortical proteins and selectively delivers signalling molecules (Lansbergen and Akhmanova, 2006). Consequently, it is not surprising that the plus end complex is a highly dynamic structure whose protein composition and web of interactions strongly varies in response to the respective needs. The binding of microtubule plus end proteins to microtubule tips was initially thought to involve a treadmilling or co-polymerization-like process. However, recent single molecule FRAP data gave rise to a “fast exchange model”. In this view, the very microtubule plus ends harbour a high number of binding sites that can rapidly bind and release microtubule tip proteins as required (Bieling *et al*., 2007; Dragestein *et al*., 2008). As polymerization proceeds, these binding sites and with them the plus end proteins are gradually lost. The current model proposes that EB1 proteins (end binding 1) represent the conserved core of the microtubule plus end complex, owing to their ability to autonomously track growing microtubule plus ends (Bieling *et al*., 2007; Bieling *et al*., 2008; Zimniak *et al*., 2009; Dixit *et al*., 2009). In turn, EB1 might then provide binding sites for other plus end proteins in a biased manner. This is supported by the fact that EB1 interacts with virtually all other plus end proteins known.

To date, more than 20 different microtubule plus end binding proteins have been described (Galjart, 2010). Besides EB1, these include proteins of the dynein/dynactin complex, the

microtubule destabilizing factor MCAK (mitotic centromere-associated kinesin), the growth promoting CLIP-170 and CLIP-115, CLASPs, LIS-1 and homologues of the microtubule polymerase XMAP215. In *Dictyostelium*, EB1, the dynein heavy and intermediate chain, LIS-1 and CP224, an XMAP215 homologue, are confirmed plus end binding proteins (Hestermann *et al*., 2002). Interestingly, unlike mammalian microtubule tip proteins, the *Dictyostelium* representatives are all permanently associated with the plus end. It remains to be tested if the increased stability of *Dictyostelium* microtubules is a consequence of this divergent behavior. In this work, TACC (Transforming acidic coiled-coil), a putative member of the microtubule plus end complex in *Dictyostelium* was characterized. TACC has been shown to strongly interact with CP224 and both proteins colocalize at the centrosome (Koch *et al*., 2006).

1.5 The ch-TOG/XMAP215 family of proteins

Along with EB1, the family of ch-TOG/XMAP215 (XMAP215) proteins are the only proteins shown to autonomously surf at microtubule plus ends *in vitro* (Bieling *et al*., 2007). This ubiquitous family of proteins is characterized by 2 - 5 N-termial TOG domains (tumor overexpressed gene) that form a conserved tubulin binding interface (Slep, 2009). In addition to its localization at microtubule tips, all members of the XMAP215 family investigated so far were shown to localize to the centrosome. This association is mediated by interaction of their conserved C-terminal third with centrosomal residents like TACC (Wang and Huffaker, 1997; Charrasse *et al*., 1998; Popov *et al*., 2001; Hestermann *et al*., 2002; Cassimeris and Morabito, 2004). Certainly the most prominent of all XMAP215 functions is its strong ability to promote microtubule growth. Its mode of action in this respect was recently described to resemble a processive tubulin polymerase that while moving with growing microtubule plus ends, repeatedly binds free single tubulin dimers and incorporates them into the microtubule lattice, possibly by stabilizing a structural intermediate in the polymerization pathway (Brouhard *et al*., 2008). However, the detailed mechanism of tubulin addition is still a matter of debate and alternative models are existing (Kerssemakers *et al*., 2006; Slep and Vale, 2007). Beyond their crucial role in microtubule dynamics, XMAP215 proteins were shown to be vital for mitotic spindle integrity (Tournebize *et al*., 2000; Severin *et al*., 2001; Cassimeris and Morabito, 2004), microtubule nucleation (Popov *et al*., 2002) and microtubule plus end interaction with the cell cortex (Hestermann and Gräf, 2004).

CP224, the *Dictyostelium* homologue of the XMAP215 proteins, has been thoroughly characterized in our lab. As most other XMAP215 proteins, it is part of the microtubule plus

end complex of interphase and kinetochore microtubules and it localizes to the centrosome throughout the entire cell cycle (Gräf *et al*., 2000a; Rehberg *et al*., 2002). With the aid of a monoclonal anti-CP224 antibody, it was found to be concentrated within the centrosomal corona (Gräf *et al*., 1999; Gräf *et al*., 2000b). CP224 was shown to be involved in centrosome duplication, cytokinesis and in dynein-dependent attachment of microtubules to the cell cortex (Gräf *et al*., 2000a; Gräf *et al*., 2003; Hestermann and Gräf, 2004). Underexpression of CP224 furthermore revealed an important role in microtubule dynamics. The corresponding cell lines exhibited significantly shortened interphase microtubules and a strongly increased sensitivity to nocodazole. As a consequence, interphase microtubules were entirely depolymerized upon nocodazole treatment, which is uncommon for *Dictyostelium* microtubules (Gräf *et al*., 2003). A recent screen for CP224 binding partners by tandem affinity purification revealed interactions with *Dictyostelium* EB1 and TACC, both of which could subsequently be confirmed by co-immunoprecipitation (Koch *et al*., 2006). The latter interaction is highly conserved and has been proposed to be crucial for the microtubule growth-promoting function of XMAP215 proteins (Lee *et al*., 2001; Srayko *et al*., 2003; Sato *et al*., 2004; Peset *et al*., 2005; Koch *et al*., 2006).

1.6 The TACC family of proteins

Originally, TACC was identified as a protein overexpressed in a human breast cancer cell line (Still *et al*., 1999). Due to its ability to transform cells and its highly acidic ~200 C-terminal amino acids that form a coiled-coil structure, it was termed Transforming acidic coiled-coil 1 (hTACC1). Soon TACC proteins were identified in many organisms ranging from yeast to humans. Three TACC family proteins are existing in humans and mice that have recently all been target of intensive study (TACC1, ACC2/ECTACC/AZU-1 and TACC3/ERIC1/AINT) (Gergely, 2002; Peset and Vernos, 2008). In lower eukaryotes, maskin (*X. laevis*), D-TACC (*D. melanogaster*), TAC-1 (*C.elegans*), TACC (*Dictyostelium*) and Alp7 (*S. pombe*) have been investigated to date (Bellanger and Gonczy, 2003; Le Bot *et al*., 2003; Srakyo *et al*., 2003; Sato *et al*., 2004; Koch *et al*., 2006). The conserved C-terminal TACC domain is the common feature of all TACC proteins. Amino acid identity within this domain lies between 50 % and 90 % for mammalian TACC proteins and maskin, and at ~30 % for D-TACC compared to other TACC family members (Gergely, 2002). *Dictyostelium* TACC (DDB0220500) seems to be slightly more divergent and shares ~20 % amino acid identity with other TACC proteins (Fig. 2). Outside the TACC domain, TACC proteins display hardly

any similarity in length or sequence. This suggests the TACC domain to be responsible for most of the functions shared by all TACC proteins.

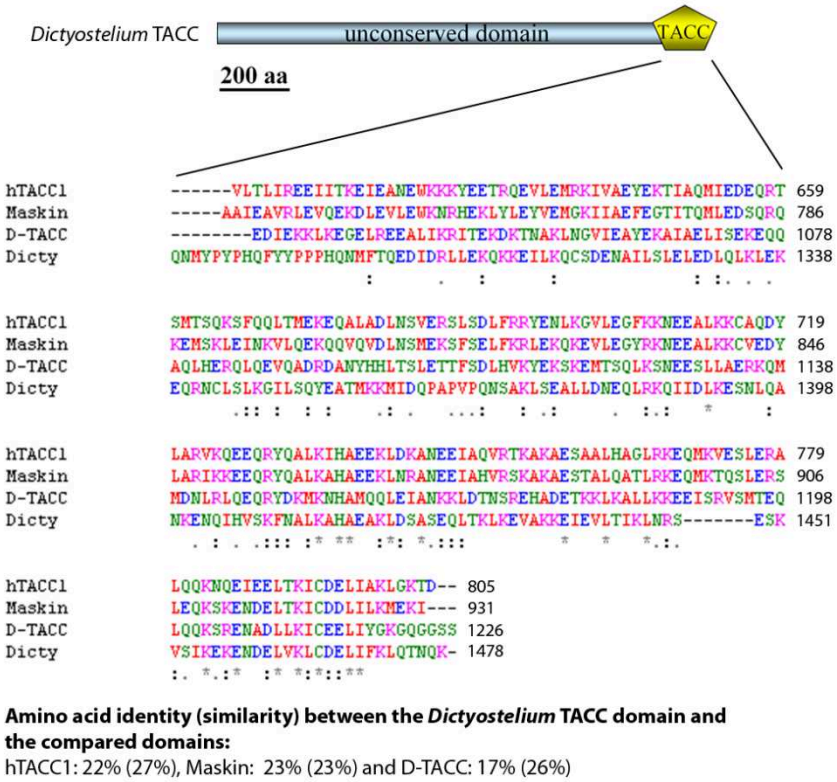

Fig. 2 Sequence homology and domain organization of *Dictyostelium* TACC (DDB0220500)
A schematic of the *Dictyostelium* TACC protein is shown on top. Sequence homology of TACC family members is limited to ~200 C-terminal residues constituting the TACC domain. The sequence alignment of various TACC domain sequences from humans (hTACC1), *Xenopus* (maskin) and *Drosophila* (D-TACC) with *Dictyostelium* TACC was generated using ClustalW (www.ebi.ac.uk/Tools/msa/clustalw2).

A role in cancer progression has been reported several times for TACC proteins in mammals. However, in this context no common role has emerged so far, since TACC proteins were frequently found to be up- and downregulated in similar types of tumors. Known TACC functions roughly fall into two categories. The first one comprises functions related to the regulation of gene expression, which includes interactions with histone acetyltransferases and the RNA processing machinery (Peset and Vernos, 2008). The second group of TACC function is closely related to its localization to microtubules and the centrosome. All TACC proteins investigated so far show recruitment to the centrosome during mitosis, and hTACC2, TAC-1 and D-TACC can also be found there during interphase, albeit to a lesser extent (Gergely *et al*., 2000a; Gergely *et al*., 2000b; Gergely, 2002; Le Bot *et al*., 2003). Moreover, maskin and TAC-1 associate with spindle microtubules and the microtubule-kinetochore

interface, while D-TACC localizes along spindle and astral microtubules (Gergely *et al*., 2000a; Gergely *et al*., 2000b; Srayko *et al*., 2003; Le Bot *et al*., 2003; Peset *et al*., 2005). GFP-D-TACC was further observed as tiny dots moving towards and away the centrosome, indicating D-TACC localization to microtubule plus ends (Lee *et al*., 2001). Multiple phenotypes described upon TACC mutation seem to be related to perturbed microtubule stability or impaired microtubule dynamics. This became evident in *Drosophila*, *C. elegans*, *X. laevis* and mammalian cells, when shortened spindles, shortened astral microtubules and sometimes shortened interphase microtubules were observed in TACC mutants (Gergely *et al*., 2000b; Le Bot *et al*., 2003; O'Brien *et al*., 2005; Peset *et al*., 2005). TACC function in promoting microtubule growth was reported to require phosphorylation by Aurora A kinase and this phosphorylation was shown to be indispensable for centrosomal TACC recruitment (Tournebize *et al*., 2000; Kinoshita *et al*., 2005; Barros *et al*., 2005; Albee *et al*., 2008). To date, all experimentally verified Aurora A phosphorylation sites lie outside the TACC domain (Peset and Vernos, 2008).

As mentioned above, interactions of TACC proteins with XMAP215 proteins are conserved and have been confirmed for all organisms investigated so far. It was proposed that this interaction is essential for correct XMAP215 protein localization, since centrosomal XMAP215 levels were found to be drastically reduced in D-TACC, maskin and TAC-1 mutant strains (Lee *et al*., 2001; Cullen and Ohkura, 2001; Srayko *et al*., 2003; Le Bot *et al*., 2003; Kinoshita *et al*., 2005). Lacking centrosomal XMAP215 might further contribute to the occurrence of the described defects observed upon TACC deficiency. Interestingly, the phenotypes of TACC and XMAP215 protein depletion are frequently similar, supporting the idea that the two proteins are acting together to stabilize microtubules. This is underlined by evidence from *Xenopus*, where maskin and XMAP215 were shown to form a complex of equimolar amounts that has an increased affinity to microtubules *in vitro* compared to the two proteins alone. Moreover, microtubules bound to the maskin-XMAP215 complex exhibited an increased resistance to the microtubule depolymerizing kinesin MCAK (Kinoshita *et al*., 2005; Peset *et al*., 2005). Although XMAP215 proteins are most concentrated at centrosomes, they mainly act on microtubule plus ends to influence microtubule dynamics (Matthews *et al*., 1998; Cullen *et al*., 1999; Tournebize *et al*., 2000; Garcia *et al*., 2001). These findings gave rise to the current model of TACC function (Fig. 3). In an Aurora A-dependent manner, phosphorylated TACC in complex with XMAP215 is enriched at the spindle poles during mitosis. As a complex the two proteins are loaded onto microtubule minus ends and emerging microtubule plus ends, where they antagonize the microtubule destabilizing kinesin MCAK

around the centrosomes (Kinoshita *et al*., 2006; Peset and Vernos, 2008). It has to be mentioned, though, that this model has recently been challenged by data from *Xenopus*, where maskin depletion did not affect the stability or dynamics of microtubules nucleated from isolated centrosomes. Instead, maskin was shown to be involved in anchoring microtubules to centrosomes in an Aurora A- dependent manner (Albee *et al*., 2008).

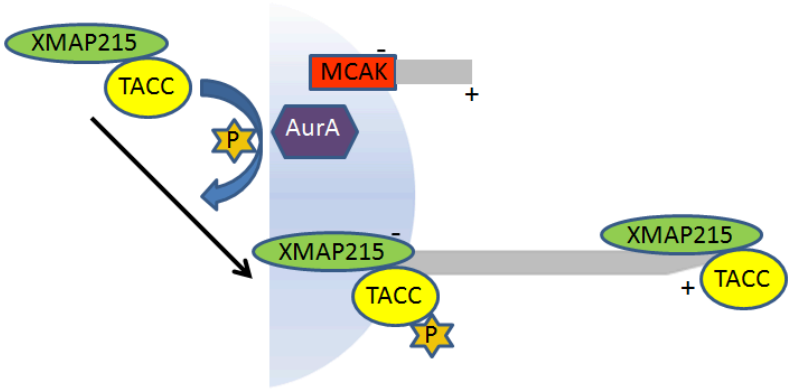

Fig. 3 Proposed model of TACC function in stabilizing microtubules
Aurora A mediated phosphorylation of TACC in complex with XMAP215 at mitotic centrosomes promotes enrichment of TACC-XMAP215 at the spindle poles. The TACC-XMAP215 complex interacts with nascent microtubules and counteracts MCAK, thereby promoting microtubule growth from spindle poles. TACC protein associated with microtubule plus ends is thought to be subsequently dephosphorylated. Microtubules are depicted as grey bars, the spindle pole as light blue semi-circle.

After *Dictyostelium* TACC was identified as an interactor of EB1 and CP224 in a tandem affinity purification approach and in co-immunoprecipitation experiments, first steps towards its characterization were conducted (Koch *et al*., 2006). A GFP-TACC-domain (GFP-TACCdom) fusion protein was expressed in *Dictyostelium* and found to localize to centrosomes during the entire cell cycle. Moreover, immunofluorescence experiments on microtubule-free, isolated centrosomes could show that TACC is a genuine centrosomal component (Koch *et al*., 2006). A rabbit polyclonal antibody generated against the TACC domain confirmed localization of endogenous TACC to the centrosomes. Unfortunately, several attempts to elucidate *Dictyostelium* TACC function by generating a knockout strain failed, initially suggesting the TACC protein to be essential. In this work, *Dictyostelium* TACC function was assessed by generating RNAi mutants, and resulting phenotypes were investigated.

1.7 The *Dictyostelium* centromeres

Centromeres are a specialized region of heterochromatin representing the site of sister chromatid cohesion and assembly of kinetochores, the attachment site for spindle microtubules during mitosis. Accurate centromere function is therefore essential for chromosome segregation and mitotic fidelity, while loss of centromere integrity can lead to chromosomal instability and cancer (Kops *et al*., 2005a; Thompson, 2010).

The *Dictyostelium* genome comprises 34 Mb of DNA organized on six distinct chromosomes and 8.8 Mb of extrachromosomal rDNA (Eichinger *et al*., 2005). Correspondingly, in a haploid *Dictyostelium* nucleus, six chromosomal regions were identified that constitute the amoebae's centromeres (Eichinger *et al*., 2005; Glöckner and Heidel, 2009; Dubin *et al*., 2010). *Dictyostelium* centromeres are telocentric and tightly clustered on the nucleoplasmic side opposite to the centrosome, where they are kept in place by a physical link with the centrosome involving the nuclear membrane protein SUN1 (Fig. 4) (Schulz *et al*., 2009a).

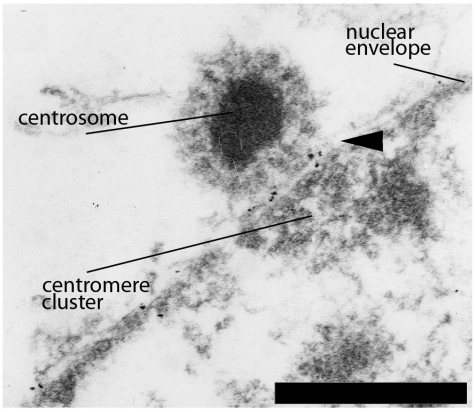

Fig. 4 *Dictyostelium* centromeres are clustered opposite to the centrosome
Immunoelectron microscopy image showing a section of an isolated nucleus with attached centrosome. The preparation was labeled with an antibody directed against *Dictyostelium* SUN1 and nanogold conjugated anti-rabbit antibody. The arrowhead points at the perinuclear space. The centrosome, centromeric cluster and nuclear envelope are indicated. Bar = 0.5 µm. The image was taken by Prof. Otto Baumann (Universität Potsdam). Modified from Schulz *et al.* (2009a).

Despite their highly conserved function, centromeres are vastly divergent on DNA level. For most eukaryotes, centromeric DNA consists of long stretches of repetitive DNA, arrays of satellite repeats and/or transposons ranging from 100 kb to 100 Mb in total (Mehta *et al*., 2010). In *Dictyostelium*, these were mainly found to be stretches of DIRS-1 (*Dictyostelium* intermediate repeat sequence 1). These long terminal repeats are restricted almost exclusively to centromers (Eichinger *et al*., 2005; Glöckner and Heidel, 2009). Centromere identity was shown to be maintained mostly by epigenetic marks (Mehta *et al*., 2010). The most important feature of core centromeric DNA in this context is the partial substitution of canonical histone H3 by a centromere-specific histone variant termed Cenp-A or CenH3 (Carroll and Straight, 2006; Buscaino *et al*., 2010), which serves to define the site of kinetochore assembly (Torras-Llort *et al*., 2009). Very recently, a Cenp-A/CenH3 orthologue could also be identified in *Dictyostelium* (Dubin *et al*., 2010). Human core centromeres furthermore contain a set of 16

nonhistone proteins known as constitutive centromere-associated network (CCAN) (Carroll *et al*., 2010). These proteins, comprising Cenp-C, Cenp-H, Cenp-I, Cenp-K through Cenp-U, Cenp-W and Cenp-X, are all permanently associated with the centromeres. However, so far none of the CCAN proteins could be identified in *Dictyostelium.* In most higher eukaryotes, including *Dictyostelium*, the Cenp-A/CenH3-containing core centromeric region is flanked by constitutive pericentromeric heterochromatin that is characterized by histone modifications such as di- or tri-methylation of H3 at lysine 9 (H3K9me2, H3K9me3) (Kaller *et al*., 2006; Dubin *et al*., 2010; Mehta *et al*., 2010). Furthermore, this chromatin region is intensely decorated with proteins of the conserved HP1 family (Heterochromatin protein 1), which play a crucial role in the assembly and maintenance of heterochromatin (Grewal and Jia, 2007). In *Dictyostelium*, pericentromeric heterochromatin represents the by far most prominent cluster of heterochromatin in the nucleus. GFP-fusion proteins of the *Dictyostelium* HP1 representatives hcpA and hcpB were shown to localize to the centromeres throughout the entire cell cycle, albeit to a lesser extent in late mitosis (Kaller *et al*., 2006). To date, hcpA, hcpB, the putative H3K9 methyltransferase SuvA, the histone variant CenpH3 and Cenp68, which was characterized in this work, are the only constitutive centromer- or heterochromatin-specific proteins known in *Dictyostelium* (Kaller *et al*., 2006; Schulz *et al*., 2009b; Dubin *et al*., 2010; Ph.D. thesis of Manu Dubin, 2010, Universität Kassel).

During mitosis, proper attachment of spindle microtubules to chromosomes is a prerequisite for accurate chromosome segregation. The link between spindle microtubules and centromeres is provided by kinetochores, macromolecular structures consisting of over 65 different proteins in *S. cerevisiae* and more than 75 in vertebrates, most of them conserved from yeast to humans. Kinetochores of higher eukaryotes exhibit a trilaminar architecture (Santaguida and Musacchio, 2009), comprising an electron-dense inner and outer plate and a middle plate of lower density. In a simplified view, the vertebrate inner plate is mostly made up of proteins of the CCAN that form an interface with centromeric chromatin, while proteins of the outer plate, essentially comprising the KNL-1/Mis12/Ndc80 complexes (KMN network), mediate the connection with the plus ends of spindle microtubules (Bharadwaj *et al*., 2004; McCleland *et al*., 2004; Obuse *et al*., 2004; Deluca *et al*., 2005; Cheeseman *et al*., 2008; Santaguida and Musacchio, 2009). The outer plate and the adjacent fibrous corona were furthermore shown to harbour proteins of the spindle assembly checkpoint (SAC), a signalling pathway that ensures accurate chromosome attachment to spindle microtubules prior to the onset of anaphase (Musacchio and Salmon, 2007; Wan *et al*., 2009). In this work, the localization of *Dictyostelium* Mad1, a putative homologue of the conserved SAC protein

Mad1 (Mitotic arrest deficient 1) was investigated. Due to its extensive complexity the SAC will not be introduced in detail here, but some features of Mad1 will briefly be mentioned.
In late prophase Mad1 and its conserved interaction partner Mad2 concentrate at kinetochores that are not yet attached to spindle microtubules (Howell *et al*., 2004). The current model states that by forming a complex with Mad2, Mad1 promotes the retention and accumulation of a fraction of total Mad2 at kinetochores (Chen *et al*., 1998; Shah *et al*., 2004; Liu *et al*., 2006). Mad1-Mad2 complex formation furthermore triggers a conformational change from open Mad2 to closed Mad2 (Luo *et al*., 2002). This kinetochore-bound complex constitutes a receptor for free open Mad2 that converts open Mad2 to Cdc20-bound (Cell division cycle 20) closed Mad2 (De Antoni *et al*., 2005). Accumulation of the Cdc20-Mad2 complex then promotes SAC activation through formation of an inhibitory complex that renders the ubiquitin ligase APC/C (Anaphase-Promoting Complex) inactive. Association of Mad1 and Mad2 with kinetochores is strongly dependent on microtubule attachment (Waters *et al*., 1998; Musacchio and Salmon, 2007). In response to bipolar spindle attachment, Mad1 and Mad2 levels at kinetochores drop drastically, thus promoting disassembly of the inhibitory complex and release of Cdc20. Upon association of Cdc20 with APC/C, Cyclin B and Securin, which are required to keep the SAC active, are ubiquitinated and degraded. This in turn activates the protease Separase, which abolishes sister chromatid cohesion by targeting the cohesin rings, thereby allowing the onset of anaphase.

1.8 Aims of this study

Tight regulation of microtubule dynamics is achieved by microtubule-associated proteins (MAPs). Considering that impaired microtubule dynamics or spindle organization can promote serious diseases such as cancer or neurodegenerative diseases, the investigation of MAP function is also of huge medical relevance.

The main focus of this study was to functionally characterize the ubiquitous microtubule-associated protein TACC in *Dictyostelium* and to gain first insights in its interplay with CP224, a conserved binding partner of the XMAP215 family. To address this issue, full length TACC and truncated derivatives had to be cloned and expressed as a GFP-fusion protein. Together with immunofluorescence data obtained by using a TACC antibody, live cell and fixed cell imaging should explicitly elucidate TACC localization.

Insight in TACC function should be gained by generating knockout or knockdown mutants. Effects of TACC depletion were identified and the molecular basis underlying the observed phenotypes should be elucidated, particularly with regard to the interplay with CP224. This included the evaluation of the effect of TACC depletion on centrosomal GFP-CP224 and GFP-α-tubulin dynamics by fluorescence recovery after photobleaching experiments (FRAP). In the course of these experiments, the unusual behavior of microtubules in *Dictyostelium* should also be addressed.

The second part of this study focused on the investigation of three yet uncharacterized *Dictyostelium* proteins, Cenp68, CP103 and Mad1. These were identified as putative centrosomal components in a proteomic screen conducted previously. This should be facilitated by expression of full length GFP-fusion proteins, followed by microscopic analysis. In addition, a polyclonal antibody against Cenp68 should be raised, allowing the investigation of the endogenous protein. Finally, by generating knockout strains and the identification of interaction partners, first steps should be carried out to unveil the function of the three proteins.

2 Materials and methods

2.1 Reagents and other materials

2.1.1 Chemicals and reagents

Unless otherwise stated, chemicals and reagents were acquired from Carl Roth (Karlsruhe), Sigma-Aldrich (St. Louis, MO, USA), Biomol (Hamburg) and AppliChem GmbH (Darmstadt). All reagents used were of *pro analysis* grade and all solutions were prepared using distilled or bi-distilled water.

2.1.2 Antibodies

Primary antibodies:

Anti-actin, mAb, 264-236-1	(Westphal *et al*., 1997)
Anti-Cenp68, rabbit antiserum	this work, (Schulz *et al*., 2009b)
Anti-CP224, mAb, 2/165	(Gräf *et al*., 1999)
Anti-CP224, DdCP224Hind, rabbit antiserum	(Hestermann and Gräf, 2004)
Anti-γ-tubulin, rabbit antiserum	(Euteneuer *et al*., 1998)
Anti-GFP, rabbit antiserum	(Faix *et al*., 2001)
Anti-GFP, mAb 264-236-1	Chemicon (Billerica, MA, USA)
Anti-H3K9me3, # 07-523, rabbit antiserum	Millipore (Billerica, MA, USA)
Anti-SUN, rabbit antiserum	(Schulz *et al*., 2009a)
Anti-TACC, rabbit antiserum	(Ph.D. thesis Dr. Katrin Pfütze (nee Koch), Universität Marburg)
Anti-tubulin, mAb YL1/2	Chemicon (Billerica, MA, USA)

Secondary antibodies:

Goat anti-mouse Alexa Fluor 488 and 568	Invitrogen (Carlsbad, CA, USA)
Goat anti-rabbit Alexa Fluor 488 and 568	Invitrogen (Carlsbad, CA, USA)
Goat anti-rat Alexa Fluor 488 and 568	Invitrogen (Carlsbad, CA, USA)
Goat anti-mouse Cy5 conjugate	Dianova (Hamburg)
Goat anti-rabbit Cy5 conjugate	Dianova (Hamburg)
Goat anti-rat Cy5 conjugate	Dianova (Hamburg)
Goat anti-mouse alkaline phosphatase conjugate	Sigma (St. Louis, MO, USA)
Goat anti-rabbit alkaline phosphatase conjugate	Sigma (St. Louis, MO, USA)
Goat anti-mouse horseradish peroxidase conjugate	Dianova (Hamburg)
Goat anti-rabbit horseradish peroxidase conjugate	Dianova (Hamburg)

2.1.3 Enzymes

Some enzymes will be described in the context of the corresponding method.

Taq polymerase	various manufacturers
Phusion polymerase	Finnzymes (Espoo, Finland)
Proteinase K	Carl Roth (Karlsruhe)
DNAse-1 (RNAse free)	Sigma (St. Louis, MO, USA)
Other DNA modifying/restriction enzymes	New England Biolabs (Ipswich, MA, USA)
Fermentas	(Burlington, Canada)

2.1.4 Antibiotics

Ampicillin	Carl Roth (Karlsruhe)
Blasticidin S	Carl Roth (Karlsruhe)
Geneticin (G418)	Carl Roth (Karlsruhe)
Penicillin/Streptomycin	PAA GmbH (Pasching, Austria)

2.1.5 Other materials

Roti-NC nitrocellulose membrane	Carl Roth (Karlsruhe)
Protein G sepharose 4 fast flow	GE Healthcare (Uppsala, Sweden)
NHS-activated sepharose 4 fast flow	GE Healthcare (Uppsala, Sweden)
Snake skin dialysis membrane, cut-off 7 kDa	Pierce (Rockford, IL, USA)
GFP-Binder coupled to NHS sepharose	Chromotek (Planegg-Martinsried)
Amylose resin E8021S	New England Biolabs (Ipswich, MA, USA)
Filtropur S plus, for sterile filtration	Sarstedt (Nümbrecht)
Polycarbonate filters, pore Ø 5µm	Whatman (Maidstone, UK)

2.1.6 Buffers and solutions

Specific buffers are described in the context of the corresponding method.

Antibody dilution buffer

0.02 % NaN_3 in 0.1 % BSA solution

6x Laemmli sample buffer for SDS-PAGE

300 mM Tris/HCl, pH 6.8; 30 % glycerol; 20 % SDS; 0.025 % bromphenol blue;

15% 2-mercaptoethanol

Urea sample buffer for SDS-PAGE

10 % SDS; 9 M urea; 5 % 2-mercaptoethanol

Mowiol (mounting medium)
120 mg/ml polyvinyl alcohol 4-88; 30 % glycerol; 0.2 M Tris-HCl, pH 8.8

PBS
70 mM Na_2HPO_4; 30 mM KH_2PO_4; 137 mM NaCl; 2.6 mM KCl; pH 7.4

50x PC (protease inhibitor cocktail)
50 mM Pefabloc SC; 1.25 mg/ml leupeptin; 0.5 mg/ml tosyl-arginine-methylester;
0.5 mg/ml soybean trypsin inhibitor; 50 µg/ml aprotinin; 50 µg/ml pepstatin;
100 mM benzamidine

SDS running buffer
100 mM Tris/HCl, pH 8.3; 0.1 % SDS; 100 mM glycin

Phosphate buffer / Soerensen buffer (Malchow *et al.*, 1972)
14.6 mM KH_2PO_4; 2 mM Na_2PO_4; pH 6.0

TAE running buffer (for agarose gel electrophoresis)
40 mM Tris; 0.1 % acetic acid; 1 mM EDTA; pH 8.3

6x TAE (loading buffer for agarose gel electrophoresis)
240 mM Tris; 6 mM EDTA; 0.6 % acetic acid; 1 % SDS; 30 % glycerol;
0.025 % bromphenol blue; pH 8.3

TBS
20 mM Tris/HCl; 150 mM NaCl; pH 7.4

TBST
20 mM Tris/HCl; 150 mM NaCl; 0.05 % Tween-20; pH 7.4

TE buffer
10 mM Tris; 1 mM EDTA; pH 8.0

2.1.7 Vectors

p1ABsr8	(Gräf *et al*., 2000a)
Cherry-histone 2B	kindly provided by Dr. Annette Müller-Taubenberger (Universität München)
GFP-CP224 (Spex Bsr)	(Gräf *et al*., 2000a)
pIS76	(Schulz *et al*., 2009b)
pIS77	(Schulz *et al*., 2009b)
pLPBLP	(Faix *et al*., 2004)
pMALc2	New England Biolabs (Ipswich, MA, USA)

2.1.8 Software

Microsoft Office 2007, Endnote X Bld 2114, ApE plasmid editor v.1.10.4, MacBiophotonics Image J v.1.42l, Carl Zeiss Axiovision 4.7 and 4.8, Carl Zeiss ZEN 2009, Adobe Photoshop CS3 Extended v10.0, Varian Cary Win UV simple reads 2.0, Biorad Quantity One 4.0.3.

2.2 Organisms and cell culture

2.2.1 Bacterial strains

Escherichia coli strains TOP10 (Invitrogen, Carlsbad, CA, USA) and DH5α were used for cloning, *Escherichia coli* KS1000 (New England Biolabs, Ipswich, MA, USA) was used for bacterial protein expression. *Klebsiella aerogenes* (Williams and Newell, 1976) was used for non-axenic cultivation of *Dictyostelium* cells.

2.2.2 *Dictyostelium discoideum* strains

D. discoideum strain AX2-214*,* an axenically growing derivate of isolate NC-1 (Raper, 1935), was used as wild type strain in this study. All mutant strains used in this study were generated by the transformation of AX2 cells. Strains used, which were not generated in the course of this work, include:

GFP-α-tubulin	(Rehberg and Gräf, 2002)
GFP-CP224	(Gräf *et al*., 2000a)
GFP-TACCdom	(Koch *et al*., 2006)
hcpA-GFP and hcpB-GFP	(Kaller *et al*., 2006), kindly provided by Prof. Wolfgang Nellen (Universität Kassel)

Strains created during this study are listed in section 2.3.15, Tab. 1.

2.2.3 Cultivation of *E. coli* strains

E. coli cells were grown in shaking culture using LB-medium (240 rpm in flasks of various diameters) or on LB-agar plates according to the standard protocol (Sambrook *et al*., 2001). To select for transformed *E.coli* clones, the medium was supplemented with a final concentration of 100 µg/ml ampicilin. Using TB-medium instead of LB-medium helped to avoid recombination of plasmid DNA in TOP10 cells while cloning GFP-TACC (full length) and GFP-TACCΔC. For long term storage, equal amounts of *E.coli* shaking culture and storage medium were mixed thoroughly and stored at -70 ºC.

LB medium
10 g/l tryptone; 5 g/l yeast extract; 10 g/l NaCl; pH 7.0

LB agar plates
LB-Medium supplemented with 1.5 % agar

Teriffic broth medium (TB-medium) (Sambrook *et al*., 2001)
900 ml of a solution consisting of 13.2 g/l tryptone, 26.4 g/l yeast extract and 4.4 ml glycerol were mixed with 100 ml of a buffer consisting of 0.17 M KH_2PO_4 and 0.72 M K_2HPO_4. Importantly, both solutions have to be autoclaved separately prior to mixing.

Storage medium
16 g/l tryptone; 10 g/l yeast extract; 5 g/l NaCl; 70 % glycerol

2.2.4 Cultivation of *Klebsiella aerogenes*

Klebsiella cells were grown on SM-agar plates at 37 ºC, or at 21 ºC when co-cultivated with *Dictyostelium*.

SM-agar plates
10 g/l peptone (Oxoid); 1 g/l yeast extract (Oxoid); 10 g/l glucose; 20 g/l bacto agar;
1.6 g/l K_2HPO_4; 2.2 g/l KH_2PO_4; 1 g/l $MgSO_4$; pH 6.5

2.2.5 Cultivation of *Dicytostelium discoideum*

Dictyostelium cells were grown axenically in HL5c medium at 21 ºC in shaking culture at 150 rpm, or as adherent culture in tissue flasks. Optionally, to select for mutant cells,

blasticidin S (4 µg/ml) and/or G418 (10 µg/ml) were added. In liquid culture, *Dictyostelium* cells were not allowed to get stationary, i.e. to grow over a density of 5 x 10^6 cells/ml. Alternatively, *Dictyostelium* was grown on lawns of *Klebsiella* using SM agar plates. This method of cultivation frequently served to keep very sick mutant strains alive.

Dictyostelium spores formed in response to starvation can be frozen and stored for many years. To do this, axenically growing *Dictyostelium* cells were harvested and washed with phosphate buffer. After resuspension in phosphate buffer, ~500 µl of cell suspension with a density of 2 - 3 x 10^8 cells/ml were plated on phosphate agar plates. Once fruiting bodies had fully developed, the spores-containing fruiting bodies were harvested with ~4 ml of sterile phosphate buffer per plate and stored at -70 ºC. To obtain axenically growing *Dictyostelium* cultures from frozen spores, ~100 µl of the latter were thawed at room temperature and resuspended in 5 ml HL5c medium.

HL5c medium

5 g/l yeast extract (Difco); 2.5 g/l bacto tryptone (Difco); 2.5 g/l casein peptone (Merck);
5 g/l proteose peptone (Oxoid); 10 g/l glucose; 1.2 g/l KH_2PO_4; 0.35 g/l Na_2HPO_4; pH 6.5

Phosphate agar plates

14.6 mM KH_2PO_4; 2 mM Na_2PO_4; 15 g/l bacto agar; pH 6.0

2.3 Molecular biology methods

2.3.1 Determination of DNA concentration

The concentration of DNA in solution was determined by measuring E_{260nm} in a Cary 50 spectrometer (Varian, Darmstadt), with E_{260nm} = 1 corresponding to 50 µg/ml dsDNA (Sambrook *et al*., 2001). Solutions of high DNA content were usually diluted prior to photometric measurements.

2.3.2 Agarose gel electrophoresis

DNA fragments were separated on gels containing 1 % agarose in TAE running buffer. Prior to loading, DNA samples were supplemented with 1/5 volume of 6 x TAE loading buffer. The separation of DNA samples according to their size was performed by applying 5 V/cm. After running, gels were stained in 1 µg/ml ethidium bromide in TAE running buffer for ~30 min.

DNA bands were visualized and documented using UV illumination in combination with the Gel Doc 2000 system (BioRad, Hercules, CA, USA).

2.3.3 Purification of PCR products and DNA extraction from agarose gels

Agarose gels were illuminated in an ECX-20-M UV-illuminator (PeqLab, Erlangen) and DNA bands were excised with a razor blade. Excised bands were purified using the Nucleospin Extract II kit (Macherey & Nagel, Düren) in accordance with the manufacturer's instructions. This kit also allows the purification of DNA obtained from PCR reactions without prior separation by gel electrophoresis. For this, an alternative protocol included in the manufacturer's instructions was used.

2.3.4 Preparation of plasmid DNA

Plasmid DNA "Mini" preparations from *E.coli* overnight shaking cultures were performed using the Plasmid-Mini Spin Isolation kit (Applichem, Darmstadt). For "Midi" preparations, the Nucleobond PC 100 kit (Macherey and Nagel, Düren) was used. For "quick and dirty Mini-preparations", the manufacturer's manual was followed except for the usage of columns. DNA was resolved in ddH_2O or 10 mM Tris pH 7.5.

2.3.5 Quick Preparation of chromosomal *D. discoideum* DNA

Dictyostelium genomic DNA suitable for PCR reactions was prepared essentially according to (Charette and Cosson, 2004). In brief, cells were harvested, washed with phosphate buffer and spun down. One volume of LyB buffer containing 20 µg of Proteinase K for every 25 µl of LyB was added and the mixture was incubated for 5 min at room temperature. To inactivate Proteinase K, the lysate was placed at 95 ºC for 5 min. Subsequently, remaining debris was removed by centrifugation with 14.000 rpm for 5 min (Hettich Universal 32R, 1653 rotor), and 1 - 2 µl of supernatant were used per PCR reaction.

LyB buffer
50 mM KCl; 10 mM TRIS pH 8.3; 2.5 mM $MgCl_2$; 0.45% NP40; 0.45% Tween 20

2.3.6 Preparation of total RNA form *D. discoideum*

Polyadenylated RNA, which mainly served as template for RT-PCR reactions, was isolated according to the manufacturer's instructions using the "Total RNA isolation spin-kit"

(Applichem, Darmstadt). Total RNA was eluted in DEPC-treated H_2O and was either immediately used for RT-PCR reactions or stored. For storage, 1/10 volume of 2 M potassium acetate pH 5.5 and 2.33 volumes of 100 % ethanol were added. The RNA precipitate was yielded by centrifugation with 14.000 rpm for 15 min (Hettich Universal 32R, 1653 rotor) and stored at -70 ºC.

2.3.7 **Polymerase chain reaction**

PCR reactions serving solely an analytical purpose were performed using Taq polymerase. Typical 25 µl reactions contained 0.2 mM dNTP (each), 25 µm primers (each), 1 U Taq-polymerase, and 2.5 µl of 10 x PCR buffer. Usually, template DNA was denatured at 94 ºC for 2 - 3 min, followed by 30 cycles of denaturation (94 ºC for 30 sec), annealing (45 – 60 ºC for 30 sec) and elongation (72 ºC for 30 – 180 sec). Finally, a last elongation step (72 ºC for 10 min) finished the reactions. For preparative reactions, Phusion high fidelity DNA polymerase (Finnzymes, Espoo, Finland) with the provided buffers "HF" and "GC" was used. Typically, 25 µl reactions contained 0.2 mM dNTP (each), 50 µm primers (each) and 0.6 U of enzyme. Denaturation, annealing and elongation steps were timed as suggested by the supplier's manual, and annealing temperatures were calculated according to (www.finnzymes.fi/tm_determination.html). Plasmid DNA, genomic DNA or cDNA were used as template.

10 x PCR buffer for Taq polymerase
100 mM Tris/HCl, pH 8.3; 500 mM KCl; 15 mM $MgCl_2$; 0.1 % gelatin

2.3.8 **Reverse transcription PCR (RT-PCR)**

RT-PCR reactions using oligo-dT primers on total RNA were performed to generate unspecific cDNA which subsequently served as template for specific PCR reactions used for cloning. RT-PCR was performed using the Protoscript first strand cDNA synthesis kit (NEB, Ipswich, MA, USA) following the supplier's instructions. Reactions were carried out in an Eppendorf Thermomixer comfort (Eppendorf, Hamburg) and 1 µg of total RNA was used per reaction. For successive PCR reactions, 2 µl of cDNA solution were used.

2.3.9 DNA cleavage with restriction endonucleases

Restriction endonucleases were obtained from NEB (Ipswich, MA, USA) or Fermentas (Vilnius, Lithuania). Cleavage reactions were conducted using the temperature, buffer, additives and amount of enzyme as recommended by the respective manufacturer. Usually, digestion reactions lasted 2 - 12 h and their completeness was assessed by agarose gel electrophoresis.

2.3.10 Ligation reactions

Purified DNA fragments and vectors exhibiting compatible sticky ends were obtained by suitable cleavage reactions (2.3.9), separation on an agarose gel (2.3.2) and subsequent purification (2.3.3). Usually twice the amount of insert compared to vector DNA was used for ligation. Insert and vector DNA concentration could be assessed on analytical agarose gels. Ligation reactions were usually carried out using 400 cohesive end units of T4-DNA ligase, (NEB, Ipswich, MA, USA) in a total volume of 20 µl containing the supplied buffer. Reactions were conducted by 6 - 12 h of incubation at 16 ºC.

2.3.11 Selected oligonucletotides used in this study

All oligonucleotides were acquired from biomers.net GmbH (Ulm).

Name (**f**orward / **r**everse)	Sequence (5’ -> 3’)
Bbp1Sal (**f**)	ATATAGTCGACTAATGCCAAGAAGGGCAACAG
Bbp2Bam (**r**)	CGGGATCCTTATCTAAAAACAGCTTCAATTAATTTG
Bbp7Bam (**f**)	CGCGGATCCATGCCAAGAAGGGCAACAG
Bbp8Sal (**r**)	ATATAGTCGACTTATCTAAAAACAGCTTCAATTAATTTG
Bbp9Hind (**f**)	GTGAAGCTTAAAAAATGCCAAGAAGGGCAAC
Bbp10Kpn (**r**)	GCGGGTACCTCTAAAAACAGCTTCAATTAATTTG
Bbp11Sal (**f**)	ATATAGTCGACGTATATTAGTGGGTGGGGTTATT
Bbp12Hind (**r**)	GTGAAGCTTCTGTTGCCCTTCTTGGCAT
Bbp13Pst (**f**)	AAAACTGCAGTGAAAATGAACAAAGATCAAATC
Bbp16KOtest (**r**)	TTATTTTATAATTTTGAAGGGATGATTATACAC
HpB1Sal (**f**)	GCACGCGTCGACTAATGGGAAAAAGAGATAAAAAAAT
HpB2Bam (**r**)	CGCGGATCCTTAACTTGGCTGACCACTATAAC
Mad1-1Sal (**f**)	ATATAGTCGACTAATGAGTCAAGAAGATGATGATA
Mad1-2Bam (**r**)	CGGGATCCTCAAGGATGAAAAGTTTGTTTTG
PM-TACC1 (**f**)	GAAATTGAAGTATTCACTATTAAATTAAATC
PM-TACC2 (**r**)	AATTTAATAGTGAATACTTCAATTTCTTTTTTG
Prp1Sal (**f**)	GCACGCGTCGACTAATGGTCATAGAATCAGAGATAAATG
Prp2Bam (**r**)	GCGGGATCCTTAAAATGGTTTTAAAAATTCGTG
TACC2Bam (**r**)	CGCGGATCCTTTTTGATTAGTTTGTAATTTAAAAAT

TACC3Sal (**f**)	TACGCGTCGACTATCACAAGATGGATTTAATTTACAATC
TACC10Afl3r (**r**)	CCCACATGTTTTGATGTGGTGGTGGATAATAAAATTG
TACC14Kpn (**f**)	GCGGGTACCATGGATAATGAAAAATTAAAAAGATTTC
TACC16Kpn (**f**)	GCGGGTACCTCACAAGATGGATTTAATTTACAATC
TACC17Bam (**r**)	CGCGGATCCTTATTTTTGATTAGTTTGTAATTTAAAAAT
TACC20Sal (**f**)	TACGCGTCGACTAATGGATAATGAAAAATTAAAAAGATTTC
TACC21Bam (**r**)	CGCGGATCCTTATTCTAATGGTGTTTCTTTCTTTGA
TACC22Afl2 (**f**)	CGCCTTAAGTAATGGATAATGAAAAATTAAAAAGATTTC
TACC23Kpn (**r**)	CGCGGTACCTTATTCTAATGGTGTTTCTTTCTTTGA
TACC31Bam (**r**)	CGCGGATCCTTATGAAATTGGTTGATGTTGTTGTG
ZW10-1Sal (**f**)	ATATAGTCGACTAATGGGCATCGATAATAAAAAGATAG
ZW10-2Bam (**r**)	CGGGATCCTTATTGTTTAGATTGTTGTTGAATTTGTTTAT

Additional oligonucleotides provided by other sources

Bsr forw (**f**)	CTCATTCCACTCAAATATACCCGAAATTAA
GFP605 (**f**)	ACCTGTCCACACAATCTGCC
Myc rev (**r**)	CTTCTTCTGATAATAATTTTTGTTCTA

2.3.12 Generation of chemically competent *E. coli* cells

A single colony of an overnight culture of TOP10 cells on LB-plates was transferred to 5 ml of ψb-medium and grown to an OD_{600} = 0.3 at 37 °C. Subsequently this culture served to inoculate 100 ml of pre-warmed ψb-medium, and cells were grown to a density of OD_{600} = 0.5. After incubation on ice for 5 min, the cells were spun down and resuspended in ice cold TfbI buffer. Once more, the suspension was incubated on ice for 5 min and spun down. Cells were resuspended in 4 ml TfbII buffer, incubated on ice for 15 min and shock frozen in liquid nitrogen in 200 µl aliquots.

ψb-medium

20 g/l tryptone; 5 g/l yeast extract; 5 g/l $MgSO_4$ (water free); pH adjusted to 7.6 using KOH

TfbI

30 mM potassium acetate; 100 mM rubidium chloride (RbCl); 10 mM $CaCl_2$; 15 % glycerol; pH adjusted to 6 using 0.2 M acetic acid and supplemented with 50 mM of $MnCl_2$; finally pH was adjusted to 5.8

TfbII

10 mM MOPS; 75 mM $CaCl_2$; 10 mM rubidium chloride (RbCl); 15 % glycerol; pH adjusted to 6.5 using KOH

2.3.13 Heat shock transformation of *E. coli* cells

200 µl of cells were thawed at room temperature and incubated on ice. After 10 min, plasmid DNA was added and the suspension was incubated on ice for another 30 - 45 min. A heat shock was performed for 90 s at 42 °C, followed by incubation on ice for 1 - 2 min. Four volumes of ψb-medium were added and the cells were shaken for 50 - 60 min at 37 °C using a Thermomixer comfort (Eppendorf, Hamburg). Finally, the suspension was plated on LB-plates containing the respective antibiotic for selection.

2.3.14 Transformation of *Dictyostelium discoideum* cells

All steps during transformation were carried out using ice cold buffers and on ice unless stated otherwise. For a single transformation, 3 - 5 x 10^7 *Dictyostelium* cells, which have not exceeded a maximum density of 5 x 10^6 cells/ml at any time during cultivation, were harvested from shaking or adherent culture and washed twice with phosphate buffer. After another washing step with electroporation buffer, the cells were resuspended in electroporation buffer with a final density of 1 x 10^8 cells/ml. The suspension was transferred to a sterile electroporation cuvette (4 mm distance between the electrodes) (Peqlab, Erlangen) and 15 - 30 µg of plasmid DNA were added. The suspension was gently mixed and the electroporation was carried out by two pulses of 1.1 kV with 3 µF in a gene pulser electroporation device (Biorad, Hercules, CA, USA). After electroporation, the suspension was left at room temperature for 10 min. Subsequently, the cells were transferred to a 1.5 ml sterile tube, 1 mM $MgCl_2$ and $CaCl_2$ each (final concentration) were added and the suspension was gently agitated on a rotator for another 15 min at room temperature. If blasticidin S was used for selection, the cells were transferred to a 24 well plate in 25 ml of HL5c medium. To prevent contamination with bacteria, penicillin/streptomycin was usually added. After 24 h of recovery time, 4 µg/ml blasticidin S (final concentration) was added. First colonies of resistant cells were usually observed after 1 - 2 weeks of cultivation.

In case of G418 resistance being used for selection, the cells were transferred to a tissue flask for recovery instead. 24 h after electroporation, the cells were harvested, washed with phosphate buffer twice and resuspended in 2.5 ml of a dense solution of *Klebsiella aerogenes* supplemented with 10 µg/ml of G418. For this, the bacteria needed to be freshly grown on SM agar plates at 37 ºC over night. One SM plate densely grown with *Klebsiella* yielded 5 ml of suspension. 500 µl of suspension containing *Dictyostelium* and *Klebsiella* cells were plated on phosphate agar plates supplemented with 100 µg/ml of G418. First feeding plaques could usually be observed after 1 - 2 weeks of cultivation. Resistant cells from the edge of feeding

plaques were transferred to liquid medium containing 10 µg/ml of G418 using a sterile pipette tip.

The cloning of transformants was achieved by plating corresponding cells on SM agar plates together with a dense suspension of *Klebsiella*. After 2 - 3 days of cultivation, cells from single feeding plaques were transferred to liquid medium containing penicillin/streptomycin and the respective antibiotic for selection.

Electroporation buffer

50 mM sucrose; 10 mM KH_2PO_4; pH 6.1

2.3.15 Generation plasmids and corresponding *Dictyostelium* strains

Except otherwise stated all coding sequences were amplified in a single PCR reaction using cDNA (section 2.3.8) or plasmid DNA as template. PCR products were purified (section 2.3.3), digested with restriction endonucleases (section 2.3.9) as indicated below, purified again and ligated into the respective vector. The fidelity of sequences was validated by sequencing (GATC Biotech, Konstanz). Primers and vectors used for each construct are listed in Tab. 1. Primer sequences are listed in section 2.3.11.

For the generation of the mRFP-tubulin vector, the GFP coding sequence was excised from pIS76 and replaced by an mRFP coding sequence obtained by PCR on an mRFP vector (Müller-Taubenberger *et al*., 2006) using HindIII and SalI linker primers. Subsequently, the α-tubulin sequence derived from a published GFP-tubulin vector (Rehberg and Gräf, 2002), was cloned into the poly-linker of the modified, mRFP-containing pIS 76 using SalI and BamHI restriction sites. The mRFP-tubulin plasmid was kindly provided by Dr. Irene Meyer.

Constructs for N-terminal fusion of GFP

PCR products flanked by SalI and BamHI restriction sites were generated and ligated into likewise digested pIS76 or pIS77 vector (Schulz *et al*., 2009b).

Constructs for C-terminal fusion of GFP

PCR products flanked by KpnI and BamHI restriction sites were generated and ligated into likewise digested p1ABsr8 vector (Gräf *et al*., 2000a). In case of Cenp68-GFP, HindIII and BamHI restriction sites were used instead.

Cloning of GFP-TACCΔC

GFP-TACCΔC was generated as generally described for the N-terminal fusion of GFP. The GFP-TACCΔC construct comprises base positions 1 - 3609 of the TACC coding sequence, corresponding to amino acids 1 - 1203.

Cloning of full length TACC

Since amplification of the entire TACC coding sequence (4437 bp) by PCR repeatedly failed, the cloning of full length TACC was carried out in two steps. First a 5' amplicon comprising base positions 1 - 3892 flanked by a SalI and an internal AflIII restriction site was generated using TACC20Sal and TACC10Afl3r primers. Then, a 3' fragment comprising base positions 3887 - 4437 was obtained by digestion of the GFP-TACCdom vector (pkk14) (Koch *et al*., 2006) with AflIII/BamHI followed by separation on an agarose gel. A ligation reaction containing the two TACC fragments in equimolar amounts and a SalI/BamHI digested pIS76 vector then yielded full length TACC in pIS76. Accurate amplification of the resulting plasmid in *E. coli* only worked when TB-medium was used for cultivation.

Cloning GFP-TACCdom

GFP-TACCdom vectors and *Dictyostelium* strains (pkk14 and pkk15) were provided by Dr. Katrin Pfütze. Both comprise base positions 3610 to 4437 of the TACC coding sequence.

Cloning of the GFP-TACCdomL1441F construct

Leucine 1441 of the TACC coding sequence was mutated to phenylalanine by a PCR approach using the GFP-TACCdom plasmid (pkk14) (Koch *et al*., 2006) as template. First, two PCR reactions were carried out that each contained a forward or reverse primer (PM-TACC1 and PM-TACC2), respectively, in which the wild type triplet -CTA-, coding for leucine, was changed to -TTC-, coding for phenylalanine. The second primers used for these reactions matched the ones used for the generation of the GFP-TACCdom construct (TACC3Sal and TACC17Bam). These PCRs yielded two amplicons, which exhibited an overlap corresponding to base positions 4309 - 4334 of the TACC coding sequence, both containing the L1441F mutation. This overlap served as priming site to complete the respective second strand during the first cycle of a successive PCR reaction containing the two PCR products but no additional primers. After the first cycle, terminal primers (TACC3Sal and TACC17Bam) were added to the reaction to start the amplification. The

yielded PCR product was digested with SalI/BamHI and ligated into a likewise cleaved pIS76 vector (Schulz *et al*., 2009b). Successful mutation of the triplet was confirmed by sequencing.

TACC-RNAi construct

The pIS193 vector, which was used to generate the RNAi construct, was obtained by substituting the GFP coding sequence by mCherry in pIS77 (Schulz *et al*., 2009b) using NheI and SalI restriction sites. The mCherry sequence was excised from a previously published mCherry-LimEΔ vector (Bretschneider *et al*., 2009). The pIS193 plasmid was kindly provided by Dr. Irene Meyer. The TACC-RNAi construct was designed according to (Martens *et al*., 2002). The transcribed RNA consists of a long inverted repeat consisting of 543 bp of the TACC coding sequence (base positions 1–543) and a stuffer fragment between the two complementary parts. Both complementary TACC fragments were amplified by PCR using linker primers. The sense fragment was flanked by SalI and BamHI sites and was cloned into the polylinker downstream of the mCherry sequence. The preceding antisense fragment was flanked by AflII and KpnI sites and replaced the first part of the mCherry sequence leaving a 196 bp stuffer fragment consisting of the remaining mCherry sequence and restriction sites.

Cenp68 KO construct

The generation of a Cenp68 knockout strain was achieved by partially replacing the chromosomal wild type Cenp68 locus by a blasticidin resistance cassette in a homologous recombination event. A schematic can be seen in Fig. 28. The Cenp68 knockout construct was generated using the pLPBLP vector (Faix *et al*., 2004). Both complementary sequences were obtained by PCR reactions using linker primers and genomic *Dictyostelium* DNA as template. The 5' fragment consisting of 941bp of the Cenp68 5' UTR was ligated into pLPBLP via HindIII and SalI restriction sites upstream to the blasticidin resistance cassette. This fragment also comprised the very first 19 bp of the Cenp68 coding sequence. Subsequently, the last 958 bp of the Cenp68 coding sequence (including introns) were inserted downstream of the blasticidin resistance cassette via PstI/BamHI restriction sites. The knockout construct was digested with PvuII and was purified prior to transformation of *Dictyostelium*.
The screening PCRs to identify knockout strains were conducted as seen in Fig. 28. Primers depicted in Fig. 28 correspond to Bsr forw (1), Bbp16KOtest (2) and Bbp1Sal (3).

MBP-Cenp68 construct

For the expression of an MBP-Cenp68 fusion protein in KS1000 *E. coli* cells, a PCR amplicon comprising the full length Cenp68 coding sequence flanked by BamHI and SalI restriction sites was generated. The fragment was purified, cleaved with SalI/BamHI and ligated in likewise digested pMALc2 vector (New England Biolabs, Ipswich, MA, USA).

Selected constructs and strains generated for this study are listed in Tab. 1.

Tab. 1 Selected plasmids and *Dictyostelium* strains generated for and used in this study.

Construct	Lab code	Target vector	Restriction sites used	Primers used	Existing *Dict.* mutant	Double mutant with
GFP-TACCΔC	#38-3	pIS76	SalI BamHI	TACC20Sal TACC31Bam	yes	-
TACC-GFP	#9-1	p1ABsr8	KpnI BamHI	TACC14Kpn TACC10Afl3r	yes	-
GFP-TACC	#17-10	pIS76	SalI BamHI	TACC20Sal TACC10Afl3r	yes	-
GFP-TACCdom	pkk15	pIS77	SalI BamHI	-	yes	mRFP-tubulin
TACC-RNAi intermediate	#13-1	pIS193	SalI BamHI	TACC20Sal TACC21Bam	no	-
TACC-RNAi	#16-5	#13-1	AflII KpnI	TACC22Afl2 TACC23Kpn	yes	-GFP-CP224 -GFP-tubulin
GFP-TACCdom-L1441F	#65-24	pIS76	SalI BamHI	PM-TACC1 PM-TACC2 TACC3Sal TACC17Bam	yes	TACC-RNAi
GFP-Cenp68	#14c-1	pIS76	SalI BamHI	Bbp1Sal Bbp2Bam	yes	-
GFP-Cenp68	#41-1	pIS77	SalI BamHI	Bbp1Sal Bbp2Bam	yes	mCherry-histone2B
Cenp68-GFP	#42-11	p1ABsr8	HindIII BamHI	Bbp9Hind Bbp10Kpn	yes	-
MBP-Cenp68	#20-3 #28-1	pMALc2	BamHI SalI	Bbp7Bam Bbp8Sal	no	-
Cenp68-KO intermediate	#43-9	pLPBLP	HindIII SalI	Bbp11Sal Bbp12Hind	no	-
Cenp68-KO	#44-24	#43-9	PstI BamHI	Bbp13Pst Bbp2Bam	yes	-GFP-Mad1 -GFP-HcpB
GFP-Mad1	#46-1	pIS76	SalI BamHI	Mad1-1Sal Mad1-2Bam	yes	-
GFP-Mad1	#49-1	pIS77	SalI BamHI	Mad1-1Sal Mad1-2Bam	yes	-Cenp68-KO -mCherry-histone2B
GFP-CP103	#48-21	pIS76	SalI BamHI	ZW10-1Sal ZW10-2Bam	yes	-
GFP-CP103	#50-1	pIS77	SalI BamHI	ZW10-1Sal ZW10-2Bam	yes	mRFP-tubulin
GFP-Prpf4B	#52-2	pIS76	SalI BamHI	Prp1Sal Prp2Bam	yes	-
GFP-HcpB	#54-13	pIS77	SalI BamHI	HpB1Sal HpB2Bam	yes	Cenp68-KO

2.4 Biochemical methods

2.4.1 Determination of protein concentration using the amido black assay

BSA samples, which were used to generate of a reference curve (e. g. 4 µg, 6 µg, 8 µg 12 µg of BSA), and protein samples were mixed with 300 µl of staining solution and were incubated for 5 min at room temperature. The precipitate was spun down at maximum speed in a desktop centrifuge, washed twice with wash solution and was resuspended in 700 µl of 0.1 M sodium hydroxide. All samples were measured at 615 nm in a Pharmacia Novaspec II photometer (GE Healthcare, Uppsala, Sweden) and the protein concentration was determined by comparison with the reference curve. Usually at least three assays of each sample were run in parallel and the mean value was used for calculations.

Wash solution
acetic acid/methanol 1:10

Staining solution
2.6 mg/ml amido black in wash solution

2.4.2 SDS-polyacrylamide gel electrophoresis (SDS-PAGE) (Laemmli, 1970)

Protein samples and molecular weight standards (Sigma, St. Louis, MO, USA) were prepared for SDS-PAGE either by adding 1/5 volume of 6 x Laemmli buffer, followed by incubation at 95 ºC for 5 min, or, alternatively, by supplementation with an equal amount of urea sample buffer, followed by incubation at 70 ºC for 120 sec. Proteins were separated using the Biorad mini system (Biorad, Hercules, CA, USA) on discontinuous gels containing 6 % or 12.5 % of polyacryamide (Tab. 2). Gels were run in SDS running buffer at a current of 15 mA for the first 15 - 20 min, followed by 30 mA for 45 - 60 min.

Separation-gel buffer
2 M Tris/HCl, pH 8.7; 0.4 % SDS

Stacking-gel buffer
0.25 M Tris/HCl, pH 6.8; 0.4 % SDS

Tab. 2 Composition of polyacrylamide gels used in this study

Stock solution	Stacking-gel for 12.5 % gels	12,5 % separation-gel	Stacking-gel for 6 % gels	6 % separation-gel
30 % acrylamide	341 µl	1.85 ml	-	-
30 % acrylamide/ 0.8 % PDA	-	-	330µl	1 ml
1 % bisacrylamide	250 µl	465 µl	-	-
Separation-gel buffer	-	1.25 ml	-	1.25 ml
Stacking-gel buffer	500 µl	-	500 µl	-
ddH_2O	889 µl	900 µl	1.2 ml	2.75 ml
10 % APS	17.5 µl	22.5 µl	15 µl	25 µl
Temed	3.5 µl	4.5 µl	2.5 µl	2.5 µl

2.4.3 Coomassie R250 staining of SDS gels

SDS gels were incubated for 1 - 2 h in Coomassie staining solution, rinsed with water and subsequently destained. Gels were scanned using a HP Scanjet 4890.

Coomassie R250 staining solution

0.25 % Coomassie R250 (Sigma-Aldrich); 50 % methanol; 10 % acetic acid

Destaining solution

25 % isopropyl alcohol; 10% acetic acid

2.4.4 Colloidal Coomassie staining of SDS gels

The colloidal coomassie staining is ~10 times more sensitive than the conventional Coomassie staining. It served to stain gels which were loaded with samples obtained from nanotrap protein interaction assays. The staining procedure was carried out using the Roti-Blue staining kit (Carl Roth, Karlsruhe).

2.4.5 Silver staining of SDS gels

Gels were gently agitated throughout the staining process. The gels were incubated in fixing solution for a minimum of 30 min and subsequently transferred to sensitizing solution for another 30 min. After washing three washing steps with ddH_2O (5 min each), the gels were stained in silver solution for 20 min. After thoroughly rinsing with ddH_2O, the gels were exposed to developing solution until the desired grade of staining intensity was reached. The reaction was stopped by addition of 0.04 M EDTA.

Fixing solution
40 % ethanol; 10 % acetic acid

Sensitizing solution
30 % ethanol; 0.2 % sodium thiosulfate; 68 g/l sodium acetate; 0.125 % glutaraldehyde (freshly added)

Silver solution
0.25 % silver nitrate; 0.015 % formaldehyde (freshly added)

Developing solution
25 g/l sodium carbonate; 0.0075 % formaldehyde (freshly added)

2.4.6 Western blotting and immunostaining

Following SDS-PAGE, proteins were blotted to a nitrocellulose membrane using a semi-dry blotting device (Peqlab, Erlangen). Blotting was essentially conducted according to (Kyhse-Anderson, 1984) using modified buffers (see below). After the proteins were transferred to the membrane by applying 1 mA/cm^2, the blot was stained in Ponceau S solution and the molecular weight standard bands were labeled. Subsequently, the blotting membrane was blocked by incubation with 5 % skim milk powder in TBST for 1 h to over night. Binding of the primary antibodies was conducted in 1.6 % skim milk powder in TBST for 1 h, followed by three washing steps using TBST. The secondary antibodies conjugated with horseradish peroxidase (see 2.1.2) were diluted 1:10.000 and applied the same way as primary antibodies. After washing two times in TBST and one time in TBS for 5 min each, detection was accomplished using ECL. To do this, the blot was transferred to an X-ray film holding device (Kisker, Steinfurt), and X-ray film (Fuji Super RX, Fujifilm, Tokyo) was applied in a darkroom. After 1 - 30 min of exposure, the X-ray film was incubated in developer (T32, Calbe Chemie, Calbe), rinsed with water and fixed in fixing solution (Superfix, Tetanal, Norderstedt).

Alternatively, western blots could also be treated with secondary antibodies conjugated with alkaline phosphatase (see 2.1.2). In this case, skim milk powder was substituted by fish gelatin (5 % in TBST, Sigma-Aldrich), and the detection was conducted in alkaline phosphatase reaction buffer supplemented with 4.5 µl/ml NBT and 3.5 µl/ml BCIP. After the

desired staining intensity was reached, the reaction was stopped by thorough rinsing with water.

Blotting buffer 1
300 mM Tris; 20 % methanol

Blotting buffer 2
30 mM Tris; 20 % methanol

Blotting buffer 3
30 mM Tris; 20 % methanol; 40 mM ε-aminocaproic acid

Ponceau S solution
0.1 % Ponceau S; 5 % acetic acid

Alkaline phosphatase reaction buffer
100 mM Tris/Cl; 100 mM NaCl; 50 mM $MgCl_2$; pH 9.5

2.4.7 Purification of MBP fusion protein

MBP-fusion proteins were expressed in KS1000 *E. coli* cells. For this, 1 l LB-medium containing ampicilin for selection and 10 mM glucose was inoculated with an overnight culture of transformed KS1000 cells and grown to an OD_{600} of 1.0 at 37 ºC. After induction by adding 0.3 M IPTG, MBP fusion protein expression was carried out at room temperature for 2 - 6 h. Cells were harvested at 4000 rpm (Hettich Rotanta 460R, 5645 rotor) and the pellets were resuspended in TE buffer. After the suspensions were pooled in a total volume of ~10 ml, the cells were frozen at -20 ºC. To prevent protein degradation, all following steps were conducted on ice and/or with ice cold buffers. After thawing, the cell suspension was sonicated for 1 min in a UP50H sonicator (Dr. Hielscher GmbH, Teltow) set to maximum. The insoluble fraction was pelleted by centrifugation at 21.000 rpm for 20 min (Beckman Avanti JE centrifuge, JA-25.50 rotor, 4 ºC). The supernatant was supplemented with NaCl (100 mM final concentration) and was carefully loaded onto a column containing 2 ml of amylose resin (NEB, Ipswich, MA, USA). The flow rate was adjusted to approximately one droplet per 10 s. The amylose resin was washed with 10 ml column buffer three times and the MBP protein was eluted by carefully applying column buffer containing 10 mM of maltose.

Alternatively, when MBP fusion protein was purified in order to be used to affinity purify antibodies, the column buffer was substituted by NHS coupling buffer. The eluate was collected in fractions of ~500 µl, whose protein concentration was assessed by measuring OD_{280}. In such measurements, a value of 1 corresponds to approximately to 0.7 mg protein per ml. To test for degradation, the integrity of fusion proteins was analyzed by SDS-PAGE.

Column buffer
200 mM NaCl; 10 mM Tris/HCl, pH 7.5; 1 mM EDTA

NHS coupling buffer
0.2 M $NaHCO_3$; 0.5 M NaCl; pH 8.3

2.4.8 Immunization of rabbits

Approximately 1 mg of MBP-Cenp68 fusion protein was generated as described in section 2.4.7 and concentrated to a final concentration of ~1 mg/ml using Centricon YM-50 devices (Millipore, Billerica, MA, USA). Immunizations of two rabbits were carried out by Biogenes GmbH (Berlin) using a standard immunization protocol comprising 4 - 5 immunizations each. Sera were received after 30 and 60 days, respectively, and tested for specificity in immunoblotting and immunofluorescence experiments. The serum producing the most promising results (day 60, rabbit No. 48) was chosen to be affinity purified (see 2.4.9).

2.4.9 Affinity purification of antibodies

Approximately 0.5 mg of MBP fusion protein (MBP-Cenp68) directly eluted in NHS coupling buffer was concentrated to a final volume of 1 ml using Centricon YM-50 devices (Millipore, Billerica, MA, USA). 1 ml of NHS activated sepharose (GE Healthcare, Uppsala), which has previously been washed with 1 mM ice cold HCl, was supplemented with the MBP fusion protein and agitated over night at room temperature. For coupling, the sepharose beads were alternatingly incubated with 5 ml of buffer A and buffer B, starting with buffer A. Incubation times for buffer A were 15 min followed by 1 h twice, while buffer B was only applied for washing. The flow through was discarded and the sephasose column was stored at 4 ºC in TBS containing 0.1 % NaN_3. Prior to usage, the column was washed with TBS three times. For antibody purification, the sera were diluted in TBS in a 1:10 ratio and loaded onto the column. The flow rate was adjusted to one droplet per 10 s. After washing with TBS three times, the specific antibodies were eluted by adding 100 mM glycine pH 2.7. Fractions of

~500 µl were collected and immediately neutralized with 1 M Tris/Cl pH 9.5. The yielded antibody fractions were tested in immunoblotting experiments and their concentration was assessed as described in (2.4.7).

Buffer A
1M Tris/Cl; 0.5 M NaCl; pH 8.5

Buffer B
0.1 M sodium acetate; 0.5 M NaCl; pH 4.0

2.4.10 Shortened protocol for the isolation of *Dictyostelium* centrosomes

To prevent protein degradation the purification process was carried out on ice, using ice cold buffers and cooled centrifuges/rotors. The yielded centrosomes served as sample for SDS-PAGE or in immunofluorescence experiments. The isolation was conducted following a modified protocol derived from Gräf *et al*. (1998). Approximately 1 x 10^9 cells with a maximum density of 4 x 10^6 cells/ml were harvested and washed with 30 ml phosphate buffer twice. A third washing step was conducted with 30 ml phosphate buffer containing 2 µM Cytochalasin A. Cells were resuspended in 10 ml lysis buffer and subjected to vortexing with maximum intensity (Vortex Genie 2) for 1 min. The lysate was pushed through a 5 µm nucleopore filter (Whatman, Maidstone, UK) and was centrifuged at 4000 rpm (Hettich Rotanta, 5624 rotor) for 10 min to spin down nuclei and associated centrosomes. The supernatant was discarded and the pellet was resuspended in 10 ml pyrophosphate buffer, vortexed for 1 min as described above and centrifuged at 4000 rpm again. The supernatant was supplemented with 2 mg heparin and incubated for 5 min on ice. The yielded solution, containing 30 % sucrose itself, was carefully loaded onto a sucrose gradient. The latter consisted of 1 ml of 80 % and 1 ml of 50 % sucrose solution and was prepared in Beckman SW-40 tubes. The gradient was centrifuged for 1 h at 40.000 g (21.000 rpm, Beckman Optima L-100K ultracentrifuge, SW-40 rotor) and was immediately placed on ice afterwards. Using a peristaltic pump and glass capillaries (flow rate ~200 µl per min), ~500 µl of the 80 % sucrose fraction were removed from the bottom of the SW-40 tube and discarded. Then, again from the bottom of the tube, 1 ml of sucrose solution was collected which contained the centrosome enriched border of the 80 % and 50 % sucrose solutions. For immunofluorescence experiments 10 - 30 µl of the centrosome fraction were diluted in 1 ml ice cold phosphate buffer and sedimented onto cover slips by centrifugation at 4.500 rpm (Hettich Rotanta, 5624

rotor). Fixation and immunolabeling of isolated centrosomes was conducted as described for whole cells (see 2.5.1). Importantly, throughout the entire isolation process, no DTT or equivalent reducing agents were used when GFP fluorescence of isolated centrosomes should be analyzed. For SDS-PAGE, the centrosomal fraction was supplemented with 1/5 volume of 6 x Laemmli buffer and incubated at 95 ˚C for 5 min.

1 x protease inhibitor cocktail
1 mM Pefabloc SC; 25 µg/ml leupeptin; 10 µg/ml tosyl-arginin-methylester;
10 µg/ml soybean trypsin inhibitor; 1 µg/ml aprotinine; 1 µg/ml pepstatine;
2 mM benzamidine; 1 mM Na-ATP

Lysis buffer
100 mM Na-PIPES, pH 6.9; 2 mM $MgCl_2$; 10 % (w/v) sucrose;
freshly added: 1 × protease inhibitor cocktail; 0.25 % Triton X-100; 1 mM DTT;
2 µM Cytochalasin A

Pyrophosphate buffer
100 mM Na-PIPES, pH 6.9; 2 mM $MgCl_2$; 30 % (w/v) sucrose;
freshly added: 1 x protease inhibitor cocktail; 40 mM tetra-sodium pyrophosphate;
1 % Triton X-100; 1 mM DTT; 2 µM Cytochalasin A

Sucrose solutions used for sucrose gradients
10 mM Na-PIPES, pH 6.9; 2 mM $MgCl_2$; sucrose (50 % or 80 %);
freshly added: 1 x protease inhibitor cocktail; 0.1 % Triton X-100; 2 mM DTT

2.4.11 Co-immunoprecipitation

All steps were conducted using ice cold buffers and cooled centrifuges. 1 x 10^8 cells were harvested and washed with phosphate buffer twice. The pellet was resuspended in 10 volumes of Co-IP buffer and firmly pushed through a 5 µm nucleopore filter (Whatman, Maidstone, UK) three times to achieve lysis. Cell debris was spun down at 14.000 rpm for 15 min (Hettich Universal 32R, 1653 rotor) and the supernatant was supplemented with 0.3 % NP40 (final concentration). 10 µg of purified polyclonal GFP antibody (Faix *et al*., 2001) or 2 µl of random pre-immune serum, respectively, were added to 600 µl of cytosolic extract and rotated for 1 h at 4 ºC. Afterwards, 20 µl of protein G beads (GE Healthcare, Uppsala,

Sweden), which have previously been blocked in 0.1 % BSA solution over night, were added and the suspension was rotated for another hour at 4 ºC. Protein G beads were washed thoroughly four times with Co-IP buffer and samples of the last washing step were collected for analysis by immunoblotting. Proteins and antibodies were eluted by addition of 50 µl of Co-IP sample buffer.

Co-IP buffer
1 x protease inhibitor cocktail; 50 mM Hepes; 100 mM NaCl; 4 mM EGTA; 2 mM $MgCl_2$;
10 % sucrose

Co-IP sample buffer
10 % SDS; 125 mM Tris/Cl, pH 6.8; 100 mM DTT, 5 % glycerol

2.4.12 The GFP nanotrap assay

The GFP nanotrap protocol was used to screen for interaction partners of various bait proteins. The assay is based on immunoprecipitation of GFP-bait fusion proteins from cellular extracts using a bead-coupled highly specific single chain GFP antibody from llamas. The assay was performed following a modified protocol derived from Rothbauer *et al*. (2008).
All steps were performed on ice using ice cold buffers and cooled centrifuges. 4 x 10^7 cells of a density no higher than 2 x 10^6 cells/ml were harvested and washed in phosphate buffer, followed by another washing step with phosphate buffer containing 2 µM Cytochalasin A. Cells were lysed by addition of 250 µl RIPA buffer and by vigorously pipetting up and down. Remaining cell debris was spun down and the supernatant was transferred to a precooled new tube. The volume was adjusted to 500 µl by addition of supplemented dilution buffer (see below). 15 - 20 µl of GFP binder sepharose (Chromotek, Planegg-Martinsried) previously equilibrated in supplemented dilution buffer were added to the cell extract and the suspension was rotated for 30 - 120 min at 4 ºC. The sepharose was collected and washed with 500 µl of dilution buffer twice. Proteins were eluted by addition of 50 µl urea sample buffer and incubation at 70 ºC for 2 min.
The assay was carried out in different ways depending on the protein used as bait. For instance, DNAse and $MgCl_2$ was added when nuclear proteins were purified, and for cytoplasmic proteins lysis buffer was used instead of RIPA buffer to avoid unnecessary, high concentrations of detergent. Furthermore, incubation times and temperatures during the binding step strongly varied depending on the susceptibility of the bait protein to degradation.

Samples obtained from nanotrap assays were subjected to SDS-PAGE, stained with colloidal Coomassie and candidate bands were excised using sterile scalpels. MALDI-TOF mass spectrometric analysis was performed by Dr. Jörg Fettke (Universität Potsdam).

Dilution buffer
10 mM Tris/Cl, pH 7.5; 150 mM NaCl; 0.5 mM EDTA

Supplemented dilution buffer
1 x protease inhibitor cocktail; 10 mM Tris/Cl, pH 7.5; 150 mM NaCl; 0.5 mM EDTA;
2 µM Cytochalasin A

RIPA buffer
1 x protease inhibitor cocktail; 10 mM Tris/Cl, pH 7.5; 150 mM NaCl; 0.1 % SDS;
1 % Triton X-100; 1 % deoxycholic acid; 5 mM EDTA; 2 µM Cytochalasin A;
5 µg/µl DNAse I; 5 mM $MgCl_2$

Lysis buffer
1 x protease inhibitor cocktail; 10 mM Tris/Cl, pH 7.5; 150 mM NaCl; 0.5 mM EDTA;
0.5 % NP40; 2 µM Cytochalasin A

2.5 Cell biological methods

2.5.1 Fixation and indirect immunofluorescence of *Dictyostelium* cells

Cells were harvested from adherent of shaking culture and diluted with phosphate buffer or HL5c medium to a density of 1 - 5 x 10^5 cells/ml. The suspension was transferred to a cover slip and cells were allowed to settle for at least 15 min. After removal of the liquid, cells were fixed with the respective fixation method (see below). Optionally, phosphate buffer containing agents such as TBZ or nocodazol was applied up to several hours prior to fixation.

Methanol fixation
100 % methanol (-20 °C) was applied and the cells were incubated at -20 °C for 2 - 3 min. Cells were washed with PBS twice and subjected to immunostaining.

Glutaraldehyde fixation

50 % PHEM buffer freshly supplemented with 0.5 % glutaraldehyde and 0.5 % Triton X-100 was applied for 5 min at room temperature. Cells were washed with phosphate buffer twice (5 min each) and 1 mg/ml of freshly solved borohydrate (in phosphate buffer) was applied for at least 10 min to quench unreacted glutaraldehyde. Cells were washed with PBS and subjected to immunostaining.

Formaldehyde fixation

PBS was supplemented with 3.7 % formaldehyde (final concentration) and applied to the cells for 5 min at room temperature. Cells were washed with acetone (-20 °C) for 1 min, washed with PBS twice and subjected to immunostaining.

The fixed samples were transferred to a moist chamber and immunostaining was conducted by incubation with one or two primary antibodies in antibody dilution buffer for 1 h at room temperature. The degree of dilution varied depending on the antibodies used. After washing with PBS three times (5 min each) to remove unbound antibodies, the secondary antibodies were applied for 1 h at room temperature in 1:1000 dilutions. Primary and secondary antibodies used for this study are listed in section 2.1.2. Subsequently, DNA was stained by addition of 1 mg/ml DAPI for 20 - 30 min. The fixed samples were washed with PBS three times (5 min each) and were embedded on a microscope slide using small droplets of Mowiol mountant.

100% PHEM buffer (Schliwa and van Blerkom, 1981)

60 mM PIPES; 25 mM HEPES; 10 mM EGTA; 2 mM $MgCl_2$; pH 6.9

2.5.2 Wide field microscopy

Immunofluorescence microscopy preparations were analyzed using a Zeiss Axiovert 200M CellObserver HS system (Carl Zeiss MicroImaging GmbH, Jena). A Sutter DG-4 (Sutter instruments, Novato, CA, USA) served as light source and the system was equipped with an ASI piezo stage (Applied Scientific Instruments, Eugene, OR, USA) and a Zeiss Axiocam MRm Rev. 3 CCD camera. Fixed cell applications were performed using Zeiss 100x/1.4 PlanApo, 63x/1.3 LCI Plan-Neofluar or 40x/1.3 Plan-Neofluar lenses, while live cell imaging was exclusively conducted with the 63x /1.3 LCI Plan-Neofluar lens. All image stacks derived from immunofluorescence preparations (with an optimal focus step size ranging from

0.175 µm to 0.275 µm, depending on the objective used) were deconvolved using a fast iterative method and maximum intensity projections were calculated for presentation.
Live cell imaging was essentially conducted as described in Samereier *et al*. (2010). In brief, usually five images per stack with a focus step size of 0.5 - 0.8 µm were taken and the inverse filter method was chosen for deconvolution. Cells with a density of 2 - 3 x 10^5 were allowed to settle on Fluorodishes (World Precision Instruments, Sarasota, FL, USA) for at least 15 min. After removal of the medium, LoFlo medium (Formedium, Hunstanton, UK) freshly supplemented with 2 mg/ml ascorbic acid (final concentration) was applied for 2 - 12 h prior to live cell imaging. Optionally, agar overlays according to Fukui *et al*. (1987b) were used to flatten cells, thereby reducing the movements of organelles and other intracellular structures in axial direction. All software applications were performed with Axiovision 4.7 (Carl Zeiss, MicroImaging GmbH, Jena) and Image J v.1.42l (http://www.macbiophotonics.ca/imagej/).

2.5.3 Evaluation of CP224 antibody fluorescence intensity in fixed cell preparations

To evaluate fluorescence intensity of CP224 antibody signals at the centrosomes of GFP-NE81 cells (control cells) and TACC-RNAi cells, both strains were mixed and fixed together, thereby avoiding differential labeling and fixation conditions. In total, thirteen images were taken using the 40x/1.3 Plan-Neofluar lens and maximum intensity projections were calculated. Imaging settings were identical for all thirteen images. The mean intensity of CP224 antibody signals of individual centrosomes was evaluated using Image J. To do this, an area of 5 x 5 pixels comprising the brightest pixels of a single centrosome was manually chosen and the mean intensity was measured. This was carried out for centrosomes of n = 485 GFP-NE81 cells and n = 304 TACC knockdown cells. Subsequently, for each of the thirteen images, the highest value was set to 1 and the relative signal intensity of all other centrosomes of the corresponding image was calculated ("normalizing"). This allowed for the comparison of signal intensities between the thirteen images. Finally, relative intensity values of the respective cell line were combined.

2.5.4 Confocal microscopy

Live cell imaging and specimen preparation was essentially performed as described in section 2.5.2 and Samereier *et al*. (2010). In brief, confocal live cell microscopy was conducted using a Zeiss LSM710 laser scanning confocal microscope employing a Zeiss PlanApo 1.4/63x lens and a piezo focusing unit. Image stacks for confocal live cell imaging usually consisted of

5 frames with a focus step size of 0.5 - 0.8 µm. For most applications, scan speed was set to almost maximum. Optionally, scan speed was doubled by using a line step value of two, where only every second line is scanned and missing lines are interpolated. Depending on the application, frame rates ranged from ~200 - 600 msec. Pinhole size was set to a value of 1 airy unit. To minimize bleaching and phototoxic effects, excitation intensity was set no higher than necessary. Typically, for imaging, AOTF (acousto optical tunable filters) transmission was set to 1 % at a laser intensity of 30 % together with a high digital gain and 450 - 550 V of detector gain. If stacks were deconvolved, Huygens essential software (SVI, Hilversum, Netherlands) was used. For imaging, Carl Zeiss ZEN 2009 software was used.

2.5.5 Fluorescence recovery after photobleaching experiments (FRAP)

All FRAP applications were performed using GFP as fluorescent protein. Imaging during FRAP experiments was carried out essentially as described in section 2.5.4. For most applications, increasing the laser intensity to above 30 % was not necessary for complete bleaching. Bleaching of box shaped, manually selected ROIs was conducted with 100 % AOTF transmission and 10 - 30 iterations, when using the same fast scan speed as for acquisition. All time series used for FRAP evaluation were taken in a way that they contained the ROI itself along with a reference ROI from another cell and background information, both needed to correct for acquisition bleaching. A schematic of information needed for evaluation is shown in Fig. 17. Importantly, the ROI and fluorescent reference structures must not laterally or axially exit the imaged area at any time during acquisition. If FRAP experiments should be compared, identical time intervals are required. For evaluation of FRAP data, maximum intensity projections were calculated using Image J. For each time point the mean fluorescence intensity within the ROI, the reference ROI (CO) and the background (BG) was determined. This was conducted by manually selecting an area of 4 x 4 pixels comprising the highest intensity values of single centrosomes or metaphase spindle poles. Since during experiments conducted for this study, background intensity was set to zero using the offset control when setting up experiments, background measurements were not carried out. As an approximation, the bleaching process during the relevant time period was considered linear. The slope of the regression line derived from the CO values (m_{ab}) can therefore be used to calculate the corrected ROI intensity values for each time point. It has to be mentioned that (m_{ab}) should have a negative value. The correction for acquisition bleaching was performed according to:

$$\frac{\mathrm{ROI}\,(t) - \mathrm{BG}}{\mathrm{ROI}\,(t = 0) - \mathrm{BG}}\ \mathrm{x}\ (1 - t\ \mathrm{x}\ m_{\mathrm{ab}}) = \mathrm{FRAP}\ (\mathrm{normalized, corrected})$$

Corrected and normalized values of corresponding experiments were combined and the standard deviation was calculated. Image J was used to measure mean intensity values, all other calculations were performed using Microsoft Excel 2007.

2.5.6 Determination of microtubule lengths from fixed cell preparations

Cells were fixed with glutaraldehyde and labeled with anti-tubulin. Evaluation of microtubule lengths was conducted using maximum intensity projection images. Cells of approximately equal size of the respective cell line were chosen randomly and microtubule length was assessed using Image J v.1.42l. To do this, microtubules were manually tracked from the very plus end to the centrosome. Especially in the proximity of centrosomes this task was frequently hampered by very high microtubule density. Therefore, in some cases, other cells had to be chosen or single microtubules were left out.

3 Results

3.1 Characterization of *Dictyostelium* TACC

3.1.1 *Dictyostelium* TACC localization

Regulation of microtubule dynamics by microtubule-associated proteins (MAPs) takes place at different places within a cell such as the centrosome, the microtubule lattice, the microtubule plus end complex or the cell cortex. When characterizing MAPs, first information on MAP function or on potential interaction partners can be derived from a detailed evaluation of MAP localization. So far, *Dictyostelium* TACC has only been shown to associate with the centrosomes/spindle poles, while its interaction partner CP224 was found at the centrosomes/spindle poles and microtubule plus ends (Rehberg and Gräf, 2002; Koch *et al*., 2006). If *Dictyostelium* TACC was to function in accordance with the current model (section 1.6, Fig. 3) (Kinoshita *et al*., 2006; Peset and Vernos, 2008), it would also be expected to associate with the plus ends of nascent microtubules. In order to address this issue, localization studies were carried out.

3.1.1.1 Endogenous TACC localizes to the centrosome and the microtubule plus ends

A polyclonal rabbit anti-TACC antibody raised against the TACC domain was available in our lab. In immunofluorescence experiments, endogenous TACC colocalized with CP224 at the centrosome and at certain spots scattered throughout the cytoplasm (Fig. 5 A). These cytoplasmic spots displayed the typical staining pattern previously observed for the verified *Dictyostelium* microtubule plus end protein CP224 (Rehberg and Gräf, 2002). During mitosis, spots visible in the vicinity of spindle poles were significantly weaker, making it difficult to interpret this staining pattern (Fig. 5 B-E). When comparing the levels of endogenous TACC at interphase and prophase centrosomes, TACC seemed significantly enriched at prophase centrosomes (Fig. 5 F-H, arrowheads).

The donut shaped arrangement of TACC at the centrosome strongly suggested TACC to be part of the centrosomal corona. This was subsequently confirmed by immunoelectron microscopy conducted by Prof. Otto Baumann (Universität Potsdam) (Samereier *et al*., 2011).

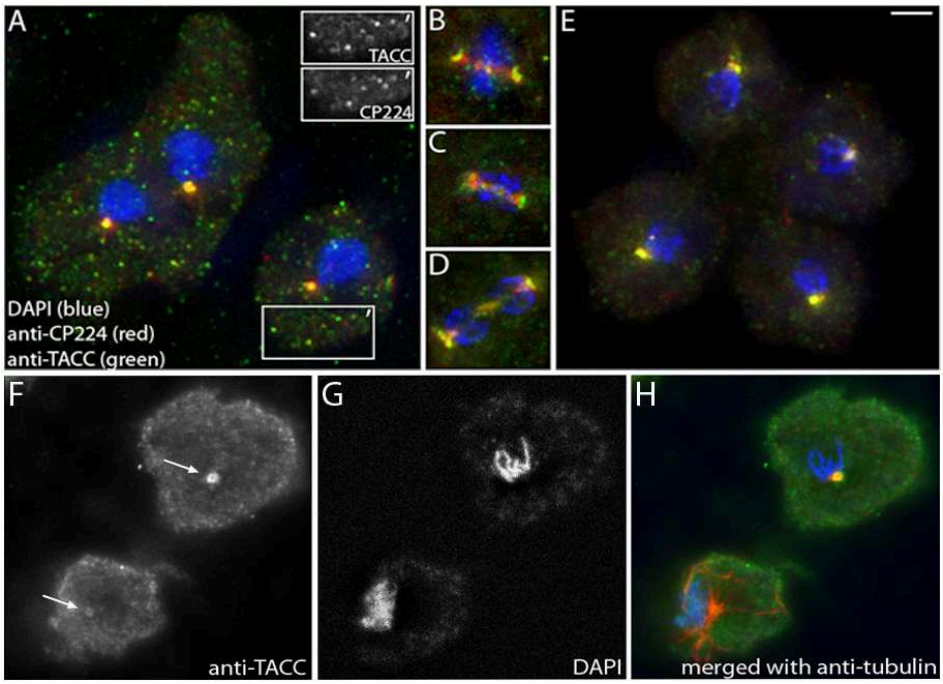

Fig. 5 Endogenous TACC localizes to centrosomes and microtubule plus ends during interphase and to spindle poles during mitosis
Dictyostelium cells were fixed with methanol and labeled with anti-TACC (green), anti-CP224 (red) and DAPI (blue). Whole cells (A, E, F-H) and mitotic spindles (B, C, D) are shown in interphase (A), metaphase (B), anaphase (C), early telophase (D) and late telophase (E). To point out TACC and CP224 colocalization at microtubule plus ends, the insets in (A) exclusively show TACC or CP224 staining within the boxed area depicted as ('). Images (F-H) show an interphase (lower) and prophase (upper) cell, respectively. Arrowheads in (F) point at the centrosomes exhibiting different levels of endogenous TACC. Bar = 2 µm.

3.1.1.2 The TACC domain is sufficient for association of TACC with the centrosome and microtubule plus ends during interphase

To confirm microtubule plus end localization and to address the question whether the TACC domain is necessary for specific TACC localization as previously reported for the *Drosophila* and *Xenopus* homologues (Gergely *et al*., 2000b; Peset *et al*., 2005), *Dictyostelium* strains expressing GFP-fusion proteins of full length TACC and a C-terminally truncated version lacking the TACC domain were generated (Fig.6 **A**). Furthermore, a strain expressing the TACC domain fused to GFP was available in our lab.

GFP-full length TACC and GFP-TACCdom were both clearly associated with the centrosome and the microtubule plus ends of apparently all microtubules, while deletion of the TACC domain abrogated all localizations of the GFP-fusion protein to specific structures (Fig. 6 **B**). Consequently, the TACC domain is sufficient and necessary for all interphase localizations of TACC. After the *Drosophila* D-TACC protein (Lee *et al*., 2001), *Dictystelium* TACC is only the second TACC protein shown to associate with microtubule plus ends *in vivo*.

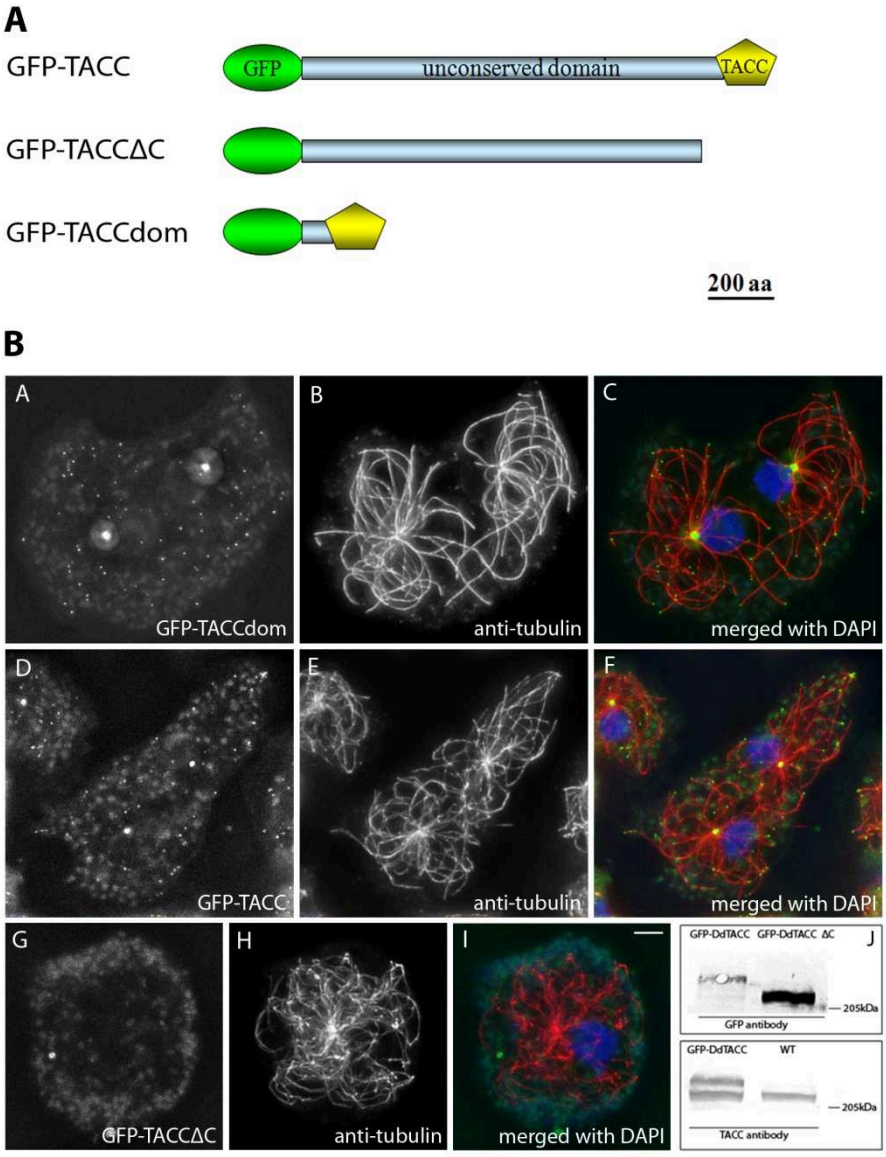

Fig. 6 The TACC domain is sufficient for localization at centrosomes and microtubule tips
(A) Schematics showing the three different GFP-TACC fusion proteins used in this study
(B) GFP-TACCdom (A-C) and GFP-full length TACC (D-F) localize to the centrosomal corona and to microtubule plus ends. By contrast, the C-terminally truncated fusion protein GFP-TACCΔC (G-I), lacking the TACC domain, does not show any specific localization. GFP (A, D, G) is shown in green, tubulin (B, E, H) in red and DNA in blue. Proper expression of GFP-TACC and GFP-TACCΔC was verified by immunoblotting. A Western blot of *Dictyostelium* whole cell lysates (J) shows labeling of GFP-TACC and GFP-TACCΔC with anti-GFP (upper panel), and of GFP-TACC and endogenous TACC with anti-TACC (lower panel). Bar = 2 µm.

3.1.1.3 TACC and CP224 are absent from microtubule tips during mitosis

In other organisms, the most striking effects on microtubule dynamics observed upon TACC depletion were reported for mitotic cells, suggesting a particular importance of TACC during mitosis (Peset and Vernos, 2008). Considering that microtubule dynamics are greatly increased during mitosis and that alterations in the composition of the plus end complex are

likely to play a key role it this process, it was interesting to know whether *Dictyostelium* TACC is still associated with the plus ends of highly dynamic microtubules in M-Phase.

Detailed investigation of mitotic TACC localization with emphasis on microtubule plus end localization was conducted with GFP-TACC and GFP-TACCdom expressing cells. Since the results did not differ at any point, only GFP-TACC images are shown (Fig. 7). As expected, GFP-TACC was associated with the spindle poles in all mitotic stages. It is noteworthy to mention that this requires TACC relocation from the centrosomal corona to the former centrosomal core structure before or while the corona is disassembled during prophase (section 1.2, Fig. 1). Surprisingly, GFP-TACC was completely absent from microtubule tips in all mitotic stages. This finding could not be due to fixation or staining artefacts, since all cells adjacent to the mitotic cells observed had a strong GFP-TACC signal at the tips of their interphase microtubules. An example for that is shown in Fig. 7 A-C. The boxed area in Fig. 7 C depicted as (´) shows a very early prophase stage, as can be seen by the cells' condensed DNA, while at the same time its interphase microtubule cytoskeleton has not yet been disassembled. The area depicted as (´´) shows a section of an interphase cell. In (´´), microtubules clearly have a GFP-TACC signal at their plus ends, while in (´) only few unspecific GFP-signals can be observed. Consequently, in prophase TACC is not lost passively from microtubule plus ends as a result of interphase microtubule depolymerization, but instead actively dissociates from the tips of microtubules beforehand, possibly in synchrony with the onset of mitosis. GFP-TACC plus end localization was usually not restored until late telophase or during the successive interphase.

Fig. 7 (next page) During mitosis GFP-TACC localizes to spindle poles, the kinetochores and the midbody region, but is virtually absent from the tips of astral microtubules
GFP-TACC (A, D, G, J, M, P, S and green in merged images) expressing cells were fixed with glutaraldehyde and stained with anti-tubulin (B, E, H, K, Q, T and red in merged images). To visualize kinetochores, the cells were also labeled with anti-Cenp68 (section 3.2.1) (N, magenta in O). DNA is shown in blue, mitotic stages are indicated on the left. In all interphase cells adjacent to the mitotic cells shown above, a clear GFP-TACC signal was visible at the microtubule plus end tips. An example for that is shown in (C). Here, the upper right cell represents an early prophase stage, as can be seen by its condensed DNA. In this cell, no GFP-TACC signal is detectable at its microtubules tips ('). In an interphase cell at the lower left ("), TACC is clearly associated with micrtotubule plus ends. Throughout mitosis, GFP-TACCdom exhibited the same behavior as GFP-TACC (not shown). Bar = 2 µm.

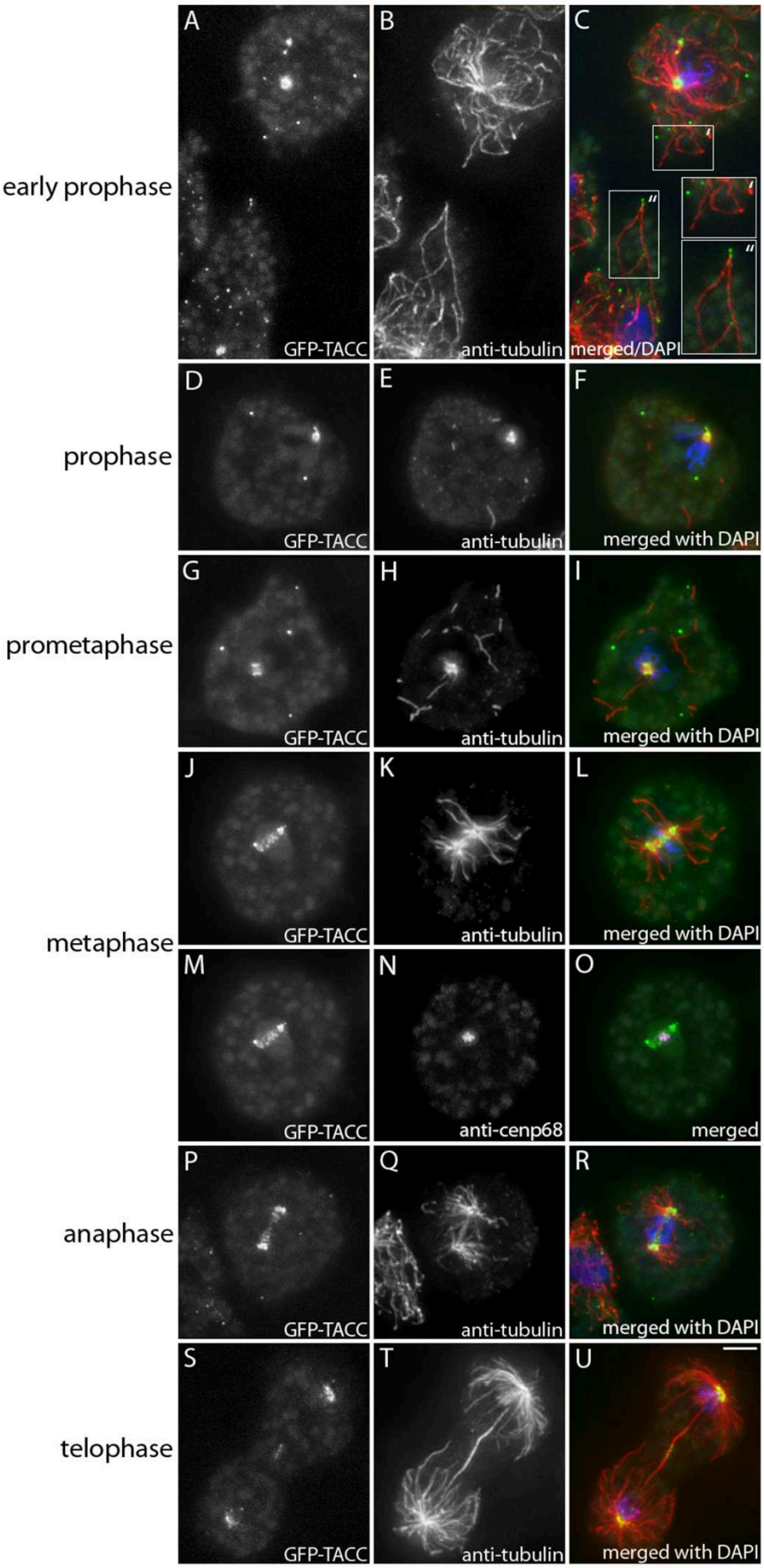
early prophase
A
GFP-TACC
B
anti-tubulin
C
merged/DAPI
prophase
D
GFP-TACC
E
anti-tubulin
F
merged with DAPI
prometaphase
G
GFP-TACC
H
anti-tubulin
I
merged with DAPI
metaphase
J
GFP-TACC
K
anti-tubulin
L
merged with DAPI
M
GFP-TACC
N
anti-cenp68
O
merged
anaphase
P
GFP-TACC
Q
anti-tubulin
R
merged with DAPI
telophase
S
GFP-TACC
T
anti-tubulin
U
merged with DAPI

Besides association with the spindle poles, GFP-TACC was also found at the kinetochores during metaphase as visualized by colocalization with the centromere marker Cenp68 (Fig. 7 M-O), and in the midbody region in telophase (Fig. 7 S-U). Finally, cytoplasmic aggregates of GFP-TACC were found in most mitotic cells from early prophase to late telophase (e.g. Fig. 7 A, D, G). These aggregates were also observed for endogenous TACC in wild type cells. Interestingly, CP224 was always strongly enriched in these aggregates (not shown).

Microtubule growth in *Dictyostelium* peaks from metaphase to telophase. Consequently, the absence of potentially growth-promoting TACC from microtubule tips during mitosis was highly surprising. Since TACC proteins were proposed to promote microtubule growth in complex with XMAP215 proteins, it was now interesting to analyze whether CP224 associates with microtubule tips during mitosis in *Dictyostelium*. Although CP224 has previously been characterized in detail by our group, this particular issue has not been addressed before. To achieve this, the monoclonal CP224 antibody was used on fixed wild type cells. As seen in Fig. 8, endogenous CP224 exhibits perfectly the same behavior as GFP-TACC and dissociates from microtubule plus ends from early prophase to late telophase. Again, all neighbouring interphase cells had strong CP224 signals at their microtubule plus ends so that staining artefacts can be excluded (Fig. 8 E, J, O).

Association of CP224 with spindle poles, kinetochores and the midbody region has been known previously (Gräf *et al*., 2000a; Rehberg and Gräf, 2002). Yet, the results of this work demonstrate for the first time *in vivo* that a TACC and XMAP215 protein can differentially localize to microtubule plus ends during interphase and mitosis. The fact that both proteins behave identically at all localizations during interphase and mitosis, supports the idea that the two proteins might function together in regulating microtubule dynamics also in *Dictyostelium*.

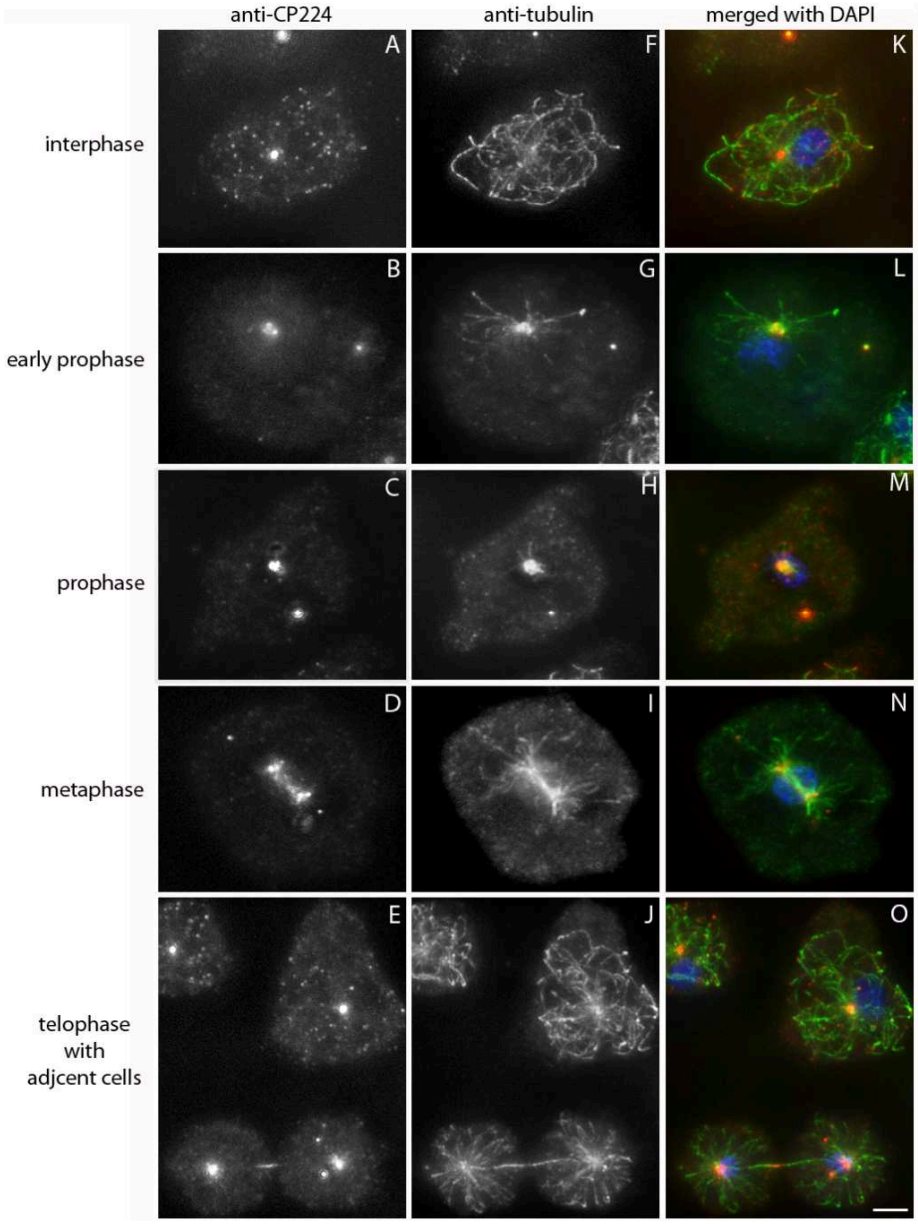

Fig. 8 CP224 is absent from plus ends of astral microtubules
Wild type cells were fixed with methanol and stained with anti-CP224 (A-E, red in merged images) and anti-tubulin (F-J, green in merged images). As GFP-TACC, endogenous CP224 is absent from the microtubule plus ends during mitosis. To exclude staining artifacts, an interphase cell exhibiting strong association of CP224 with microtubule tips is shown in (E-O). Mitotic stages are indicated on the left and antibody staining on top. DNA is shown in blue. Bar = 2 µm

3.1.1.4 TACC is enriched at prophase spindle poles

Enrichment of TACC proteins at the centrosomes during mitosis in an Aurora A-dependent manner seems to be evolutionally conserved (Peset and Vernos, 2008; Albee *et al*., 2008). In *Dictyostelium*, immunofluorescence experiments using the TACC antibody on wild type cells revealed an increase in centrosomal TACC levels during prophase as well (Fig. 5 F-H). In

order to study mitotic TACC enrichment at spindle poles more thoroughly, a GFP-TACCdom expressing strain was further transformed with mRFP-α-tubulin. Fluorescence live cell imaging revealed an enrichment of GFP-TACCdom precisely at the time when the corona is shed off from the centrosome together with the microtubules in prophase (Fig. 9, 23m 20s - 24m 20s) (Ueda *et al*., 1999). Interestingly, GFP-TACCdom persists at the spindle pole even when tubulin is absent.

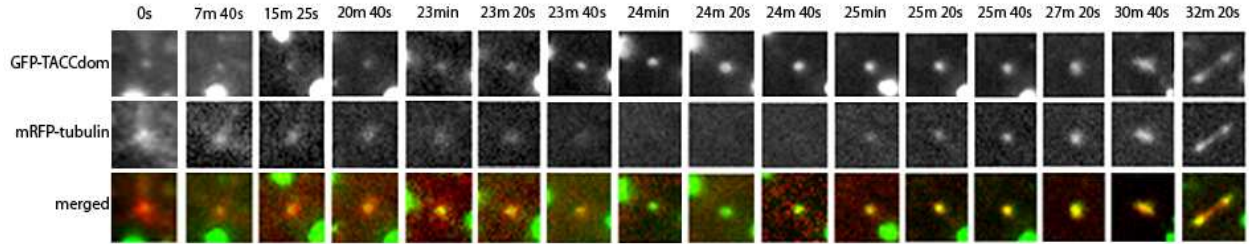

Fig. 9 GFP-TACCdom is enriched at the spindle poles in prophase
Shown is a time series of widefield microscopy images of a mitotic cell co-expressing GFP-TACCdom (upper panel) and mRPF-α-tubulin (middle panel). Due to spatial limitations, only a square region around the centrosome of selected time points is shown. Please note that additional bright GFP-signals outside the centrosome represent aggregates of GFP-TACCdom, which have been frequently observed upon strong overexpression of the TACC domain or during mitosis. The time series starts ~20 minutes prior to M-Phase (0s) and the last image (32m 20s) shows a metaphase spindle. The shown cell normally finished mitosis. Time points are indicated on top, shown fluorescent fusion proteins are indicated on the left. For each time point, a z-stack consisting of 5 images (focus step size 0.5 µm) was taken. Shown are maximum intensity projections.

3.1.2 *Dictyostelium* TACC function

3.1.2.1 Knockdown of TACC by RNAi

TACC proteins were reported to contribute to microtubule stabilization or spindle organization in a variety of organisms (section 1.6). Nothing was known about *Dictyostelium* TACC function so far, but its localization at the centrosome and the microtubule plus ends was in agreement with such functions.

Initially, *Dictyostelium* TACC function should be assessed by characterizing a knockout mutant. Since no such mutants could be isolated, TACC expression was suppressed by RNAi. This was achieved by transcription of an RNA fragment containing long inverted repeats which consisted of 543 bp from the 5' end of the TACC coding sequence. These sequences were separated by an interjacent stuffer fragment that allows folding to a hairpin-like structure (Martens *et al*., 2002) (Fig. 10 A).

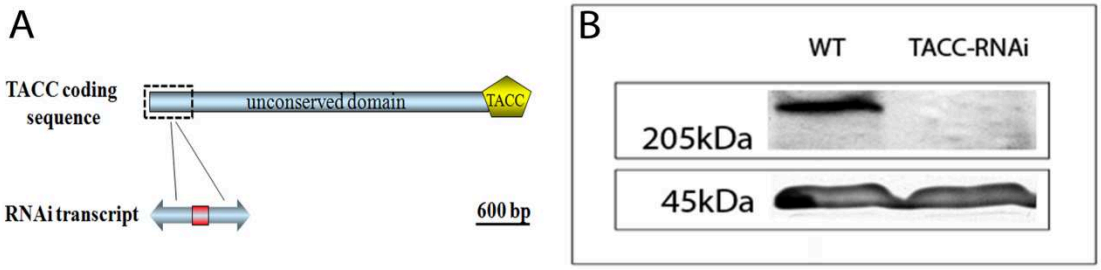

Fig. 10 Knockdown of TACC expression by RNAi
(**A**) Schematic of the TACC knockdown construct used. Arrows indicate the orientation of the transcribed RNA. The stuffer fragment that allows folding of the inverted repeats to double stranded RNA is shown in red. (**B**) Upon RNAi treatment, TACC is no longer detectable in immunoblots. Western blots of whole cell lysates were stained with anti-TACC (upper panel). Anti-actin staining (lower panel) served to demonstrate equal amounts of protein were loaded. Molecular weight is shown on the left and strains used are indicated on top of the respective lanes.

After determining the TACC expression of isolated transformants by immunoblotting, several clones with clearly reduced TACC levels could be identified. In those strains the remaining TACC expression ranged from ~90 % to levels undetectable by immunoblotting. For further analysis the clone with the most pronounced knockdown effect was chosen (Fig. 10 B). Importantly, due to the integration of the transfected vector into the *Dictyotelium* genome, the RNAi transcript is permanently and stably transcribed. Consequently, the RNAi effect was found to remain unaltered over long periods of cultivation, development or after transfection with further expression vectors.

3.1.2.2 TACC is required for interphase microtubule length

To test for involvement of TACC in organizing an interphase microtubule cytoskeleton, immunofluorescence experiments using a tubulin antibody were carried out. These experiments revealed a moderate reduction of interphase microtubule length in TACC-RNAi cells compared to wild type cells (Fig. 11 A, E and B, F). Quantification of microtubule lengths in the respective cell lines further demonstrated this effect of TACC depletion (Tab. 3). Since the RNAi construct used, was directed against the very N-terminus of the TACC protein, expression of the C-terminal TACC domain as a GFP-fusion protein was not affected in TACC-RNAi cells (Fig. 11 I). Therefore, the ability of GFP-TACCdom to rescue the reduced interphase microtubule length could be determined. These experiments revealed that although there clearly was a positive effect on microtubule length, a completely normal microtubule cytoskeleton was not restored in many cells (Fig. 11 C, G and Tab. 3).

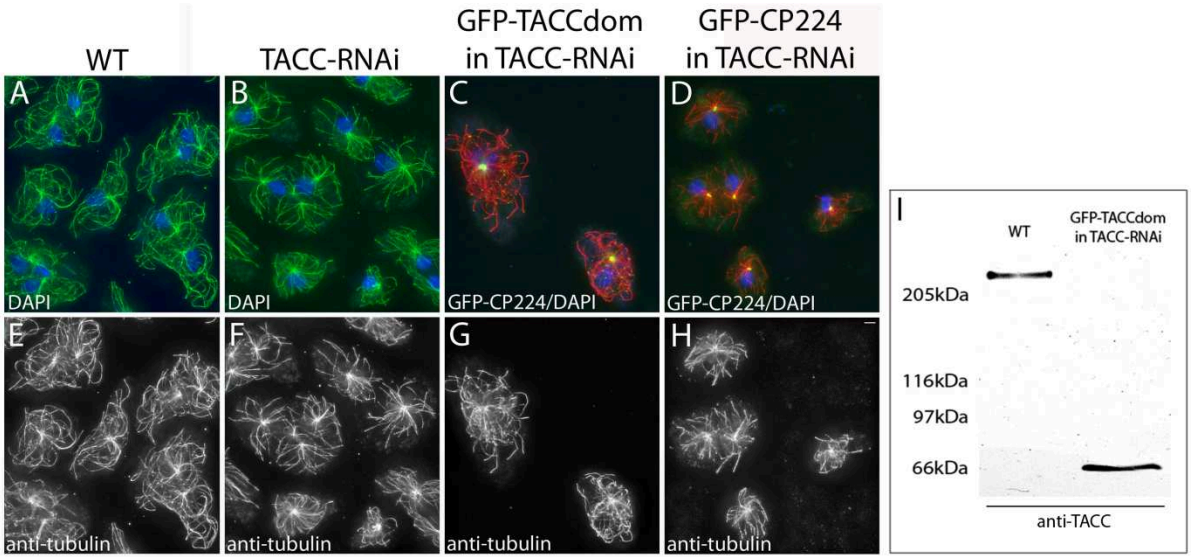

Fig. 11 Microtubule length is significantly reduced upon TACC-RNAi and rescued by expression of the TACC domain as GFP-fusion protein
Cell types indicated on top were fixed with glutaraldehyde and stained with anti-tubulin (E-H, green in A, B and red in C, D). Compared to wild type cells, microtubule length is reduced in TACC-RNAi cells. Although GFP-TACCdom and GFP-CP224 expressed in TACC-RNAi cells both localize normally (green in C and D), only GFP-TACCdom expression partially restores wild type-like microtubule length in a large number of cells. The upper panel shows merged images of anti-tubulin, DNA (blue) and the respective GFP-fusion proteins in (C) and (D). Bar = 2 µm. An immunoblot of whole cell lysates stained with anti-TACC demonstrates that upon transfection of TACC-RNAi cells with GFP-TACCdom, the RNAi effect remains strong and no full length TACC was detected (I). GFP-TACCdom is expressed normally in this cell line. Molecular weight is depicted on the left, strains used are indicated on top of the respective lanes.

Tab. 3 Microtubule length in wild type and TACC mutant cells

cell line	microtubule length µm (*n*)
Control cells (strain AX2)	8,68 ± 2,59 (135)
TACC-RNAi	6,17 ± 1,62 (132)
GFP-TACCdom in TACC-RNAi	6,83 ± 2,38 (127)
GFP-CP224 in TACC-RNAi	6,34 ± 1,89 (129)

In order to compare microtubule lengths, the respective strains were fixed with glutaraldehyde and labeled with anti-tubulin. Evaluation of microtubule length was accomplished with Image J on maximum intensity projection images (section 2.5.6).

It is noteworthy that GFP-TACCdom properly localizes to the centrosome and the microtubule plus ends in TACC-RNAi cells. Importantly, this applied for cells with strong rescue effect as well as for cells with no rescue effect. In a similar experiment, the conserved interaction partner CP224 was expressed as a GFP-fusion protein in TACC-RNAi cells, in

order to determine if overexpression of CP224 could compensate the lack of TACC. In these experiments the microtubule length was not significantly increased upon expression of GFP-CP224 in TACC-RNAi cells (Fig. 11 D, H and Tab. 3).

3.1.2.3 TACC is involved in the formation of astral microtubules

Although TACC was shown to be absent from the tips of astral microtubules (section 3.1.1.3), the protein appears to be vital for their formation. This became evident upon analyzing spindle formation in mitotic TACC-RNAi cells, where the effect of TACC depletion was much more pronounced than during interphase. Astral microtubules of wild type cells frequently exhibit a considerable length in late metaphase or early anaphase (Fig. 12 C-F). In TACC-RNAi cells, however, astral microtubules could not be observed at all until anaphase (Fig. 12 K-N). Unlike astral microtubules, spindle microtubules were not affected by RNAi treatment. Accordingly, chromosome segregation as visualized by the centromere/kinetochore marker Cenp68 (section 3.2.1) proceeded accurately (Fig. 12, green in A-P). In contrast to the phenotype observed for interphase microtubules (3.1.2.2), expression of GFP-TACCdom in TACC-RNAi cells fully restored normal astral microtubule length (Fig. 12 Q-X).

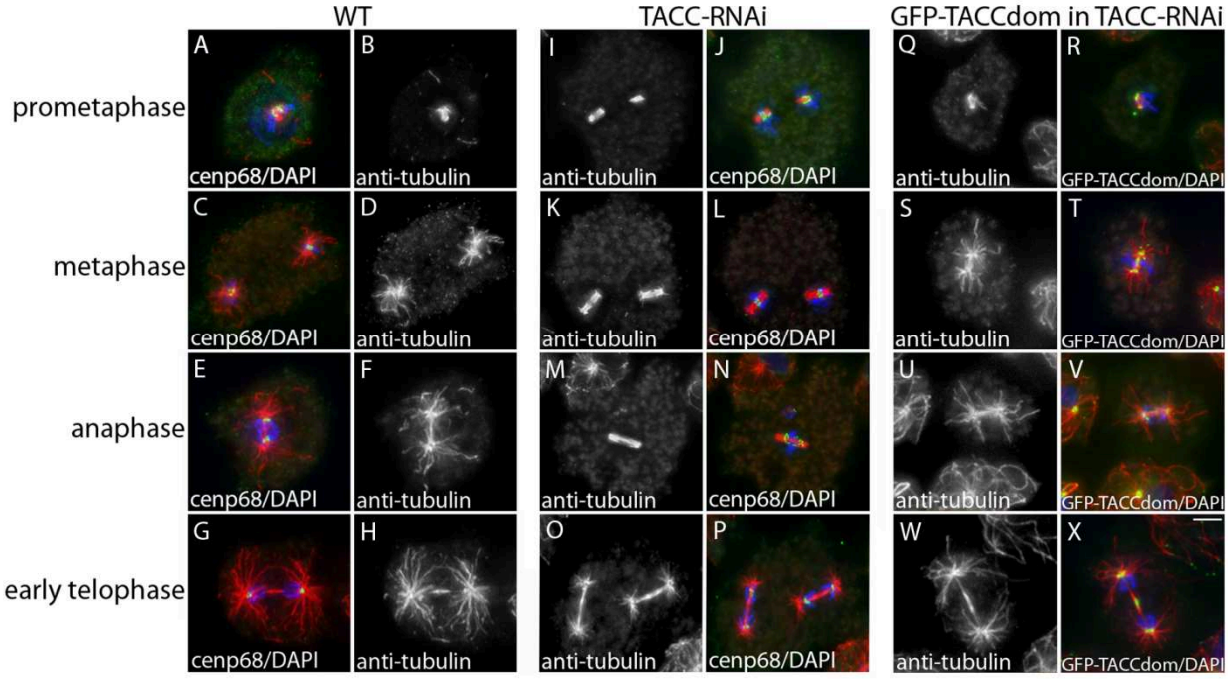

Fig. 12 Astral microtubule formation is impaired upon TACC-RNAi
Cell types indicated on top were fixed with glutaraldehyde and labeled with anti-tubulin (greyscale images and red in merged images) and anti-Cenp68 as a kinetochore marker (green in merged images A, C, E, G and J, L, N, P). Aster formation is heavily impaired upon TACC-RNAi treatment, while spindle microtubules are unaffected (I-P). Expression of GFP-TACCdom in TACC-RNAi cells (green in merged images R, T, V, X) restores normal astral microtubule length (Q-X). DNA is shown in blue. Bar = 2 µm.

3.1.2.4 Depletion of TACC does not affect cytokinesis

Astral microtubules were reported to play an important role in determining the site of cleavage furrow formation (Werner and Glotzer, 2008). Therefore, the pronounced effect of TACC depletion on astral microtubules during mitosis raised the question whether TACC-RNAi treatment would give rise to defects in cytokinesis or mitosis. Such defects could manifest in the occurrence of multi-nucleated cells or in a ratio of centrosomes to nuclei other than 1:1. To test this, the number of centrosomes and nuclei of ~1000 wild type cells and TACC-RNAi cells, each, were counted (Tab. 4). In this context it has to be mentioned that *Dictyostelium* cells sometimes naturally contain more than one nucleus. For this experiment, cells with no more than two nuclei were regarded as normal and only cells with three or more nuclei were counted.

Tab. 4 TACC depletion does not obviously affect cytokinesis

	wild type	TACC-RNAi
(*n*)	1048	1047
Cells with supernumerary centrosomes	7	41
Cells with nuclei > 2	40	25

In order to evaluate the impact of TACC knockdown on cytokinesis, the number of nuclei and centrosomes in wild type cells and TACC mutants were counted. To do this, cells grown in adherent culture were fixed with methanol and stained with anti-CP224, anti-tubulin and DAPI. Cells, centrosomes and nuclei were subsequently counted in maximum intensity projections.

A slight increase in supernumerary centrosomes of ~3 % compared to wild type cells was determined for TACC-RNAi cells. This, however, does not compare to results from other cell lines such as CP224 overexpressing cells, where 42 % of the cells had too many centrosomes (Gräf *et al*., 2003). Finally, no increase in multi-nucleated cells was observed upon TACC-RNAi, and TACC mutants were not found to be arrested in mitosis.

3.1.2.5 TACC depletion causes TBZ hypersensitivity

Cells depleted of TACC are unable to form astral microtubules until anaphase and exhibit shortened interphase microtubules. The latter observation strongly resembled the phenotype reported for cells underexpressing CP224 (Gräf *et al*., 2003). Furthermore, depletion of CP224 diminished resistance to microtubule depolymerizing drugs like nocodazole or

thiabendazole (TBZ). Therefore, it was obvious to analyze the effect of TACC depletion on thiabendazole sensitivity.

After treatment of wild type cells with 100 µm TBZ for 3 h, microtubules are usually only partially depolymerized and significant microtubule stubs are left (Fig. 13A, E). In contrast, the majority of CP224 underexpressing cells displayed a completely depolymerized microtubule cytoskeleton with remnants of tubulin at the centrosome only (Gräf *et al*., 2003). A similar result was produced when TACC-RNAi cells were challenged with TBZ (Fig. 13 B, F). Upon expression of GFP-TACCdom in TACC-RNAi cells, TBZ hypersensitivity caused by TACC depletion could be fully rescued (Fig. 13 C, G), while overexpression of GFP-CP224 in TACC-RNAi cells could not compensate for the lack of TACC (Fig. 13 D, H).

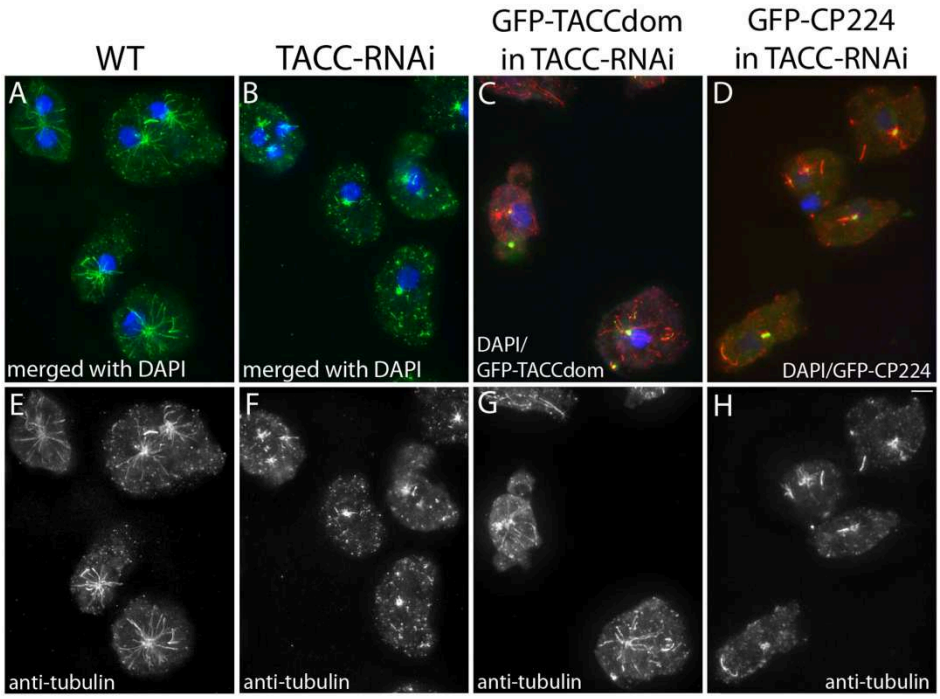

Fig. 13 Cells depleted of TACC are hypersensitive to thiabendazole
Cell types indicated on top were treated with 100 µM thiabendazole for 3 h and microtubules were labeled with anti-tubulin (E-H, green in A, B and red in C, D). TBZ treatment clearly has an effect on all cell types, but compared to wild type cells, remaining microtubules in TACC-RNAi cells are significantly shorter. Expression of GFP-TACCdom (green in C) rescues the hypersensitivity phenotype, while overexpression of GFP-CP224 (green in D) has no significant effect. In merged images DNA is shown in blue. Bar = 2 µm.

3.1.3 Functional analysis of *Dictyostelium* TACC

There is little doubt that the conserved interaction between TACC and XMAP215 proteins plays a crucial role in connecting TACC protein function to the regulation of microtubule assembly. The proposed function of TACC in this context is to recruit XMAP215 proteins to

the centrosome or, more frequently, to the mitotic spindle poles. Upon depletion of TACC, XMAP215 protein localization to the spindle poles was reported to be heavily impaired or completely lost in *C. elegans*, *S. pombe*, *D. melanogaster* and *X. laevis* (Lee *et al*., 2001; Bellanger and Gonczy, 2003; Le Bot *et al*., 2003; Sato *et al*., 2004; O'Brien *et al*., 2005). Concomitantly, overexpression of D-TACC was shown to raise spindle pole levels of msps, the *D. melanogaster* XMAP215 homologue, to above normal (Lee *et al*., 2001). After being recruited to the centrosome in a TACC-dependent manner, XMAP215 proteins were suggested to be loaded onto the plus ends of nascent microtubules in a complex with TACC to promote microtubule assembly.

3.1.3.1 Does TACC function in a complex with CP224?

Considerable evidence exists from other organisms that TACC and XMAP215 proteins act as a complex in stabilizing microtubules (Kinoshita *et al*., 2005; Peset *et al*., 2005). In order to test whether this was also true for *Dictyostelium*, a recently identified point mutation that was reported to disrupt the interaction between *C.elegans* TAC-1 and the XMAP215 homologue ZYG-9 (Bellanger *et al*., 2007) was reproduced for *Dictyostelium* TACC. The idea was to examine if a GFP-TACCdom fusion protein that no longer interacts with CP224, was still able to rescue the phenotypes of TACC depletion in the same way as non-mutated GFP-TACCdom. The corresponding residue for the *Dictyostelium* TACC domain was identified by sequence analysis (Fig. 14 A).

In accordance with the point mutation identified in *C.elegans*, leucine 1441 within the GFP-TACCdom expression construct was point mutated to a phenylalanine (GFP-TACCdomL1441F). The presence of the correct mutation within the expression construct was verified by sequencing. Unfortunately, co-immunoprecipitation experiments revealed that the affinity of GFP-TACCdom to endogenous CP224 was not altered upon point-mutating leucine 1441 (Fig. 14 B). Furthermore, GFP-TACCdomL1441F localized normally and could rescue the TACC depletion phenotypes (not shown). Consequently, this approach was not suitable to investigate the importance of the interaction between *Dictyostelium* TACC and CP224.

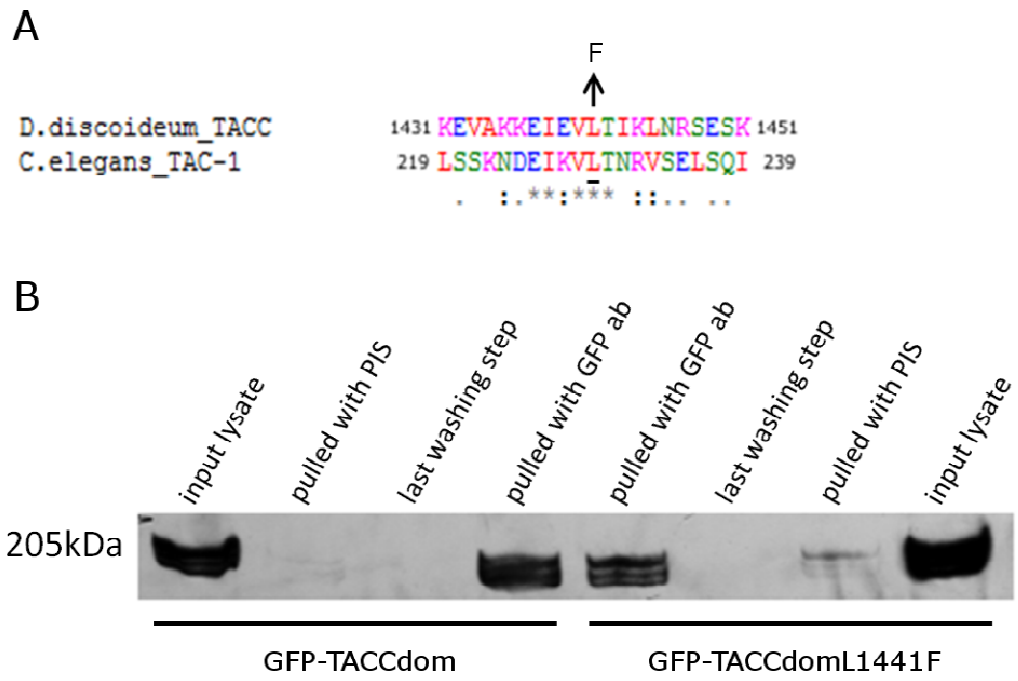

Fig. 14 Point mutation of *Dictyostelium* TACC (L1441F) does not impair interaction with CP224
Point mutation of L229 to phenylalanine in *C.elegans* TAC-1 abrogates interaction with ZYG-9.
(**A**) Shown is an alignment of the corresponding sequences in *C.elegans* and *Dictyostelium.* In both organisms the respective residues are situated within the C-terminal third of the TACC domain. In analogy to the point mutation in *C.elegans*, *Dictyostelium* TACC L1441 was mutated to phenylalanine. The alignment was generated using ClustalW (www.ebi.ac.uk/Tools/msa/clustalw2). Alignment is modified. (**B**) Co-immunoprecipitation experiments revealed that substitution of L1441 with phenylalanine in *Dictyostelium* TACC does not affect the interaction with CP224. Cytosolic extracts of GFP strains, as indicated on bottom, were incubated with rabbit polyclonal anti-GFP antibody or a random rabbit pre-immune serum (PIS) as control. After recovery of the antibodies by addition of protein G beads, the yielded eluates were subjected to western blotting and stained with anti-CPP224. Molecular weight is shown on the left.

3.1.3.2 Association of CP224 with the centrosome is hardly impaired by TACC depletion

If *Dictyostelium* TACC, as other TACC proteins, was involved in recruiting XMAP215/CP224 to the centrosome, TACC depletion should be accompanied by a decrease in centrosomal CP224 levels. To investigate this, centrosomal CP224 levels in TACC-RNAi cells and control cells were compared. This was achieved by measuring the fluorescence intensity of CP224 antibody signals at interphase centrosomes in both cell lines (see section 2.5.3). In order to provide identical fixation and labeling conditions, both cells types were mixed and fixed together. Given that limitations in fixation and labeling techniques did not allow using the TACC antibody to identify TACC depleted cells in this experiment, GFP-NE81 expressing cells were used as control. Since GFP-NE81 localization is limited to the

nuclear envelope, alterations in CP224 localization due to NE81 overexpression are very unlikely, but cannot be ruled out.

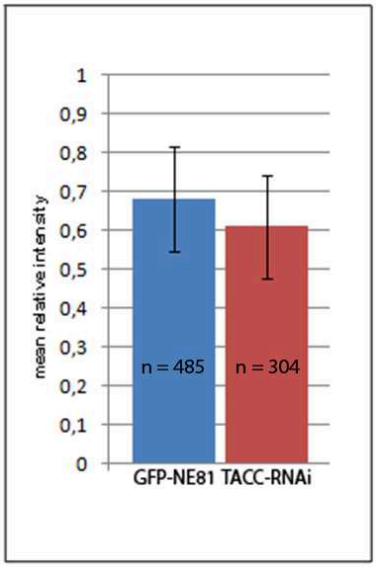

Fig. 15 Depletion of TACC hardly affects CP224 recruitment to interphase centrosomes
TACC knockdown leads to a ~10 % reduction in endogenous CP224 levels at the centrosome. To quantify the loss of centrosomal CP224 in TACC mutant cells compared to GFP-NE81 cells, both cell types were mixed and fixed together and stained with anti-CP224 antibody. The NE81-GFP label served to distinguish between TACC mutant cells and cells normally expressing TACC. Maximum intensity projection images were used for measurements. The mean intensity of CP224 antibody signals of individual centrosomes (*n*) was measured using Image J (section 2.5.3). Signal intensity values were normalized to allow for comparison of values derived from different images, and relative intensity values of the respective cell line were combined. Standard deviation is shown as error bars on top of columns.

As summarized in Fig. 15, centrosomal CP224 levels were on average ~10 % lower in TACC depleted cells compared to GFP-NE81 cells. Considering the impact of TACC depletion on XMAP215 protein localization reported for other organisms, this is a very minor effect. It has to be mentioned, however, that corresponding experiments in other species have mostly been conducted for mitotic spindle poles rather than for interphase centrosomes. Since the processes behind mitotic and interphase XMAP215 protein recruitment to the centrosome could be fundamentally different, it might not be possible to compare these results. Unfortunately, collecting sufficient data for a similar evaluation of mitotic CP224 localization upon TACC depletion in *Dictyostelium* was not feasible, since Dictyostelium cells cannot be properly synchronized in mitosis. Observing mitotic CP224 localization in individual TACC-RNAi cells, however, did not reveal any obvious differences compared to wild type cells (Fig. 16).

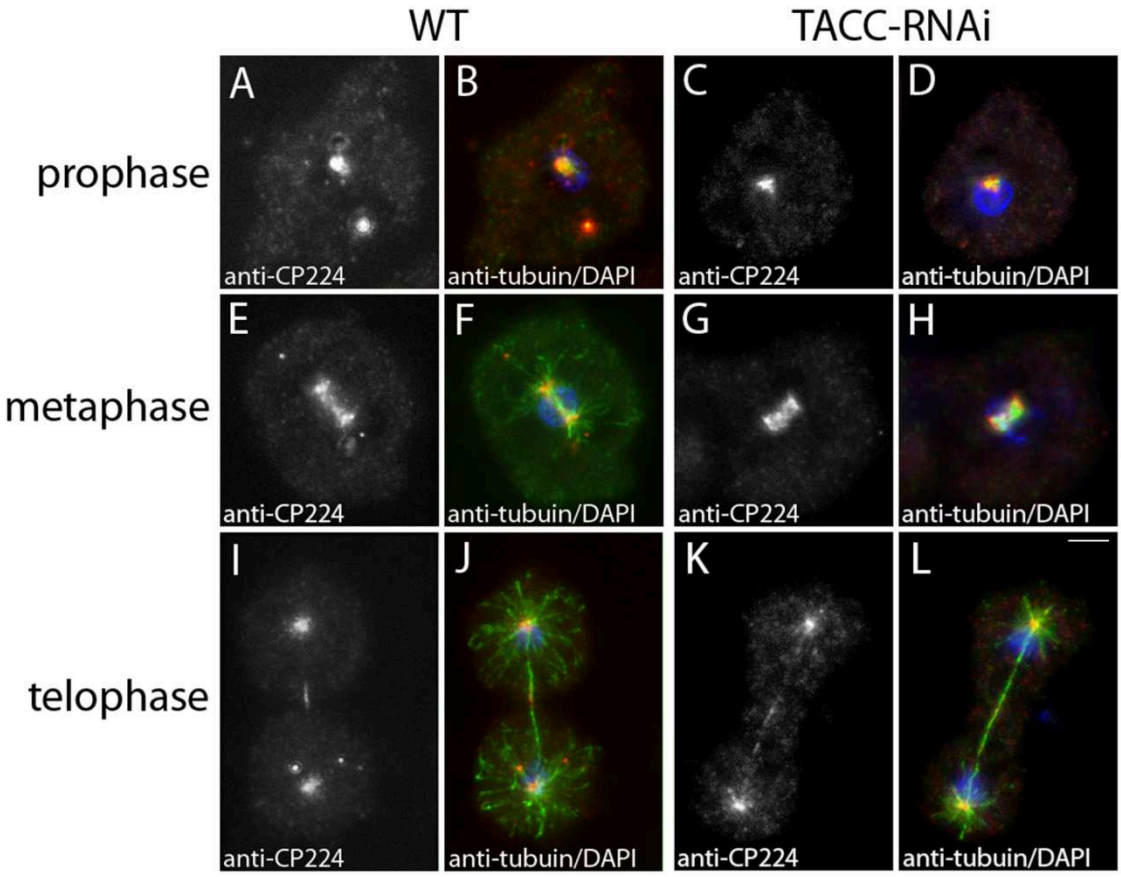

Fig. 16 Depletion of TACC does not obviously impair mitotic CP224 localization
Wild type cells (A, B, E, F, I, J) and TACC-RNAi cells (C, D, G, H, K, L) were fixed with methanol and labeled with anti-CP224 (greyscale images, red in merged images) and anti-tubulin (green in merged images). Association of CP224 with mitotic spindle poles, kinetochores and the midbody region is not perturbed in the absence of TACC. Mitotic stages are indicated on the left and cell types on top. To facilitate comparison, selected images, which have previously been shown in Fig. 8, were added (A, B, E, F, I, J). In merged images DNA is shown in blue. Bar = 2 µm.

3.1.3.3 Depletion of TACC does not affect CP224 dynamics at the centrosome

The experimental setup described in section 3.1.3.2 restricted thorough evaluation of centrosomal CP224 levels upon TACC depletion to interphase. Furthermore, a GFP-NE81 expressing cell line had to be used as control for cells normally expressing TACC. To circumvent this weaknesses an assay based on fluorescence recovery after photobleaching (FRAP) was carried out. In these experiments, the recovery of GFP-CP224 at interphase centrosomes and metaphase spindle poles was determined in a wild type and TACC-RNAi background, respectively. In brief, this was accomplished by confocal 4D live cell imaging of GFP-CP224 expressing cells lines. The area to be bleached was defined manually around whole centrosomes or individual metaphase spindle poles. A schematic of typical ROIs drawn (region of interest) is shown in Fig. 17.

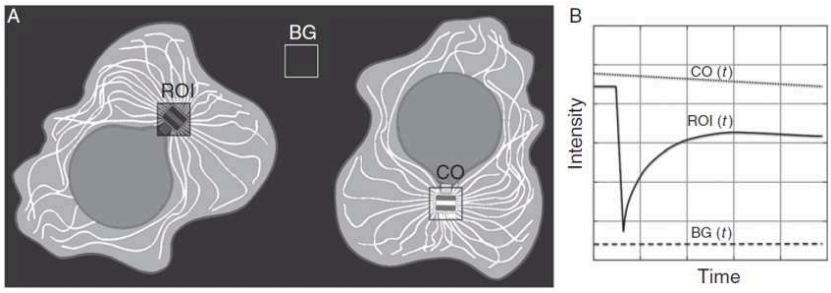

Fig. 17 Schematic drawing of selected regions for FRAP experiments
(**A**) ROI = bleached region of interest, BG = background region of interest, CO = control region of interest to correct for acquisition bleaching. (**B**) Facilitated display of bleaching and recovery processes, plotting fluorescent intensity versus time.

The recording of time series started shortly before the bleaching process and lasted 60 sec with an interval of 1.19 sec. This was usually long enough to observe the maximum level of GFP-CP224 recovery. Fluorescence intensity within the region of interest was determined using Image J on maximum intensity projection images. Subsequent evaluation of GFP-CP224 recovery, including the correction for acquisition bleaching, was conducted with Microsoft Excel (section 2.5.5) (Samereier *et al*., 2010). Regions depicted as CO (control region) and BG (background region) in Fig. 17 A were used for correction. An idealized graphic display of bleaching and recovery processes occurring during FRAP analyses is shown in Fig. 17 B. Representative examples of time series used for FRAP analysis are included as movie on CD (Mov. 1-4).

The FRAP data revealed rapid turnover of centrosomal GFP-CP224 in cells expressing TACC as well as in TACC-RNAi cells during interphase (Fig. 18 A, B) and mitosis (Fig. 18 C, D). No significant difference in the half time of recovery between both cell lines was detected. However, recovery of GFP-CP224 was faster during metaphase, indicating that CP224 dynamics are increased during mitosis regardless of TACC expression.

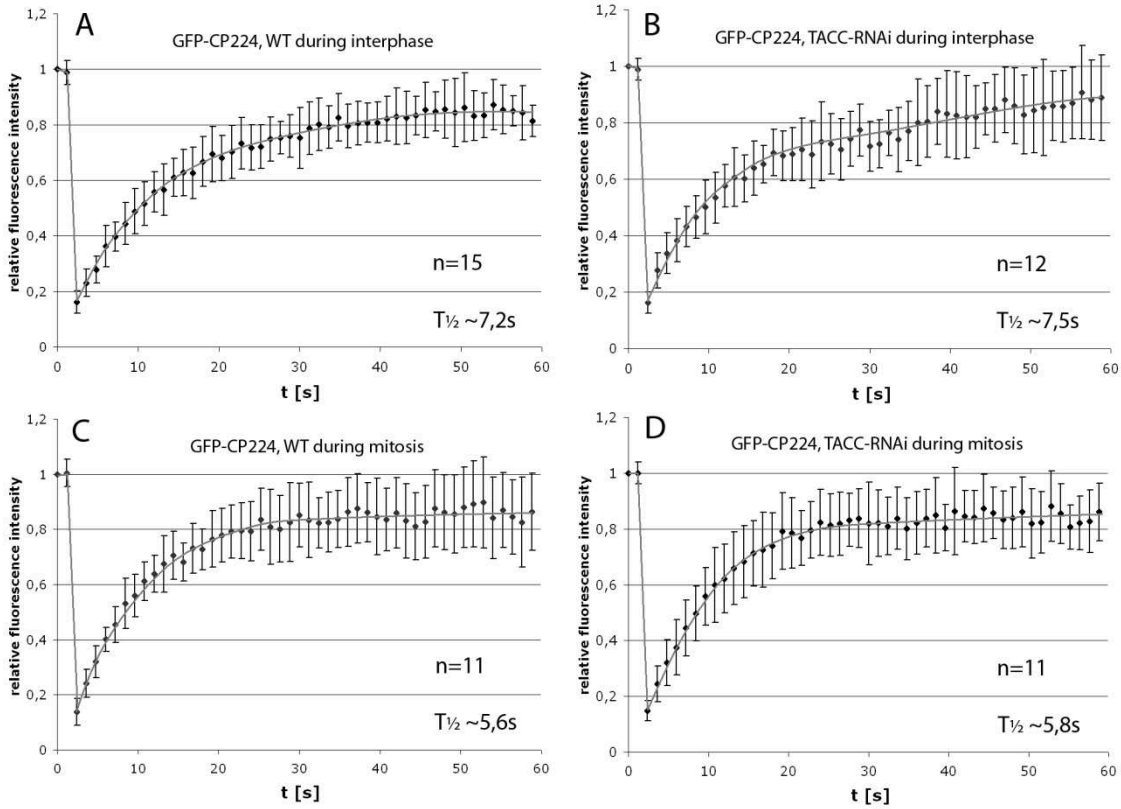

Fig. 18 Centrosomal dynamics of GFP-CP224 are largely unaffected by TACC depletion
FRAP of GFP-CP224 in TACC-RNAi cells and in a wild type background was compared. In interphase cells, whole centrosomes were bleached. For analysis of GFP-CP224 dynamics during mitosis, exclusively metaphase cells were chosen and a single spindle pole was bleached. The cell cycle position and the cell type used are indicated on top of the respective graph. The half time of recovery (T½) and the number of individual experiments combined (*n*) are indicated on the lower right. The standard deviation is indicated as error bars.

Taken together, the slight reduction in centrosomal CP224 levels observed in fixed interphase TACC-RNAi cells (section 3.1.3.2) could not be corroborated by FRAP analyses. Instead, the FRAP data indicates that unlike in most other organisms, recruitment of CP224 to the centrosome in interphase and mitosis is independent of TACC expression. Consequently, the phenotypes observed upon TACC depletion do not seem to be due to impaired CP224 localization at the centrosome.

3.1.3.4 TACC is required for CP224 localization to microtubule tips

Dictyostelium TACC was shown to be dispensable for the recruitment of CP224 to the centrosome. However, if TACC was involved in loading centrosomal CP224 onto nascent microtubule plus ends as previously suggested (Kinoshita *et al*., 2006; Peset and Vernos, 2008), association of CP224 with microtubule tips might be disturbed in the absence of TACC.

To investigate this, the intensity of CP224 antibody signals at microtubule plus ends of TACC-RNAi cells and GFP-NE81 cells was compared. Due to varying labeling intensities of the CP224 antibody, it was necessary to pool both cell lines prior to fixation according to the assay previously described in section 3.1.3.2. Since TACC and CP224 do not localize to the tips of astral microtubules, this experiment was conducted for interphase cells only.

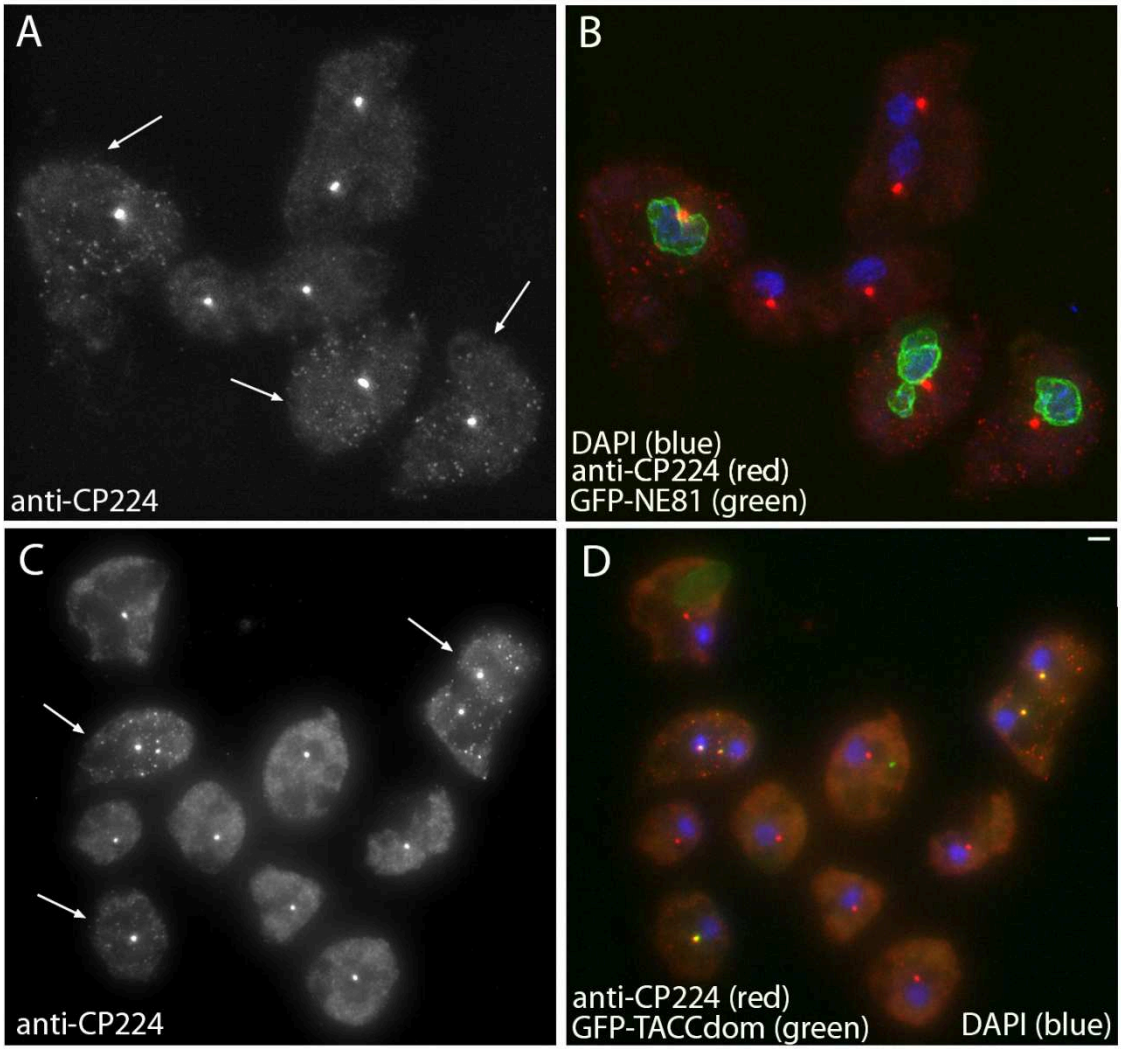

Fig. 19 CP224 localization at the microtubule plus ends is heavily impaired upon TACC depletion and depends on the presence of the TACC domain
TACC-RNAi cells were mixed with GFP-NE81 cells, fixed with methanol and stained with anti-CP224 (A, B). The GFP-NE81 signal at the nuclear envelope (green in B) allows the identification of cells normally expressing TACC (marked with arrowheads in A). The typical staining pattern of CP224 at mictrotubule tips can only be observed in cells expressing GFP-NE81, while centrosomal CP224 can be seen in both cell types (A, and red in B). Expression of GFP-TACCdom restores association of CP224 with microtubule tips. To demonstrate this, TACC-RNAi cells were mixed with TACC-RNAi cells expressing GFP-TACCdom and stained with anti-CP224 (C, D). By means of the centrosomal GFP-TACC signal (green in D), cells expressing the TACC domain can be easily identified (marked with arrowheads in C). CP224 can be found exclusively at microtubule plus ends of TACC-RNAi cells that express GFP-TACCdom (C, red in D). DNA is shown in blue, bar = 2 µm.

In immunofluorescence experiments, CP224 signals at microtubule plus ends appear as tiny dots scattered throughout the cytosplasm (section 3.1.1.1). The latter were clearly visible in GFP-NE81 cells (Fig. 19 A, arrowheads), but almost undetectable in TACC-RNAi cells (Fig. 19 A, B). Moreover, expression of GFP-TACCdom in TACC depletion mutants (Fig. 19 C, arrowheads) rescued this effect and restored CP224 recruitment to microtubule tips (Fig. 19 C, D). Importantly, the TACC-RNAi cells shown in Fig. 19, exhibit no obvious reduction in centrosomal CP224 levels. Therefore, absence of CP224 at microtubule tips cannot be due to insufficient CP224 at centrosomes. Furthermore, overall CP224 levels remained largely unaffected by TACC-RNAi treatment (Fig. 20). This demonstrates for the first time *in vivo*, that a TACC protein is crucial for the association of an XMAP215 protein with microtubule tips.

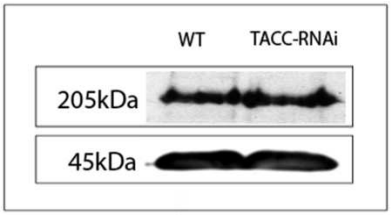

Fig. 20 TACC-RNAi treatment does not alter the level of CP224 expression
Immunoblots of whole cell lysates were stained with anti-CP224 (upper panel). Anti-actin staining (lower panel) served to demonstrate equal amounts of protein were loaded. Molecular weight is indicated on the left and strains used are shown on top of the respective lanes.

3.1.3.5 TACC-RNAi treatment does not affect tubulin turnover at centrosomes

During interphase, TACC and CP224 promote microtubule assembly or stabilization presumably at microtubule plus ends (section 3.1.2.2) (Gräf *et al*., 2003). During mitosis, however, both proteins are lost from microtubule tips in early prophase and do not return until the end of M-Phase (section 3.1.1.3). Consequently, the phenotype of absent or drastically shortened astral microtubules observed upon TACC depletion is likely to originate from impaired spindle pole function. Such defects could manifest in disturbed centrosomal tubulin dynamics. Evidence for that comes from *C.elegans*, where TACC depletion caused slower FRAP of GFP-α-tubulin in the vicinity of spindle poles (Bellanger and Gonczy, 2003).
To investigate whether TACC depletion affects GFP-α-tubulin dynamics in *Dictyostelium* as well, GFP-α-tubulin turnover at centrosomes and spindle poles was analyzed by FRAP experiments in a wild type and TACC depletion background. The FRAP assay was conducted as previously described in section 3.1.3.3. Representative examples of time series used for FRAP evaluation are included as movie on CD (Mov. 5-8).

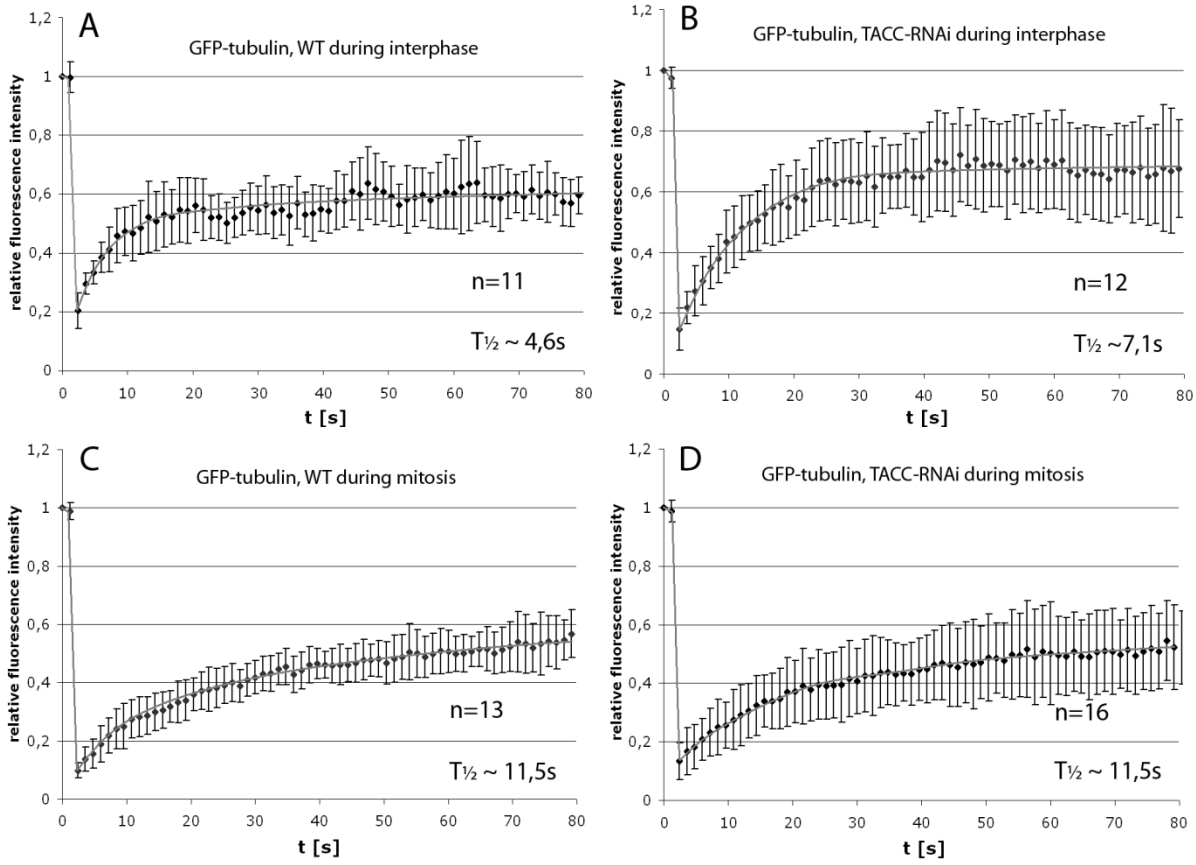

Fig. 21 Centrosomal dynamics of GFP-α-tubulin are largely unaffected by TACC depletion
Recovery of GFP-α-tubulin in TACC-RNAi cells was compared to FRAP of GFP-α-tubulin in a wild type background. In interphase cells, whole centrosomes were bleached. For analysis of GFP-α-tubulin dynamics during mitosis, exclusively metaphase cells were chosen and a single spindle pole was bleached. The cell type used and the cell cycle position are shown on top of the respective graph. The half time of recovery (T½) and the number of individual experiments combined (*n*) are indicated on the lower right. The standard deviation is indicated as error bars.

These experiments revealed no significant effect of TACC depletion on centrosomal GFP-α-tubulin dynamics, neither in interphase (Fig. 21 A, B) nor in mitosis (Fig. 21 C, D). At first, GFP-α-tubulin turnover seems to be slightly slowed down in interphase TACC-RNAi cells (Fig. 21 B) compared to TACC expressing cells (Fig. 21 A). This, however, can be explained by an apparently larger fraction of mobile GFP-α-tubulin in TACC depletion mutants, which certainly takes longer to replenish. Consequently, recruitment of tubulin to the centrosome still proceeds efficiently in the absence of TACC. Generally, after bleaching GFP-α-tubulin at centrosomes or spindle poles, fluorescence never recovered to pre-bleach levels. This suggests the existence of an immobile GFP-α-tubulin fraction that is stably incorporated into the centrosome. Surprisingly, these experiments further demonstrated that there was almost no recovery of fluorescence at microtubules close to the centrosome, despite of quick recovery of GFP-α-tubulin at the centrosome itself. This behavior was observed regardless of TACC

expression and leads to a “black halo-like” appearance upon bleaching a square region around the centrosome, suggesting the minus ends of *Dictyostelium* microtubules to be non dynamic. An example is available on CD (Mov. 5), and selected still images are shown in Fig. 22.

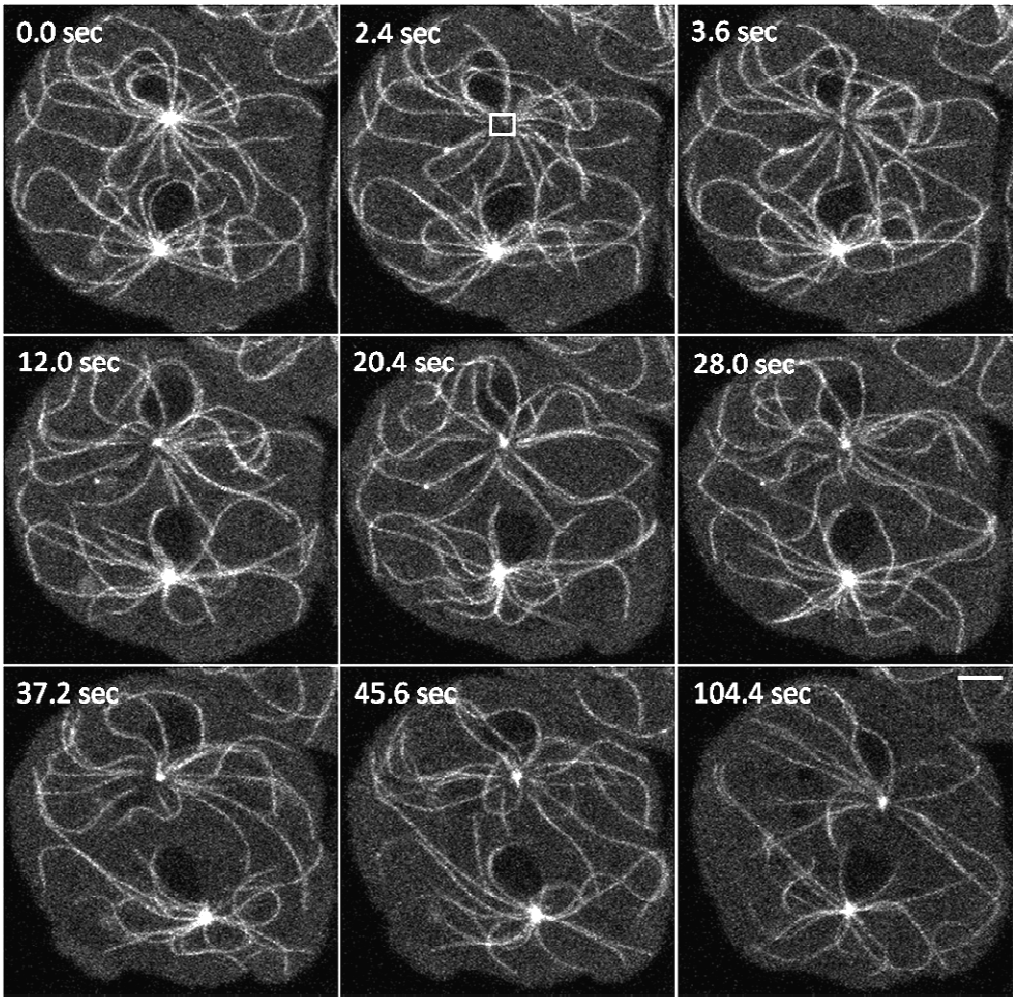

Fig. 22 *Dictyostelium* microtubules are not dynamic at their minus ends
A square region around the centrosome of a GFP-α-tubulin expressing cell was bleached (indicated by a white square) and followed by 4D confocal live cell imaging (Mov. 5). GFP-α-tubulin recovers rapidly, albeit only partially, at the centrosome itself. By contrast, virtually no recovery of GFP-fluorescence can be observed at microtubule minus ends. For each time point, a z-stack consisting of 5 images with a focus step size of 0.5 µm was taken. Shown are maximum intensity projections. The time interval is indicated on the upper left. Bar = 2 µm.

3.1.4 Microtubule plus end dynamics in *Dictyostelium*

Apart from the activity of MAPs, tubulin concentration is the crucial factor influencing microtubule dynamics. If the amount of available tubulin dimers is lowered below the critical concentration for the given set of MAPs, microtubules depolymerize. Drugs like TBZ or nocodazole cause such decrease in concentration of free polymerization-competent tubulin dimers and consequently promote microtubule depolymerization. Although microtubules in

Dictyostelium seem very stable in length, TBZ treatment causes partial tubulin depolymerization, leaving microtubule stubs at the centrosome after treatment. This raised the question whether the significant effect of TBZ on *Dictyostelium* microtubules was due to yet unknown dynamics of microtubules in *Dictyostelium*. A GFP-α-tubulin expressing cell exhibiting the typical three-dimensional movements of interphase microtubules in *Dictyostelium* is available on CD (Mov. 9).

3.1.4.1 Live cell imaging of GFP-TACCdom reveales dynamic microtubules in *Dictyostelium*

Analyses of dynamic processes like catastrophe and rescue events of individual microtubules in GFP-α-tubulin expressing cells are complicated by the rapid three-dimensional movements of *Dictyostelium* microtubules (Koonce and Khodjakov, 2002; Brito *et al*., 2005). Therefore, additional labelling of microtubule plus ends could certainly facilitate the tracking of single microtubules. Unfortunately, microtubule plus end proteins such as DdEB1 and CP224 do not only associate to microtubule tips, but instead distribute alongside the whole microtubule when overexpressed as a GFP-fusion protein (Gräf *et al*., 2000a; Rehberg and Gräf, 2002). Overexpressed GFP-TACC and GFP-TACCdom, however, still produce specific GFP signals at microtubule plus ends, as can be seen in cells expressing GFP-TACCdom and mRFP-α-tubulin (Fig. 23). This makes TACC a promising tool to analyze microtubule dynamics in *Dictyostelium*. Unfortunately, mRFP-α-tubulin is very prone to bleaching, which usually resulted in comparably short time series.

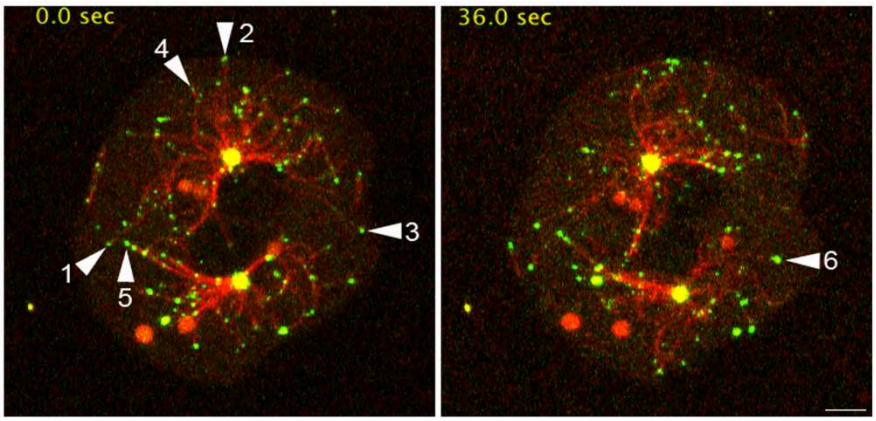

Fig. 23 Dynamic behavior of individual microtubules in the cell periphery of cells expressing mRFP-α-tubulin and GFP-TACCdom
Cells co-expressing GFP-TACCdom (green) and mRFP-α-tubulin (red) were followed by 5D confocal live cell imaging. For each time point, a z-stack consisting of 5 images with an interval of 0.5 µm was taken. Shown are maximum intensity projections of two still images of (Mov. 10). Tips of individual microtubules where movements are traceable are labeled with arrowheads. Bar = 2 µm.

In agreement with previous reports, tracking of individual microtubules revealed no complete rescue or catastrophe events (Koonce and Khodjakov, 2002). If at all, net growth of interphase microtubules could only be observed to a minor extent. In several cases, however, microtubule ends seemed to undergo movements, which distantly resembled small-scale catastrophe and rescue events alternating with high frequency. Such behavior could perfectly explain the partial sensitivity of *Dictyostelium* microtubules to TBZ and nocodazole. Due to their mode of action these agents should only affect dynamic microtubules. If the movements described above were furthermore restricted to the distal ends of microtubules, this would explain the significant microtubule stubs which are usually left at the centrosome after TBZ treatment. An example for such movements can be seen in a time series (Mov. 10) corresponding to the still images seen in Fig. 23. The arrowheads point at six microtubules that undergo movements as described. However, due to insufficient time resolution of our confocal microscopic system, distinguishing between real dynamic instability events and the extensive lateral bending movements of *Dictyostelium* microtubules was very difficult and not always unambiguously.

3.1.4.2 FRAP experiments indicate tubulin turnover at microtubule plus ends in *Dictyostelium*

To rule out misinterpretations due to lateral bending movements, *Dictyostelium* microtubule plus end dynamics was investigated by a different approach. The behavior observed in section 3.1.4.1, would have to be accompanied by rapid exchange of tubulin dimers at the

microtubule tips. To test this, FRAP of GFP-α-tubulin incorporated into microtubules close to the plus ends was monitored *in vivo*. FRAP experiments were generally conducted as described previously (section 3.1.3.3). Reliabe tracking of individual microtubules was still a difficult task and consequently only a few, yet fruitful, time series could be recorded. Upon bleaching microtubule plus ends, rapid recovery of fluorescence starting at the very tip of microtubules proceeding towards the minus end could be observed (Fig. 24). The corresponding time series is available on CD (Mov. 11).

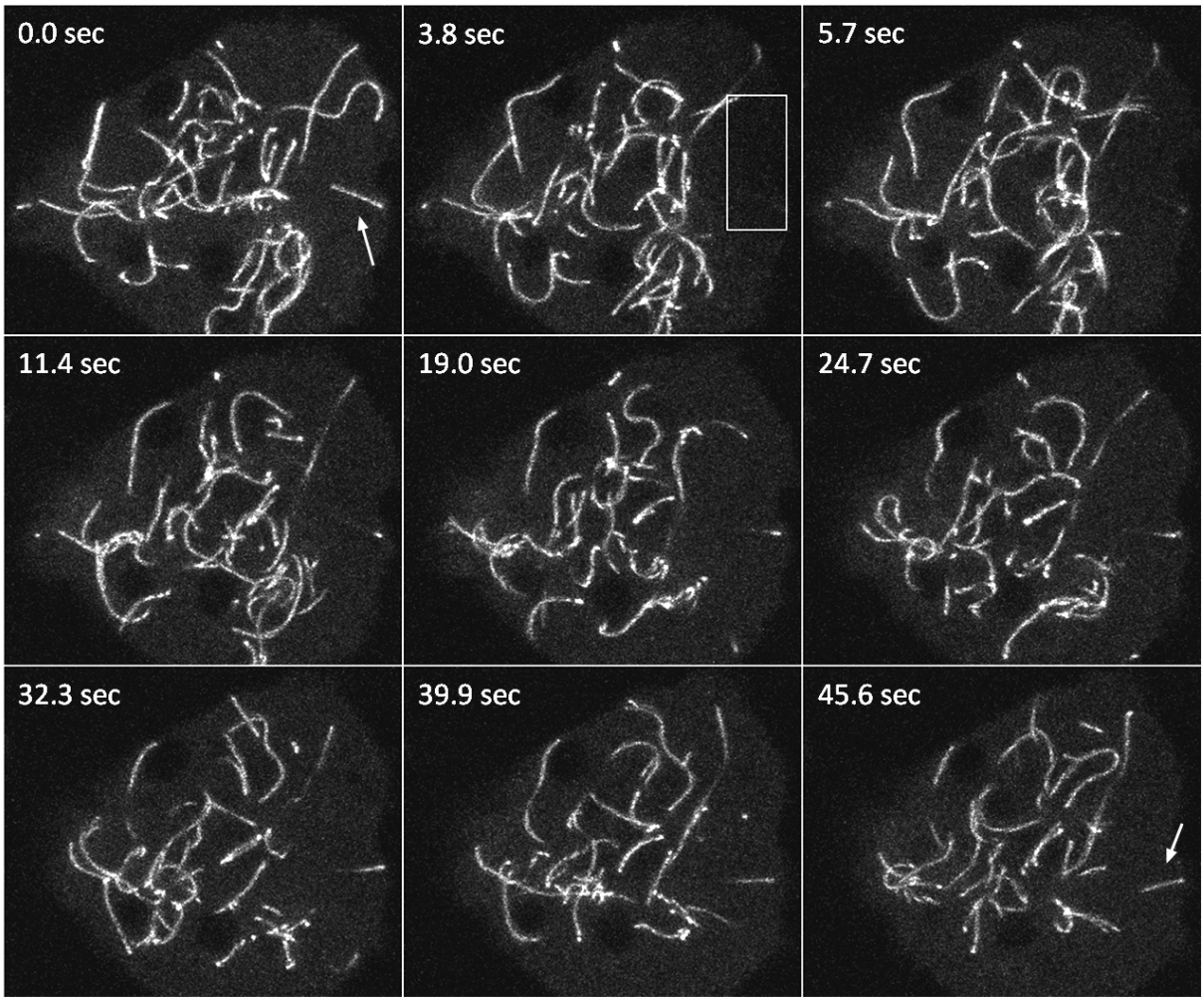

Fig. 24 *Dictyostelium* microtubules exhibit GFP-α-tubulin turnover at their plus ends
In a cell expressing GFP-α-tubulin, the region indicated by a white rectangle was bleached and monitored by 4D confocal microscopy (Mov. 11). For each time point, a z-stack consisting of 5 images with a focus step size of 0.5 µm was taken. Z-stacks recorded were chosen in the very cell periphery, which is why no centrosome is visible and microtubules cannot be traced to their minus end. The arrowheads point to a microtubule displaying rapid fluorescence recovery. The time interval is indicated on the upper left. Bar = 2 µm.

This significant turnover of incorporated tubulin dimers in the cell periphery indicates that *Dictyostelium* interphase microtubules are in fact dynamic at their plus ends, although hardly exhibiting net growth or shrinkage. The origin of this dynamic behavior might lie in rapid

changes between growth and shrinkage phases that are easily overlooked due to the much more prominent three-dimensional movements.

3.2 Investigation of centrosomal candidate proteins in *Dictyostelium*

Revealing the molecular composition of the *Dictyostelium* centrosome is an important task in the quest for a deeper understanding of this organelle. Without doubt, one of the most comprehensive approaches to identify new centrosomal proteins in *Dictyostelium* was carried out by Reinders and Schulz (Reinders *et al*., 2006). By applying differential proteomic techniques, more than 70 new candidate proteins were identified, some of which have already been confirmed as genuine centrosomal residents by cell biological and biochemical methods. Still, several candidate proteins remain to be verified. In this work the subcellular localization of three such proteins, Cenp68, Mad1 and CP103 should be elucidated and first steps to reveal their yet unknown function were conducted (Schulz *et al*., 2009b).

3.2.1 Characterization of *Dictyostelium* Cenp68

Cenp68 (Centromeric protein 68, DDB0233901) consists of 575 aa and the protein contains no conserved domains. Within 140 residues, a BLASTp search revealed 28 % amino acid identity with the *S. cerevisiae* Bbp1 protein (evalue 0,067). Bbp1 is a permanent resident of the yeast the spindle pole body (SPB) and localizes to the periphery of the central plaque. There it plays an important role in SPB duplication and in tethering the SPB to the nuclear envelope (Schramm *et al*., 2000). Cenp68 localization was addressed by expression of a GFP-fusion protein and the generation of a rabbit polyclonal antibody against Cenp68 for immunofluorescence microscopy.

3.2.1.1 GFP-Cenp68 localizes to the centromeric region

Full length Cenp68 was fused to GFP and expressed in a wild type background. Surprisingly, no GFP-Cenp68 was detected at the centrosomes. Instead, the fusion protein was strongly enriched inside the nucleus (Fig. 25 A-D). There it predominately localized to a major spot opposite to the centrosome, where, in interphase cells, the *Dictyostelium* centromeres are tightly clustered and retained by a physical link with the centrosome (Eichinger *et al*., 2005; Kaller, 2006; Schulz *et al*., 2009a). GFP-Cenp68 fusion protein outside this cluster was uniformly distributed throughout the nucleoplasm. In late G2 cells the tight cluster spilt up

and up to six single foci, presumably representing the six *Dictyostelium* centromeres, could be counted (Fig. 25 E-H). While in prophase and prometaphase, the GFP-Cenp68 foci were still arranged around the centrosome, they were found to be aligned in the center of the spindle during metaphase. In anaphase the foci divided and moved towards the spindle poles, with which they remained attached throughout telophase. This staining pattern strongly resembles the one described for the three established centromeric proteins known in *Dictyostelium,* hcpA, hcpB and CenH3 (Kaller *et al*., 2006; Dubin *et al*., 2010). Some of the cells shown in Fig. 25 seem to be diploid cells. In these cases, of course, twice the number of centromeres can be distinguished. Interestingly, during prometaphase the majority of GFP-Cenp68, which is not associated with the centromeres, rapidly exits the nucleus. This observation is consistent with previous reports of hcpA/B-GFP and GFP fused to a nuclear localization signal (Zang *et al*., 1997; Kaller *et al*., 2006) and suggests that although *Dictyostelium* undergoes a closed mitosis, the *Dictyostelium* nuclear envelope becomes permeabilized in prophase. It is tempting to speculate that in the amoebae, this process takes place in a similar manner as in *Aspergillus nidulans*, where permeabilization of the nuclear envelope during a closed mitosis is mediated by partial disassembly of the nuclear pore complexes (De Souza *et al*., 2004). Time series of mitotic cells expressing GFP-Cenp68 and cherry-histone 2B are available as Mov. 12 and 13.

Fig. 25 (next page) GFP-Cenp68 associates with the centromeres throughout the cell cycle
GFP-Cenp68 (A, E, I, M, Q, U, Y, CC and green in merged images) expressing cells were fixed with glutaraldehyde (E-FF) or methanol (A-D) and were stained with anti-tubulin (F, J, N, R, V, Z, DD and red in merged images), anti-CP224 (B) and DAPI (C, G, K, O, S, W, AA, EE and blue in merged images). Mitotic stages are indicated on the left. Bar = 2 µm.

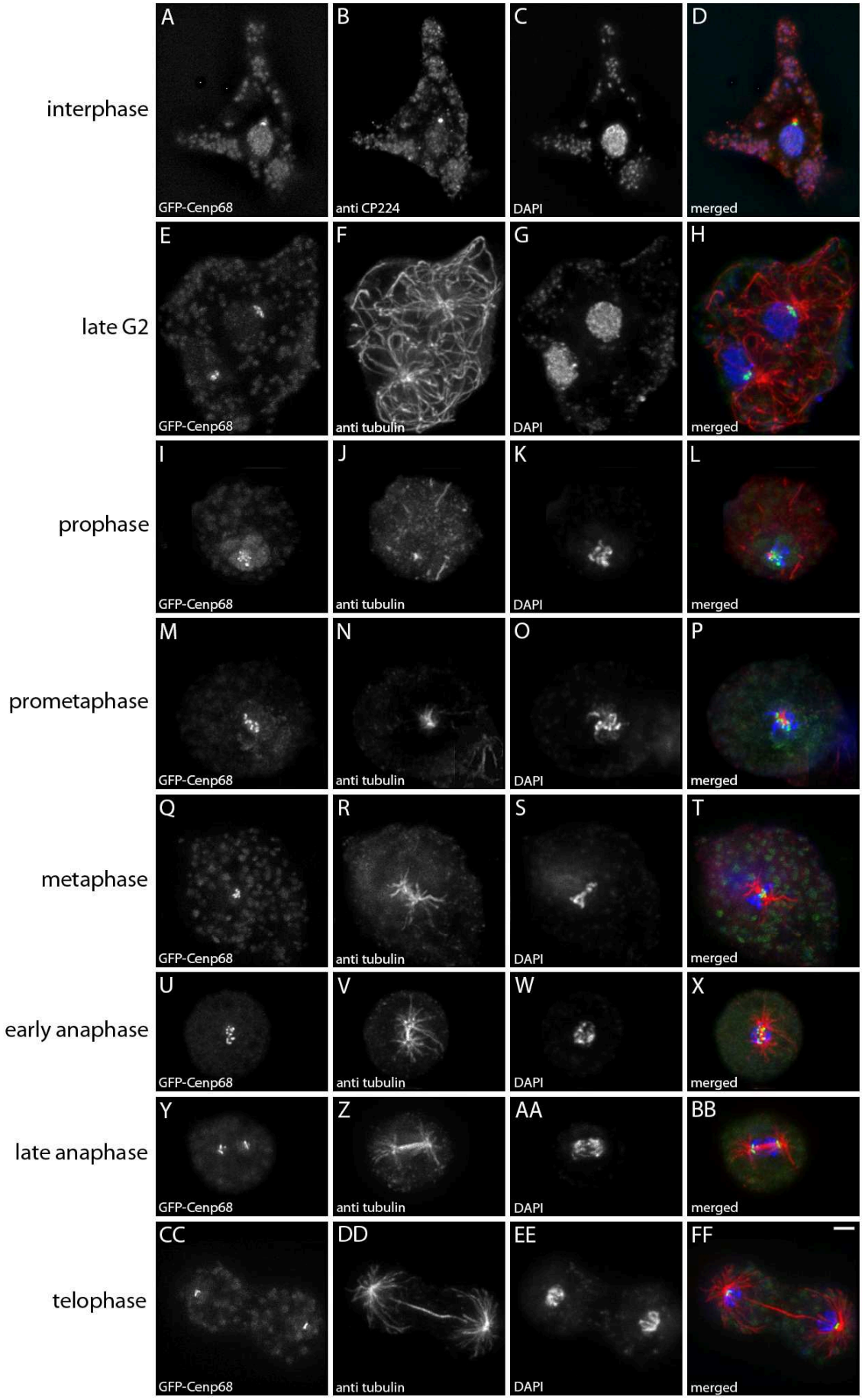
interphase
A
GFP-Cenp68
B
anti CP224
C
DAPI
D
merged
late G2
E
GFP-Cenp68
F
anti tubulin
G
DAPI
H
merged
prophase
I
GFP-Cenp68
J
anti tubulin
K
DAPI
L
merged
prometaphase
M
GFP-Cenp68
N
anti tubulin
O
DAPI
P
merged
metaphase
Q
GFP-Cenp68
R
anti tubulin
S
DAPI
T
merged
early anaphase
U
GFP-Cenp68
V
anti tubulin
W
DAPI
X
merged
late anaphase
Y
GFP-Cenp68
Z
anti tubulin
AA
DAPI
BB
merged
telophase
CC
GFP-Cenp68
DD
anti tubulin
EE
DAPI
FF
merged

3.2.1.2 Generation of a rabbit polyclonal anti-Cenp68 antibody

The behavior of GFP-Cenp68 suggested Cenp68 to be a centromere- or pericentromeric heterochromatin-specific protein. However, it cannot be excluded that the GFP-tag interfered with Cenp68 localization to centrosomes in above described experiments (3.2.1.1). In order to elucidate endogenous Cenp68 localization and to be able to conduct colocalization studies with other centromeric proteins, a rabbit polyclonal antibody was generated. Thus, Cenp68 was expressed as an MBP-fusion protein in *E.coli* (Fig. 26 A) and the recovered protein was used to raise antibodies in rabbits. In immunoblotting and immunofluorescence experiments the antisera did not produce satisfying results. Therefore, they were affinity purified using MBP-Cenp68 protein coupled to NHS-activated sepharose. In Western blot analyses, the purified antibody recognized a single ~80 kDa band of endogenous Cenp68 and the GFP-fusion protein (Fig. 26 B). Furthermore, it nicely stained the centromeric region in immunofluorescence experiments with only minor background.

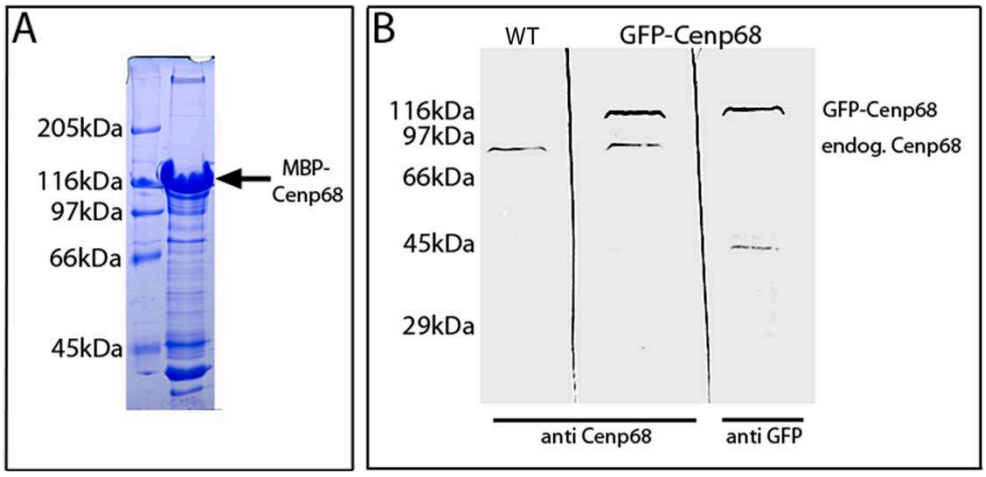

Fig. 26 The Cenp68 antibody recognizes a single band at ~80 kDa
(**A**) Expression of full length Cenp68 as MBP-fusion protein. MBP-Cenp68 was purified, subjected to SDS-PAGE and stained with Coomassie. The prominent band at ~116 kDa corresponds to MBP-Cenp68. Molecular weight is shown on the left. (**B**) Endogenous Cenp68 and GFP-Cenp68 is detected by affinity purified Cenp68 antibody. Whole cell lysates of strains as indicated on top of the respective lanes were subjected to SDS-PAGE and immunoblotting. Antibodies used are indicated on bottom. Molecular weight is shown on the left.

These experiments also demonstrated that Cenp68 is actually expressed in vegetative *Dictyostelium* wild type cells. As the GFP-Cenp68 fusion protein, the purified antibody did not label centrosomes in immunofluorescence analyses. Since the results of localization

studies performed with the Cenp68 antibody are virtually identical to those using the GFP-fusion protein, these images are not shown in this section. However, Fig. 32 in section 3.2.2, which deals with the investigation of the kinetochore protein Mad1, shows a set of images using the Cenp68 antibody that covers the entire cell cycle.

To date, the Cenp68 antibody is the only existing antibody directed against a constitutive centromere- or pericentromeric heterochromatin-specific *Dictyostelium* protein and has proven to be a useful tool for the investigating of centromere behavior in the amobae. This became evident when the Cenp68 antibody allowed the detection of centromere dislocation upon overexpression of the nuclear membrane protein Sun1 (Schulz *et al*., 2009a).

3.2.1.3 Cenp68 colocalizes with hcpA and hcpB

The *Dictyostelium* HP1 protein homologues hcpA and hcpB were shown to permanently associate with the prominent cluster of pericentromeric heterochromatin, which flanks the CenH3-containing core centromeric chromatin. Both proteins were furthermore found in smaller spots of constitutive heterochromatin in other nuclear regions (Kaller *et al*., 2006; Dubin *et al*., 2010). Therefore, the two proteins are perfect candidates to verify the centromeric localization of Cenp68. Strains expressing GFP-fusion proteins of hcpA and hcpB were kindly provided by Prof. Wolfgang Nellen (Universität Kassel). In immunofluorescence experiments, the Cenp68 antibody signal clearly colocalized with that of hcpA-GFP and hcpB-GFP, regardless of whether the centromeres were tightly clustered as in interphase cells, or split up as in late G2 cells (Fig. 27). However, although the three proteins always exhibited the same staining pattern, Cenp68 and hcpA/B-GFP signals did not match perfectly in some cases. It remains to be tested whether this could be due to the association with distinct centromeric chromatin regions such as core centromeres and pericentromeric heterochromatin. Importantly, while hcpA and hcpB localized to additional foci of constitutive heterochromatin (Kaller *et al*., 2006) (Fig. 27, arrowheads), Cenp68 was never found in these spots. This finding clearly argues against Cenp68 to be a heterochromatin-specific protein.

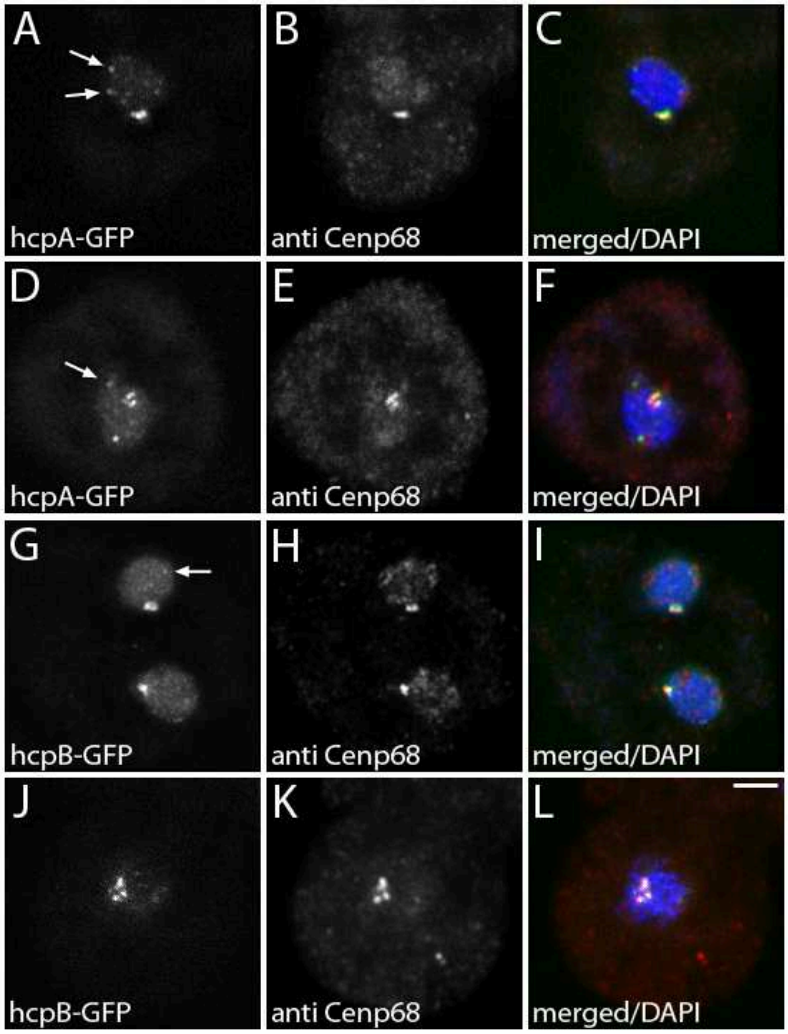

Fig. 27 Cenp68 colocalizes with hcpA and hcpB
HcpA-GFP (A-F) and hcpB-GFP expressing cells (G-L) were fixed with glutaraldehyde and stained with anti-Cenp68 (B, E, H, K and red in merged images). HcpA-GFP is shown in (A, D and green in C, F) and hcpB-GFP in (G, J and green in I, L). Selected examples of hcp-protein localization to non-pericentromeric heterochromatin are indicated with arrowheads. Endogenous Cenp68 is not enriched in these foci. Strains expressing hcpA-GFP and hcpB-GFP were kindly provided by Prof. Wolfgang Nellen (Universität Kassel). DNA is shown in blue. Bar = 2 µm.

3.2.1.4 Generation of a Cenp68 knockout strain

In order to get first insights in Cenp68 function, a knockout mutant was created. This was achieved by transformation of a linearized targeting vector, essentially comprising a blasticidin resistance cassette (bsr cassette) flanked by genomic Cenp68 sequences (Fig. 28 A) (section 2.3.15). In the resulting knockout strains, the majority of the chromosomal Cenp68 coding sequence was replaced by the bsr cassette in a homologous recombination event. Primer combinations used to identify potential knockout clones by PCR were selected as indicated in Fig. 28 A. In this way, a total of three Cenp68 null mutant strains could be isolated that were obviously not contaminated with wild type cells (Fig. 28 B, C). Disrupted Cenp68 expression was furthermore verified on protein level (Fig. 28 D).

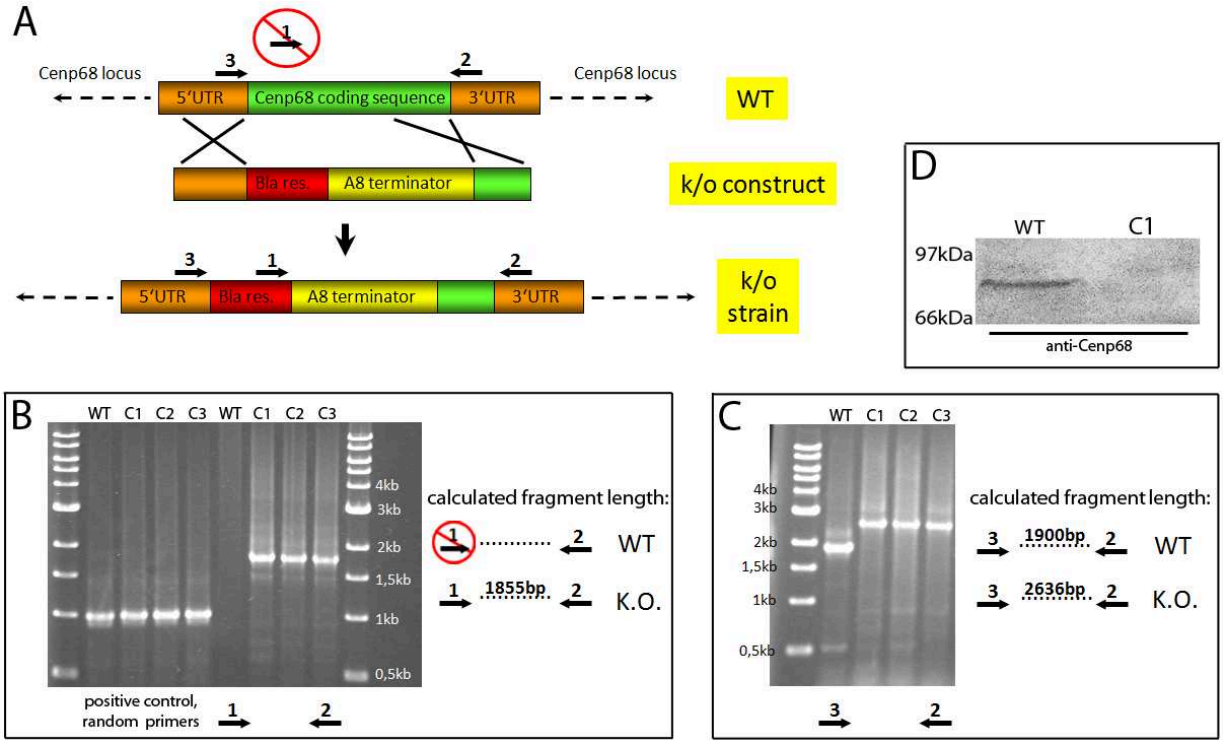

Fig. 28 Generation of a Cenp68 knockout mutant by homologous recombination
(**A**) Shown is s schematic of a homologous recombination event to knock out Cenp68. In such events, the wild type coding sequence is largely replaced by a bsr cassette (depicted as Bla res. and A8 terminator), which abrogates Cenp68 expression and confers resistance to blasticidin. Arrows indicate the binding sites of primers 1-3 used to screen for specific integration of the resistance cassette. (**B**, **C**) Specific integration of the bsr cassette at the Cenp68 locus was verified by PCR. Primer combinations used to identify k/o clones are depicted on the right of the respective gels together with the calculated fragment lengths to identify either wild type or k/o strains. Oligonucleotide names and sequences corresponding to primers 1-3 are listed in section 2.3.15. PCR products loaded are shown on bottom and the tested strains are indicated on top. (**D**) To confirm absence of Cenp68 on protein level, a western blot of whole cell lysates was stained with anti-Cenp68. Molecular weight is shown on the left and strains used are indicated on top of the respective lanes.

3.2.1.5 Cenp68 knockout cells do not exhibit an obvious phenotype

Despite being expressed in vegetative wild type cells, absence of Cenp68 protein did not lead to any obvious perturbations. The weakly homologous protein Bbp1 from *S. cerevisiae* is involved in connecting the SPB to the nucleus. However, the centrosome-nucleus distance in Cenp68 mutants was found to be normal, indicating that Cenp68 is not involved in a similar process (Fig. 29 A-C). In order to visualize the centromeres in Cenp68 null cells, an antibody directed against human heterochromatin-specific histone H3 tri-methylated at lysine 9 (H3K9me3) was used in immunofluorescence experiments. The specificity of the H3K9me3 antibody in *Dictyostelium* has recently been proven (Ph.D. thesis of Manu Dubin, 2010, Universität Kassel). As seen in Fig. 29 A-C, centromeres are normally clustered in the absence of Cenp68 and, as centromeres in wild type cells, seem to be connected to the centrosome. Moreover, GFP-hcpB localized perfectly normal in Cenp68 mutants (Fig. 29 D-

F). Taken together, examination of the Cenp68 knockout strain could not shed light on Cenp68 function.

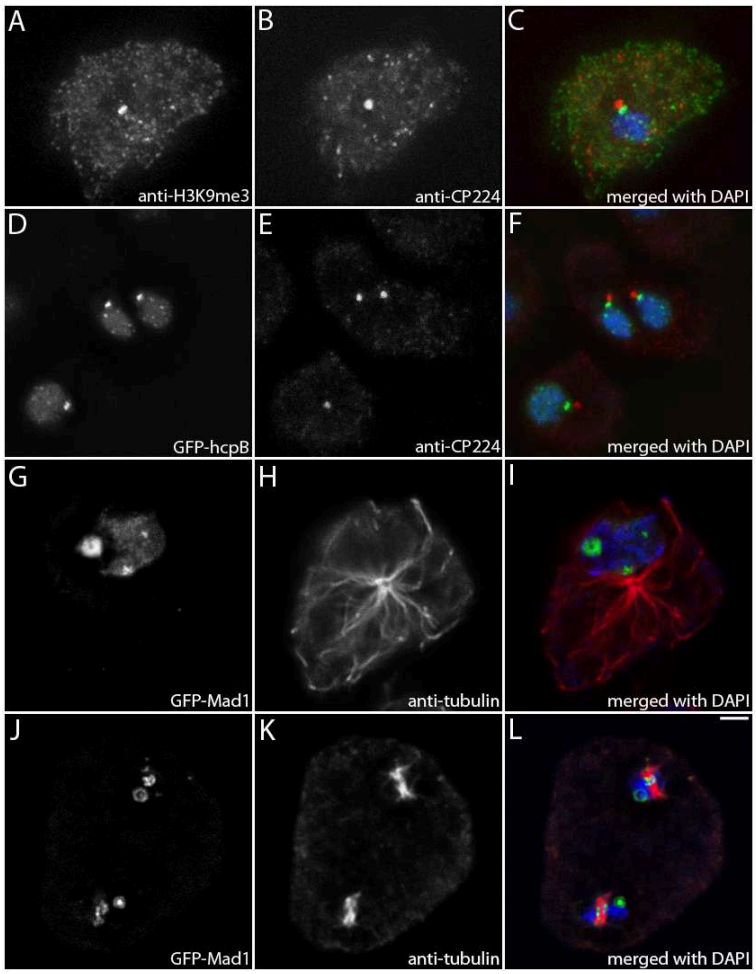

Fig. 29 Centromere clustering is not affected in the absence of Cenp68, and GFP-hcpB and GFP-Mad1 are normally recruited to the centromeres in the knockout strain
Centromeres are normally clustered and associated with the centrosome in Cenp68 mutants. Cenp68 knockout cells were fixed with methanol and stained with anti-H3K9me3 (A, green in C) and anti-CP224 (B, red in C). To investigate recruitment of hcpB to the centromeres in the absence of Cenp68, the knockout cells were transfected with GFP-hcpB (D, green in F), fixed with methanol and stained with anti-CP224 (E, red in F). GFP-Mad1 association with kinetochores is not impaired upon Cenp68 knockout in late G2 (G-I) and early metaphase cells (J-L). Cenp68 mutants were transfected with GFP-Mad1 (G, J and green in I, L), fixed with glutaraldehyde and stained with anti-tubulin (H, K and red in I, L). DNA is shown in blue. Bar = 2 µm.

3.2.1.6 Revealing potential interaction partners of Cenp68

To approach the investigation of Cenp68 function in a different way, a search for potential interaction partners of Cenp68 was conducted. To do this, the GFP-nanotrap protocol was chosen, which advantageously involves the expression of the bait protein fused to GFP (Rothbauer *et al*., 2008) (section 2.4.12). Unfortunately, after the purification process, the yielded eluates frequently contained a multitude of non-specific contaminants, thus causing substantial background. Therefore, in the case of GFP-Cenp68, only two bands were excised, one of which could be successfully identified by MALDI-TOF mass spectrometry (Fig. 30 A, arrowhead). MALDI-TOF analyses were kindly carried out by Dr. Jörg Fettke (Universität Potsdam, group of Prof. Martin Steup).

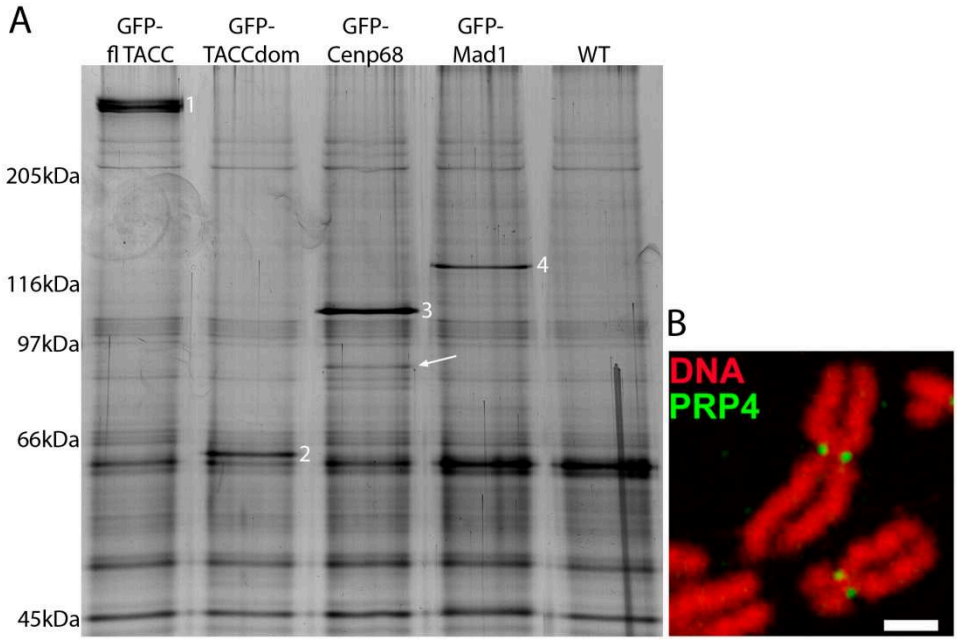

Fig. 30 The nanotrap assay reveals a potential interaction between Cenp68 and prpf4B
(**A**) Eluates collected after nanotrap experiments were subjected to SDS-PAGE and silver-stained. By contrast, gels whose bands were analyzed by mass spectromerty were stained with colloidal Coomassie. The nanotrap assay was carried out using various GFP-fusion proteins, however, the only promising result was yielded for GFP-Cenp68. Examples in this figure include GFP-full length TACC (depicted as 1), GFP-TACCdom (depicted as 2), GFP-Cenp68 (depicted as 3) and GFP-Mad1 (depicted as 4). The band marked with an arrowhead was exclusively found when GFP-Cenp68 was used as bait. This band was identified as prpf4B. Molecular weight is shown on the left and strains used are indicated on top of the respective lanes. (**B**) The human homologue of prpf4B localizes to the kinetochores of isolated chromosomes from mitotic HeLa cells. Image is taken from Montembault *et al*. (2007). Bar = 2 µm.

This band was found to correspond to the prpf4B protein (Pre-mRNA Processing Factor 4 homolog B**,** DDB0216281), a putative homologue of the mammalian serin/threonine prp4 kinase. In *Dictyostelium* this kinase has not been investigated in depth, but mammalian counterparts were shown to be constituents of the nuclear speckles and to be involved in pre-mRNA splicing (Kojima *et al*., 2001; Dellaire *et al*., 2002). It is known that splicing factors are frequent contaminators in such approaches, however, *Dictyostelium* prpf4b was never identified in comparable assays conducted in our group before (Dr. Katrin Pfütze, unpublished). More importantly, in HeLa cells, this kinase was found to localize to the kinetochores and to be essential for the recruitment of SAC proteins Mps1, Mad1 and Mad2 (Montembault *et al*., 2007) (Fig. 30 B). Coincidentally, the putative *Dictyostelium* homologue of Mad1 (DDB0304834) was one of the proteins that should be investigated for association with the centrosome (section 3.2.2). Although a direct role of the constitutive centromeric protein Cenp68 in the spindle assembly checkpoint does not seem very likely, it was tested whether GFP-Mad1 is normally targeted to the kinetochores in the absence on Cenp68.

Expectedly, Cenp68 deletion did not alter GFP-Mad1 localization in late G2 (Fig. 29 G-I) and early metaphase cells (Fig. 29 J-L).

3.2.1.7 Prpf4B does not specifically localize to centromeres and kinetochores

Interaction between two proteins requires colocalization. In order to reveal whether prpf4B and Cenp68 colocalize at centromeres or kinetochores, full length prpf4B was C-terminally fused to GFP and expressed in wild type cells. During interphase, GFP-prpf4B was found to be irregularly distributed throughout the nucleoplasm, however, without resembling the staining pattern of nuclear speckles (Fig. 31 A-C). During mitosis, the GFP-prpf4B signal appeared more homogeneously and the fusion protein seemed to partially exit the nucleus without associating with any specific structure (Fig. 31 D-F). At no time GFP-prpf4B was found to be specifically enriched in the centromeric region, which does not support the idea of Cenp68 and prpf4B interaction. Unfortunately, Co-IP experiments to investigate a putative interaction between the two proteins failed due to rapid degradation of the GFP-prpf4B fusion protein in cell lysates. Furthermore, a yeast two-hybrid assay using the LexA system failed to confirm interaction between the two proteins (not shown). Based on these observations, a direct interaction between Cenp68 and prpf4B is unlikely.

Finally, it has to be mentioned that expression of GFP-prpf4B seems to cause phenotypes such as the occurrence of multinucleated cells and the enlargement of nuclei, which frequently are associated with more than one centrosome (Fig. 31). These phenotypes, however, were not evaluated statistically and not pursued further.

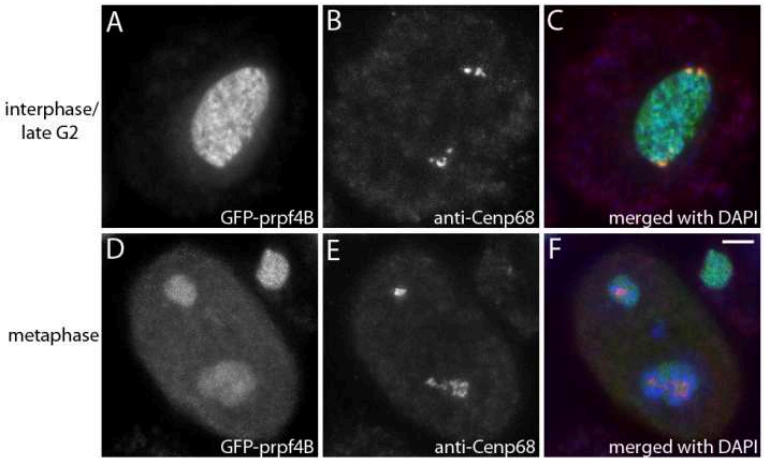

Fig. 31 Prpf4b is a nuclear protein that does not specifically associate with centromeres or kinetochores
Shown is an interphase (A-C) and metaphase (D-F) cell expressing GFP-prpf4B (A, D, green in merged images). Cells were fixed with glutaraldehyde and stained with anti-Cenp68 to visualize the centromeres/kinetochores (B, E, red in merged images). DNA is shown in blue. Bar = 2 µm.

3.2.2 Investigation of the putative *Dictyostelium* Mad1 homologue

Dictyostelium Mad1 (Mitotic arrest deficient 1, DDB0304834) is a ~96 kDa protein that shares 35 % amino acid identity with human Mad1 within its 200 C-terminal residues (evalue 0,0018). As Cenp68, it was identified as potential centrosomal component (Reinders *et al*., 2006). To investigate whether *Dictyostelium* Mad1 localizes to the centrosome or, as other Mad1 homologues, is a SAC protein that associates with unattached kinetochores in late prophase (Howell *et al*., 2004), a GFP-Mad1 fusion protein was expressed in wild type cells. During interphase GFP-Mad1 was found to be enriched inside the nucleus, where it was uniformly distributed throughout the nucleoplasm (Fig. 32 A-D). Most interphase nuclei, however, contained small aggregates of GFP-Mad1 that did not associate with any specific structure and strongly varied in size and number depending on the degree of overexpression (Fig. 32, arrowhead in A). Association of GFP-Mad1 with centromeres/kinetochores could first be observed in late G2 cells and persisted throughout prophase and prometaphase (Fig. 32 E-P). In most metaphase cells, Mad1 was still found to be present at kinetochores, however, the GFP signal intensity was frequently weaker and in some cases only a subset of kinetochores exhibited GFP fluorescence (Fig. 32 Q-X). In other organisms, Mad1 is sequestered from kinetochores upon attachment of spindle microtubules (Waters *et al*., 1998; Musacchio and Salmon, 2007). If a similar mechanism existed in *Dictyostelium*, this might lead to a staining pattern as seen in Fig. 32 U (arrowhead).

Fig. 32 (next page) *Dictyostelium* Mad1 is a putative SAC protein that associates with centromeres/kinetochores in late G2, and is sequestered from kinetochores during metaphase
GFP-Mad1 expressing cells were fixed with glutaraldehyde and stained with anti-Cenp68 to visualizes kinetochores (B, F, J, N, R, V, Z, DD, red in merged images C, G, K, O, S, W, AA, EE), anti-tubulin (red in merged images D, H, L, P, T, X, BB) and anti-CP224 (red in merged image FF). GFP-Mad1 is shown in (A, E, I, M, Q, U, Y, CC and green in merged images). The arrowhead in (A) points to a typical interphase aggregate of GFP-Mad1, and the arrowhead in (U) points to GFP-Mad1 that is clearly concentrated at three individual metaphase kinetochores, while it is absent from all others. A weak GFP-Mad1 signal can be observed at the spindle poles during telophase (CC). The cell cycle stage is indicated on the left, DNA is shown in blue. Bar = 2 µm.

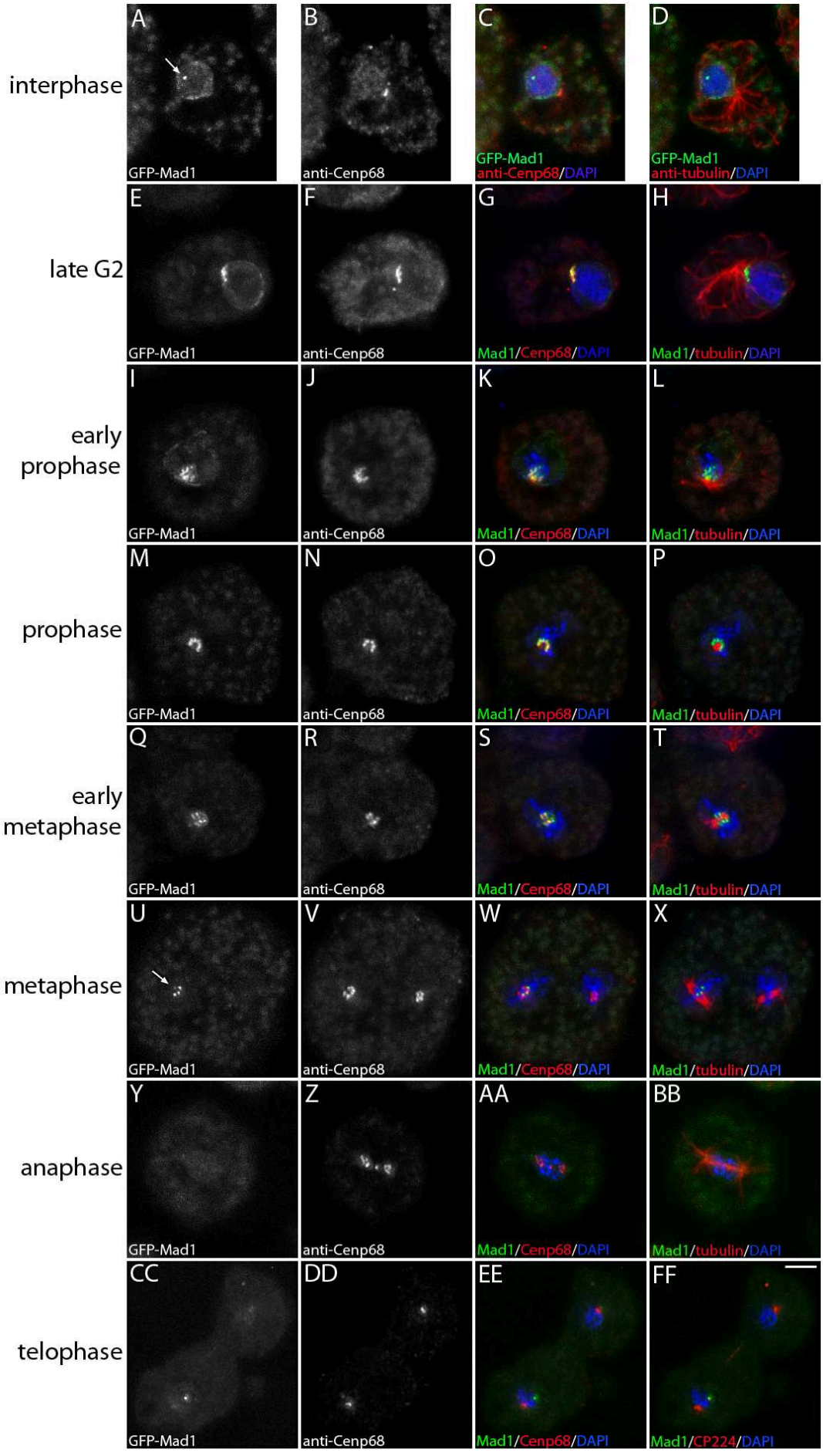
interphase
A
GFP-Mad1
B
anti-Cenp68
C
GFP-Mad1
anti-Cenp68/DAPI
D
GFP-Mad1
anti-tubulin/DAPI
late G2
E
GFP-Mad1
F
anti-Cenp68
G
Mad1/Cenp68/DAPI
H
Mad1/tubulin/DAPI
early prophase
I
GFP-Mad1
J
anti-Cenp68
K
Mad1/Cenp68/DAPI
L
Mad1/tubulin/DAPI
prophase
M
GFP-Mad1
N
anti-Cenp68
O
Mad1/Cenp68/DAPI
P
Mad1/tubulin/DAPI
early metaphase
Q
GFP-Mad1
R
anti-Cenp68
S
Mad1/Cenp68/DAPI
T
Mad1/tubulin/DAPI
metaphase
U
GFP-Mad1
V
anti-Cenp68
W
Mad1/Cenp68/DAPI
X
Mad1/tubulin/DAPI
anaphase
Y
GFP-Mad1
Z
anti-Cenp68
AA
Mad1/Cenp68/DAPI
BB
Mad1/tubulin/DAPI
telophase
CC
GFP-Mad1
DD
anti-Cenp68
EE
Mad1/Cenp68/DAPI
FF
Mad1/CP224/DAPI

During anaphase and telophase GFP-Mad1 was absent from kinetochores in most cells observed. In some strongly overexpressing cells, however, a weak signal remained and little GFP-Mad1 could also be observed at the spindle poles during late mitotic stages. It remains to be tested whether this observation is merely an overexpression artifact or if endogenous Mad1 in a wild type background also associates with the centrosome in anaphase and telophase. Such behavior would be consistent with the fact that several SAC proteins, including Mad2, were reported to be stripped from kinetochores and transported towards the spindle poles in a dynein-dependent manner (Howell *et al*., 2001; Wojcik *et al*., 2001; Basto *et al*., 2004; Howell *et al*., 2004). This process was shown to be crucial for the SAC inactivation. A time series of a mitotic *Dictyostelium* cell co-expressing GFP-Mad1 and cherry-histone 2B, which confirms GFP-Mad1 behavior as observed in fixed cells, is available on CD (Mov. 14).

3.2.3 CP103 is a genuine centrosomal component

Dictyostelium CP103 (Centrosomal protein 103, DDB0304837) is a 103 kDa protein that contains a domain characteristically for ZW10 proteins (Zeste white 10), a family of conserved kinetochore-associated proteins. These were shown to play differential roles in interphase and mitosis. In mitotic animal cells, ZW10 is part of the Rod/ZW10/Zwilch (RZZ) complex that is essential for the targeting of SAC components Mad1/Mad2 and the dynein-dynactin complex to kinetochores (Starr *et al*., 1998; Kops *et al*., 2005b). Interestingly, by providing a connection with dynein-dynactin, the RZZ complex is also necessary for sequestering SAC proteins from kinetochores after spindle microtubule attachment. By contrast, during interphase, ZW10 proteins are part of a vesicle tethering complex, termed Dsl1 in yeast and syntaxin18 in mammals. These complexes reside at the ER membrane and assist in membrane trafficking between the ER and the Golgi apparatus (Vanrheenen *et al*., 2001; Hirose *et al*., 2004).

To elucidate *Dictyostelium* CP103 localization, a GFP-fusion protein was expressed in wild type cells. During interphase and mitosis GFP-CP103 was found to associate with the centrosome and spindle poles, respectively (Fig. 33 A-F). Centrosomal GFP-signals exhibited a donut shaped appearance (Fig. 33 J, K), indicating CP103 localization to the centrosomal corona. Although a weak nuclear staining could be observed in most cells, GFP-CP103 was not found to be enriched in the centromeric/kinetochore region at any time. This finding certainly does not support a role of ZW10 in targeting SAC components to kinetochores in

Dictyostelium. *Bona fide* centrosomal components are considered to associate with the centrosome independently of microtubules (Gräf *et al*., 1998). In order to prove that CP103 is a genuine centrosomal protein, its presence at microtubule free, isolated centrosomes had to be demonstrated. Thus, centrosomes of a GFP-CP103 expressing strain were isolated (see section 2.4.10), fixed with methanol and counterstained for CP224 as a marker for the centrosomal corona (Gräf *et al*., 1999; Gräf *et al*., 2000a). As seen in Fig. 33 G-I, GFP-CP103 is clearly associated with isolated centrosomes. A plot showing the spatial distribution of fluorescence intensity along a line through the center of a representative centrosome, demonstrates subcentrosomal colocalization of GFP-CP103 with the corona marker CP224 (Fig. 33 J, K).

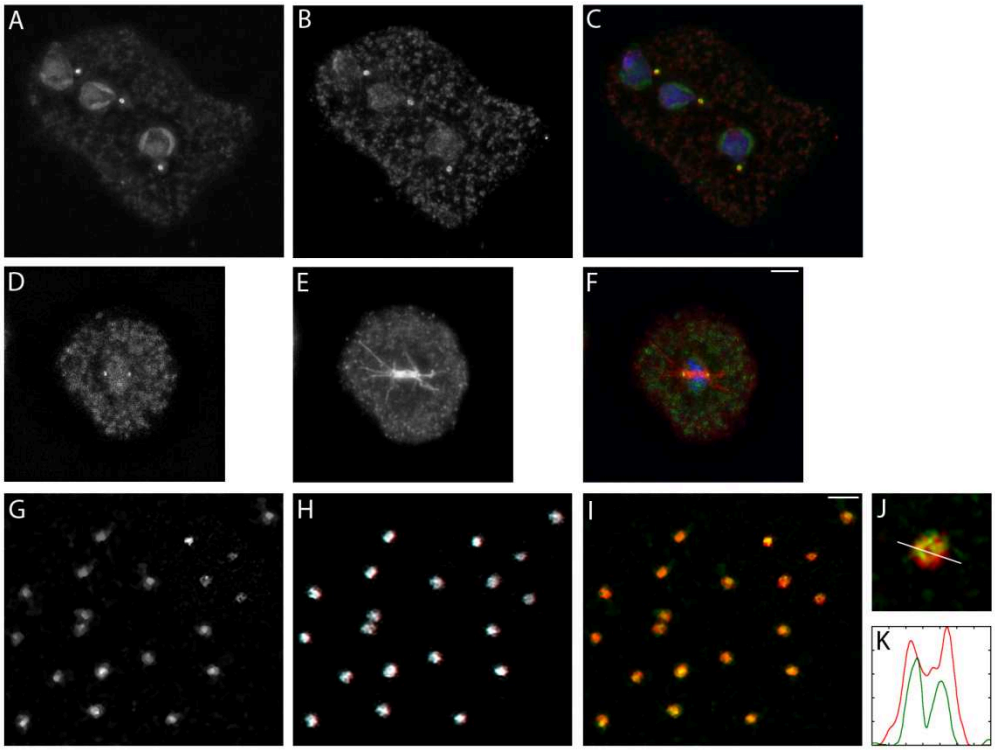

Fig. 33 CP103 is a genuine centrosomal corona protein
Shown is an interphase (A-C) and metaphase (D-F) cell expressing GFP-CP103 (A, D, green in merged images). Cells were fixed with methanol and stained with anti-CP224 (B and red in C) or anti-tubulin (E and red in F). GFP-CP103 localizes to the centrome in interphase and to spindle poles during mitosis. Throughout the cell cycle, GFP-CP103 is weakly enriched in the nucleus. DNA is shown in blue. Bar = 2 µm (A-F). Isolated centrosomes of cells expressing GFP-CP103 (G-I) were centrifuged onto a cover slip, fixed with methanol and stained with the corona marker anti-CP224 (H, red in I, J). GFP-CP103 (G, green in I, J) is clearly associated with microtubule free, isolated centrosomes. An intensity distribution plot (K) along an axis through the center of a centrosome (J), demonstrates colocalization of GFP103 (green in K) with CP224 (red in K) in the centrosomal corona. Bar = 1 µm (G-I). Modified from Schulz *et al*. (2009b).

Unfortunately, to date, all attempts to investigate CP103 function by creating a knockout strain failed. Moreover, interaction studies using the GFP-nanotrap protocol with GFP-CP103 as bait did not yield any plausible candidate proteins. Thus, CP103 function remains unknown.

4 Discussion

4.1 Characterization of *Dictyostlium* TACC

4.1.1 TACC localization

Endogenous TACC, GFP-full length TACC and GFP-TACCdom could be shown to associate with the centrosome throughout the cell cycle and with the microtubule plus ends during interphase (Figs. 5, 6, 7). Besides D-TACC, *Dictyostelium* TACC is the only TACC family protein known to bind to microtubule tips *in vivo* (Lee *et al*., 2001). Surprisingly, except at kinetochore microtubules, TACC was not found at microtubule tips during mitosis, when microtubule growth in *Dictyostelium* peaks (Fig. 7). A GFP-fusion protein lacking the TACC domain did not localize to any specific structure (Fig. 6). This finding is consistent with results from other organisms, where the TACC domain alone is sufficient and necessary for correct TACC localization (Gergely *et al*., 2000b; Peset *et al*., 2005).

Throughout the entire cell cycle, the TACC localization pattern perfectly matches that of its conserved interaction partner CP224 (Fig. 8). The strong interplay between both proteins is further underlined by the occurrence of aggregates consisting of TACC and CP224 during mitosis. These aggregates varied in size and number and could be found in many mitotic wild type and GFP-TACC expressing cells, while they usually did not form during interphase. Examples can be seen in Fig. 7. Strong overexpression of GFP-TACCdom, however, gave rise to the formation of aggregates during interphase as well (Fig. 9, 0s). This is consistent with observations in HeLa cells, where overexpressed human TACC proteins assembled into highly ordered cytoplasmic polymers that strongly interacted with ch-TOG, the human XMAP215 homologue (Gergely *et al*., 2000a). In wild type cells, this mechanism might serve to sequester excess CP244 and TACC protein in the cytoplasm, which is released from microtubule plus ends upon entry into mitosis.

In early prophase, CP224 and TACC were shown to be released from the plus ends of remaining interphase microtubules that are still attached to the centrosome (Fig. 7 A-C and Fig. 8 B, G, L). Consequently, the two proteins are not lost passively from microtubule tips upon depolymerization of interphase microtubules, but instead actively dissociate from the plus ends of existing microtubules in synchrony with the onset of mitosis. It is tempting to speculate that this behavior is part of a microtubule destabilizing process prior to complete disintegration of interphase microtubules in late prophase. Here, as in TACC-RNAi cells,

absence of CP224 and TACC from microtubule plus ends might cause microtubule destabilization. In fact, there is a short period in early prophase of wild type cells, which is characterized by the occurrence of shortened microtubules that strongly resemble the ones of TACC-RNAi cells during interphase (Mov. 15) (Rehberg *et al*., 2005). After mitosis, loading of CP224 and TACC back onto microtubule plus ends takes place in a similar direct manner as their dissociation in early prophase. Both proteins are not associated with the plus ends of growing telophase astral microtubules that eventually constitute the interphase microtubules once M-Phase has ended (Fig. 7 S-U and 8 E, J, O). Furthermore, live cell imaging of later mitotic stages in GFP-TACC expressing cells revealed that the typical staining pattern of microtubule plus end proteins cannot be observed until mitosis has ended (Mov. 16). Since no signs of plus end-directed transport of TACC or CP224 along the microtubules could be observed, this suggests that CP224 and TACC are recruited to microtubule tips directly from the cytoplasm rather than from their respective centrosomal pool. Consequently, CP224 and TACC seem to be able to dock on and off the microtubule plus ends independently of the centrosome. Investigation of TACC and CP224 turnover at microtubule tips by FRAP analysis could shed further light on plus end dynamics of these proteins. Unfortunately, however, all attempts to address this issue failed due to the limitations of the available microscopic systems or insufficient labeling of mictotubule plus ends by the GFP-fusion proteins.

4.1.2 Regulation of *Dictyostelium* TACC

Several observations suggest tight cell cycle-dependent regulation of *Dictyostelium* TACC properties. These include the simultaneous release of GFP-TACC from microtubule tips at G2/M, the occurrence of cytoplasmic TACC protein aggregates in wild type cells exclusively during mitosis and the enrichment of TACC at the centrosome in prophase (Figs. 7, 9). To date, no protein has been identified that triggers these events. However, in all other organisms investigated so far, TACC proteins were shown to be regulated through phosphorylation by their conserved interaction partner Aurora A (Peset and Vernos, 2008). The latter proteins are serin/threonine kinases that were shown to be active predominantly at centrosomes in G2- and M-Phase, and to play crucial roles in processes like centrosome maturation, centrosome separation and spindle assembly (Barr and Gergely, 2007). With regard to regulating TACC function, Aurora A was shown to mediate TACC recruitment to the centrosome during mitosis in several organisms. Evidence for this comes from the finding that phosphorylated

TACC is predominantly localized to the spindle poles and that TACC proteins are not efficiently recruited to the centrosome in Aurora A mutants (Giet *et al*., 2002; Barros *et al*., 2005; Kinoshita *et al*., 2005; Peset *et al*., 2005). Furthermore, mutation within the conserved Aurora A consensus sequence abrogates TACC localization to centrosomes (Peset *et al*., 2005). Since recruitment to the mitotic centrosome and sudden changes in TACC properties in G2/M could also be observed for *Dictyostelium*, a similar way of governing TACC function by phosphorylation seemed conceivable in the amoebae. This was further supported by the recent identification of a *bona fide* Aurora kinase in *Dictyostelium* (Li *et al*., 2008). Moreover, the *Dictyostelium* TACC sequence contains a motif at its very N-terminus (34 KE**S**L 37), which matches the proposed Aurora A consensus sequence {KR} X {**S**T} {ILV} (Cheeseman *et al*., 2002; Peset *et al*., 2005). However, no differences in the behavior of full length TACC and the GFP-TACC domain fusion protein were observed with regard to localization, although the latter does not contain the putative S36 phosphorylation site. Thus, if relevant in this context, DdAurora phosphorylation needs to take place at other or additional sites that are also included in the GFP-TACCdom fusion protein.

4.1.3 *Dictyostelium* TACC function

Several attempts to examine *Dictyostelium* TACC function by establishing a knockout strain failed, initially suggesting TACC to be essential. Surprisingly, when TACC expression was suppressed by RNAi, the knockdown effect turned out to be virtually complete. In three TACC-RNAi strains, endogenous TACC was no longer detectable by immunblotting (Fig. 10 B) or in immunofluorescence microscopy experiments (not shown). Considering the comparatively moderate phenotypes upon a very pronounced TACC depletion, it appears unlikely that disruption of the *Dictyostelium* TACC gene is lethal. However, it certainly cannot be excluded that a very small amount of TACC protein is required for the viability of the amoebae. Reports from other organisms are not uniform in this respect, since some TACC proteins seem to be essential, while others are not (Gergely *et al*., 2000b; Piekorz *et al*., 2002; Schuendeln *et al*., 2004; Lauffart *et al*., 2007).

As in many other organisms, the effects of TACC depletion on microtubule dynamics in *Dictyostelium* were found to be much more prominent during mitosis than in interphase (Lee *et al*., 2001; Srayko *et al*., 2003; Peset *et al*., 2005). TACC-RNAi cells exhibited a moderate reduction in interphase microtubule length, but severely shortened astral microtubules in metaphase and anaphase (Figs. 11-12). Furthermore, TACC mutants were shown to be

hypersensitive to the microtubule depolymerizing drug thiabendazole (Fig. 13). These phenotypes were also observed in a second, independent strain of TACC-RNAi cells, which exhibited a similar level of TACC depletion (not shown). Moreover, expression of GFP-TACCdom in TACC-RNAi cells could partially or fully rescue the observed phenotypes, thus demonstrating that the aforementioned effects are really due to TACC depletion. Association of TACC with kinetochores (Fig. 7 J-O) suggested it to play a role in the formation of spindle microtubules as well. The spindle, however, seemed to develop perfectly normal even in the absence of TACC. Accordingly, the segregation of chromosomes and kinetochores was not affected by TACC depletion (Fig. 12 I-P).

Although TACC and CP224 were found to be associated with microtubule plus ends exclusively during interphase, TACC was shown to promote microtubule growth throughout the entire cell cycle. Therefore, TACC seems to act on microtubule dynamics from the plus ends during interphase and from the spindle poles in mitosis. This indicates that TACC can affect microtubule dynamics in two different ways, depending on the cell cycle stage. Concomitantly, expression of GFP-TACCdom in TACC RNAi mutants was sufficient to fully rescue the phenotype of TACC depletion during mitosis but only partially in interphase (Figs. 11-12, Tab. 3). This suggests that interphase, but not mitotic TACC function, requires the N-terminal part of the protein. Such differential behavior might reflect a change in interaction partners in a cell cycle-dependent manner. This idea would be consistent with the finding that XMPAP215, the *Xenopus* homologue of CP224, was shown to interact with an entirely different set of MAPs during interphase and mitosis (Niethammer *et al*., 2007).

4.1.4 TACC mode of action during interphase

XMAP215 proteins have been shown to be conserved interaction partners of TACC proteins (Lee *et al*., 2001; Srayko *et al*., 2003; Conte *et al*., 2003; Sato *et al*., 2004; Peset *et al*., 2005; Koch *et al*., 2006) and to act as microtubule polymerases (Brouhard *et al*., 2008). Therefore, CP224 is an ideal candidate to link *Dictyostelium* TACC function to promotion of microtubule growth. In most other organisms, TACC was described as being crucial for the recruitment of XMAP215 proteins to the centrosome (Lee *et al*., 2001; Bellanger and Gonczy, 2003; Le Bot *et al*., 2003; Sato *et al*., 2004; Kinoshita *et al*., 2005). Therefore, an important question was whether *Dictyostelium* TACC is involved in a similar process. When centrosomal levels of endogenous CP224 in TACC-RNAi cells and GFP-NE81 expressing cells were compared, only a slight reduction of 10 % was detected in TACC mutants

(Fig. 15). In agreement with these experiments, depletion of TACC did not significantly affect the kinetics of CP224 recruitment to the centrosome in FRAP analyses (Fig. 18). Thus, although the overall capacity of TACC-depleted centrosomes to bind CP224 may be perturbed to a small extent, targeting CP224 to the centrosome does not seem to be a primary function of TACC in *Dictyostelium*.

While CP224 levels at the centrosome remained largely unaffected by TACC depletion, the XMAP215 homologue was found to be no longer associated with the tips of interphase microtubules in TACC-RNAi cells. However, when GFP-TACCdom was expressed in these cells, loading of CP224 onto microtubule plus ends was restored (Fig. 19). Since both proteins were found at normal levels at microtubule tips in virtually all cells of the rescue strain, their recruitment seems to occur as efficiently as in wild type cells. This demonstrates for the first time *in vivo* that a TACC protein is necessary for the association of an XMAP215 homologue with microtubule plus ends. As discussed above, in *Dictyostelium*, this is likely to be achieved by directly recruiting a complex of CP224 and TACC from the cytoplasm. Unfortunately, the attempt to further investigate the interdependence of both proteins for plus end localization and the ability to rescue the TACC depletion phenotypes failed, since introducing a point mutation in GFP-TACCdom did not abrogate the interaction with CP224 as expected (Fig. 14).

Although expression of the TACC domain in TACC-RNAi cells perfectly rescued CP224 association with all microtubule tips, the length of interphase microtubules was only partially restored in the rescue strain and several microtubules still exhibited a clear TACC depletion phenotype (Fig. 11 and Tab. 3). This indicated that full length TACC promotes growth of interphase microtubules beyond its role in recruiting CP224 to microtubule tips, because loss of CP224 from microtubule plus ends alone, cannot account for the reduction of interphase microtubule length. Assuming that *Dictyostelium* CP224 can function as a microtubule polymerase as its *Xenopus* homologue XMAP215 (Brouhard *et al*., 2008), it might be speculated that the large N-terminal part, which is not included in the GFP-TACCdom fusion protein used for the rescue experiments, is required for full catalytic activity of CP224. This idea would be consistent with the observation that XMAP215 activity in promoting microtubule growth is positively stimulated by the presence of the *Xenopus* TACC homologue maskin (Kinoshita *et al*., 2005).

4.1.5 TACC mode of action during mitosis

Absence of CP224 and TACC from microtubule plus ends in mitosis leaves only the spindle poles as site of TACC function in promoting mitotic aster formation. The importance of TACC at mitotic centrosomes is further underlined by the fact that in many organisms, including *Dictyostelium*, TACC proteins are being enriched at the spindle poles during early mitosis (Figs. 5, 9) (Gergely *et al*., 2000a; Gergely *et al*., 2000b; Bellanger and Gonczy, 2003; Kinoshita *et al*., 2005). But unlike its homologues, *Dictyostelium* TACC is not involved in the recruitment of CP224 or of tubulin dimers to the spindle poles (Figs. 18, 21). The lack of either protein at the centrosome can therefore not account for the failure of TACC-RNAi cells to assemble astral microtubules in metaphase (Fig. 12). Interestingly, in contrast to astral microtubules, spindle microtubules developed perfectly normal in the absence of TACC, indicating that the two types of microtubules are regulated differentially (Fig. 12). This furthermore demonstrates that TACC is not generally indispensable for microtubule assembly during prometaphase and metaphase.

According to the current model of TACC function (Fig. 3), the growth-promoting complex of TACC and XMAP215 proteins associates with the plus ends of nascent microtubules, where it antagonizes MCAK proteins (mitotic centromere-associated kinesin), members of the kinesin-13 family (Tournebize *et al*., 2000; Kinoshita *et al*., 2005; Peset *et al*., 2005). These proteins have been shown to be potent microtubule depolymerases, whose inhibition by XMAP215 proteins occurs locally at the spindle poles and strongly depends on the association of XMAP215 with phosphorylated TACC (Kinoshita *et al*., 2005; Kinoshita *et al*., 2006). Since many XMAP215 homologues do not localize to the centrosome during interphase (Matthews *et al*., 1998; Charrasse *et al*., 1998; Cullen *et al*., 1999; Garcia *et al*., 2001), MCAK inhibition also requires targeting of XMAP215 proteins to the spindle poles by TACC proteins prior to mitosis (Lee *et al*., 2001; Bellanger and Gonczy, 2003; Srayko *et al*., 2003; Le Bot *et al*., 2003; Sato *et al*., 2004; Kinoshita *et al*., 2005). Of course, this work cannot provide sufficient data to assess whether an analogous mechanism to govern astral microtubule length does exist in *Dictyostelium*. Also, in contrast to their homologues, CP224 and TACC are permanently associated with the centrosome throughout the entire cell cycle, which is not consistent with the idea of XMAP215 regulation through TACC-dependent recruitment to the centrosome. However, the fact that XMAP215 proteins require the association with TACC proteins in order to be able to counteract MCAK, could nicely explain why astral microtubule formation is perturbed in TACC-RNAi cells, despite the presence of CP224 at the centrosome. To date, no *bona fide* MCAK homologue has been identified in *Dictyostelium* yet, but recently

Tikhonenko *et al* speculated that *Dictyostelium* Kif9 might have microtubule depolymerizing activity similar to MCAK proteins (Tikhonenko *et al*., 2009). Therefore, one of the next steps in revealing the mechanisms underlying astral microtubule formation in *Dictyostelium*, might be to investigate Kif9 function in this respect.

4.2 Microtubule dynamics in *Dictyostelium*

During interphase, *Dictyostelium* microtubules appear very stable in length (Mov. 9). In this work, as in previous studies, no complete catastrophe or rescue events could be observed (Koonce and Khodjakov, 2002). Yet, *Dictyostelium* microtubules are clearly shortened by treatment with microtubule depolymerizing drugs such as TBZ or nocodazol (Gräf *et al*., 2003) (Fig. 13 A, E). Owing to their mode of action, these should only affect dynamic microtubules. In order to address this paradox, 5D live cell imaging of cells co-expressing mRFP-α-tubulin and GFP-TACCdom was performed (Fig. 23, Mov. 10). The latter fusion protein turned out to be the first suitable marker to study the dynamics of microtubule plus ends in living *Dictyostelium* cells. The corresponding experiments revealed a considerably more pronounced dynamic behavior of microtubules than expected. Many microtubule tips seemed to rapidly alternate between small-scale growth and shrinkage events, suggesting *Dictyostelium* microtubules to be dynamic in the cell periphery. Due to the difficulty to follow individual microtubule tips in GFP-α-tubulin cells without using an additional plus end marker, this behavior might have been overlooked in earlier studies. In accordance with these results, the microtubule dynamics in the cell periphery could be confirmed by FRAP analysis (Fig. 24, Mov. 11). By contrast, when a square region around the centrosome was bleached, no GFP-α-tubulin recovery was observed for the microtubules in the pericentrosomal area (Fig. 22). Taken together, these findings suggest *Dictyostelium* microtubules to be rather stable near their minus ends and dynamic at their plus ends. This idea is also in perfect agreement with the observation that TBZ treatment depolymerizes microtubules in the cell periphery, but leaves significant microtubule stubs at the centrosome. Interestingly, recovery of GFP-α-tubulin at the centrosome itself proceeded rapidly, but never to pre-bleach levels (Fig. 21 A), indicating the existence of two populations of centrosomal tubulin. The first population, recovering rapidly from photobleaching, seems to comprise a highly dynamic pool of free tubulin dimers at the centrosome. The second population, showing no fluorescence recovery, might be incorporated into microtubules whose minus ends are non-dynamic and firmly attached to the centrosome.

4.3 Investigation of three centrosomal candidate proteins

A proteomic approach to identify yet unknown components of the *Dictyostelium* centrosome yielded several candidate proteins, three of which should be investigated during this study. Two out of three candidate proteins could not be confirmed as centrosomal components, but instead were found to associate with centromeres and kinetochores, respectively. For the proteomic approach mentioned above, large quantities of isolated centrosomes were purified and subjected to mass spectrometric analysis after separation of their proteins by differential techniques (Reinders *et al*., 2006; Schulz *et al*., 2006). During the isolation process of *Dictyostelium* centrosomes, the latter have to be separated from the nuclei. Since these two organelles are firmly associated, the use of comparably harsh treatment including the disintegration of nuclei by shearing forces, detergent, heparin and sodium pyrophosphate is required (Gräf *et al*., 1998). The most likely explanation how these two centromeric proteins ended up in the centrosome enriched fraction is that such harsh treatment partially destroys the centromere structure, whose remainders are then co-isolated due to their strong connection to the centrosome. This idea is consistent with the fact that further non-centrosomal proteins such as the nuclear envelope protein NE81 were also identified in the screen. Accordingly, GFP-NE81 was frequently found to be associated with isolated centrosomes in immunofluorescence microsocopy, presumably by association with patches of nuclear envelope that were ripped out during the purification process (Schulz *et al*., 2009b).

4.3.1 *Dictyostelium* Cenp68 associates with the centromeres

Endogenous Cenp68 and GFP-Cenp68 could not be detected at centrosomes throughout the cell cycle (Figs. 25, 32). Instead, Cenp68 localization was found to perfectly match the one described for the *Dictyostelium* HP1 homologues hcpA and hcpB, and the core centromeric histone variant CenH3 (Kaller *et al*., 2006; Dubin *et al*., 2010). Colocalization experiments with hcpA-GFP and hcpB-GFP further validated association with the centromeric cluster (Fig. 27). Therefore, after hcpA, hcpB, SuvA and CenH3, Cenp68 represents the fifth constitutive centromere-associated protein identified in *Dictyostelium* to date (Kaller *et al*., 2006; Dubin *et al*., 2010; Ph.D. thesis of Manu Dubin, 2010, Universität Kassel). The data obtained during this work, however, cannot specify subcentromeric localization of Cenp68 to either the CenH3-containing core centromeric region or to pericentromeric heterochromatin. Yet, Cenp68 does not seem to be a heterochromatin-specific protein, since it does not associate with additional foci of heterochromatin outside the centromeres as observed for hcpA and

hcpB (Kaller *et al*., 2006) (Fig. 27, arrowheads). Centromeric levels of hcpA-GFP and hcpB-GFP were shown to strongly decrease in late mitotic stages (Kaller *et al*., 2006), whereas association of endogenous Cenp68 with centromeres remained constant throughout the cell cycle (Fig. 32). Concomitantly, GFP-hcpB was normally targeted to pericentromeric heterochromatin in Cenp68 knockout mutants (Fig. 29 D-F). Both observations suggest that Cenp68 and the *Dictyostelium* HP1 representatives are recruited to centromeres independently. This is corroborated by observations in FRAP experiments, where GFP-Cenp68 turnover did not appear to be slowed down in late mitotic stages when centromeric hcpA and hcpB protein levels are low (Mov. 17 compared to Mov. 18).

However, FRAP analysis of GFP-Cenp68 did not yet yield a clear general picture. This is because during interphase and mitosis, GFP-Cenp68 could be observed to recover rapidly upon bleaching a square region around the centromeres in some of the cells investigated, while it was found to be rather stable in others (Mov. 19 and 20). Several mammalian centromeric proteins comprising CENP-B, -C, -H and –T were reported to exhibit differential and cell cycle-specific dynamic behavior at centromeres (Hemmerich *et al*., 2008; Hellwig *et al*., 2008). Therefore, it is tempting to speculate that such behavior also applies for Cenp68, and that the differential dynamics observed in the FRAP experiments of this work was not an artifact. Certainly a larger number of single experiments covering the entire cell cycle will be necessary to reveal the dynamic behavior of Cenp68 in a statistical approach.

4.3.2 Cenp68 function remains unknown

Since neither Cenp68 overexpressing cells nor a knockout mutant displayed any obvious phenotype, assessing Cenp68 function turned out to be a difficult task. Sequence analysis did not reveal any conserved domains or motifs. Furthermore, BLASTp searches only revealed one potential homologue, the *S.cerevisiae* protein Bbp1, which is part of the yeast SPB and functions in tethering the SBP to the nuclear envelope (Schramm *et al*., 2000). Cenp68 localization at centromeres, however, is entirely different from Bbp1 localization at the SPB. Moreover, connection of the centromeres with the nuclear envelope or the centrosome was not obviously perturbed in the absence of Cenp68 (Fig. 29 A-C). These observations do not suggest Cenp68 to be a functional homologue of Bbp1.

In a GFP-nanotrap assay, the prpf4B kinase was identified as a putative interactor of Cenp68 (Fig. 30). The human counterpart was shown to be involved in two distinct processes, namely pre-mRNA splicing and the spindle assembly checkpoint (SAC) (Kojima *et al*., 2001; Dellaire

et al., 2002; Montembault *et al*., 2007). Since SAC proteins associate with the kinetochores, this process seems more likely to involve Cenp68. However, unlike human prp4, *Dictyostelium* prpf4B could not be detected at the kinetochores at any time (Fig. 31). Moreover, neither co-immunoprecipitation experiments nor a yeast-two-hybrid assay could confirm interaction between the two proteins (not shown). Without successful confirmation by additional methods, interaction between Cenp68 and prpf4B certainly remains very doubtful. Since GFP-prpf4B furthermore does not specifically localize to kinetochores, a common role in the SAC seems very unlikely. Suitable future experiments to investigate a cell cycle-dependent interaction between the two proteins at kinetochores or at other nuclear structures in living cells could comprise split-GFP experiments (Ghosh *et al*., 2000) or fluorescence resonance energy transfer assays (FRET) (Wouters and Bastiaens, 2006).

During interphase, *Dictyostelium* centromeres are known to be clustered inside the nucleus opposite to the centrosome (Eichinger *et al*., 2005). The mechanism underlying this clustering, however, has yet to be discovered. Recently, we could show that anchoring the centromeres to the centrosome is at least partially mediated by the nuclear membrane protein SUN1 (Schulz *et al*., 2009a). Upon overexpression of GFP-SUN1, ~28 % of the cells exhibited severely dislocated centromeres, which were still associated with the nuclear membrane, but appeared to be no longer connected to the centrosome (Fig. 34). Interestingly, the clustering itself was not affected by centromere displacement, suggesting the two processes to be independent from each other.

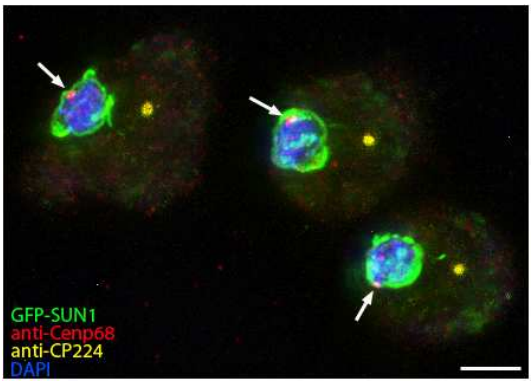

Fig. 34 Overexpression of GFP-SUN1 causes detachment of the centromeric cluster from the site of centrosome-nucleus attachment
GFP-SUN1 (green) overexpressing cells were fixed with methanol and stained with anti-Cenp68 (red) and anti-CP224 as a centrosomal marker (shown in yellow). DNA is shown in blue. The arrowheads point at the displaced centromere clusters. Bar = 2 µm. Modified from Schulz *et al.* (2009a).

In order to test whether Cenp68 is involved in the clustering process, the centromeric region in Cenp68 knockout cells was visualized using anti-H3K9me3 antibody (Fig. 29 A-C). It turned out, however, that Cenp68 is neither required for the formation of centromeric clusters during interphase, nor for their connection to the centrosome.

4.3.3 *Dictyostelium* Mad1 is a putative component of the spindle assembly checkpoint

Recruitment of the Mad1-Mad2 complex to unattached kinetochores in early mitotis and subsequent dissociation upon attachment of spindle microtubules are central events in SAC regulation. While bound to unattached kinetochores, the Mad1-Mad2 complex causes the accumulation of the Mad2-Cdc20 complex, which in turn renders the SAC active and thereby prevents anaphase onset (Musacchio and Salmon, 2007). Upon bipolar spindle attachment, the Mad1-Mad2 complex is stripped from kinetochores causing SAC inactivation and transition to anaphase (Howell *et al*., 2001; Howell *et al*., 2004).

Little is known about the existence or the functionality of a SAC in *Dictyostelium*. However, *Dictyostelium* Mad2 is highly similar to its human homologue and the Mad2-binding motifs of human and *Dictyostelium* Mad1 are almost identical (Fig. 35). This suggests that *Dictyostelium* Mad1 and Mad2 can form this evolutionary conserved complex as well. Moreover, besides Mad1 and Mad2, a variety of other core SAC components such as Cdc20, Separase, Bub1 and Bub3 seem to be conserved in the haploid amoebae, supporting the idea of an existent SAC in *Dictyostelium*.

When *Dictyostelium* cells are treated with microtubule destabilizing drugs, which prevent proper spindle assembly, the amoebae cannot undergo normal mitosis and are temporarily arrested in a prometaphase-like state (Kitanishi *et al*., 1984). After several hours of exposure, these cells were shown to re-enter interphase as a dipolid cell without having successfully completed mitosis. This behavior, termed “checkpoint slippage”, has been observed for many cell types (Rieder and Maiato, 2004) and therefore does not necessarily argue against a functional SAC in *Dictyostelium*.

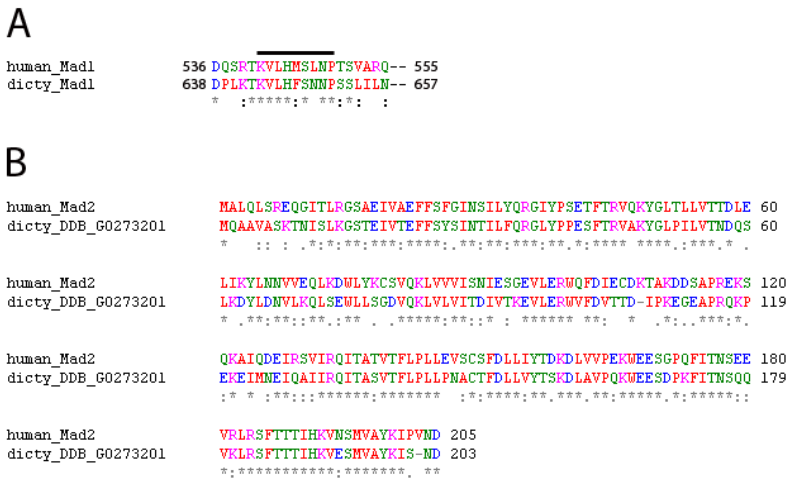

Fig. 35 Sequence homology between human and *Dictyostelium* Mad2 proteins and corresponding Mad2 binding motifs
(**A**) Mad1 proteins interact with Mad2 proteins via their Mad2 binding motif (highlighted by a black bar above the alignment). The *Dictyostelium* and human Mad 2 binding motifs are highly similar and only differ in two positions. Shown are amino acids 536-555 of human Mad1 and amino acids 638-657 of *Dictyostelium* Mad1. Mad2 binding motifs were identified using the Eukaryotic linear motif sequence analysis tool (ELM) (http://elm.eu.org/). Alignment is modified. (**B**) Sequence alignment of human Mad2 and the putative *Dictyostelium* Mad2 protein (DDB_G0273201). Both alignments were generated using ClustalW (www.ebi.ac.uk/Tools/msa/clustalw2).

The investigation of putative *Dictyostelium* SAC components has not yet been systematically addressed, which is why virtually no experimental data is available. In this work, Mad1 behavior was investigated, whose localization was found to be in accordance with a potential role in SAC regulation. As human Mad1, *Dictyostelium* GFP-Mad1, albeit being enriched inside the nucleus, did not associate with interphase centromeres (Fig. 32 A-D) (Howell *et al*., 2004). In cells that appeared to be in late G2 phase, GFP-Mad1 was found to be concentrated at centromeres/kinetochores, where it remained until prometaphase or metaphase (Fig. 32 E-T, Mov. 14). During metaphase, the GFP-Mad1 signal was frequently found to be significantly weaker, or even to be absent from kinetochores. Interestingly, in a few cases, individual metaphase kinetochores could be observed, which were still heavily decorated with GFP-Mad1, whereas the latter was completely absent from other kinetochores of the same cell (Fig. 32 U-X). This suggests that the cell cycle stage is not the only determinant for triggering GFP-Mad1 dissociation from kinetochores, since in that case one would rather expect GFP-Mad1 to dissociate from all kinetochores simultaneously. Although little is known to date about a fucntional SAC in *Dictyostelium*, our observation of Mad1 behavior and the fact that several key SAC components are conserved in *Dictyostelium*, both support the idea of an existent SAC in the amoebae.

The declustering of *Dictyostelium* centromeres in early mitosis has been previously reported (Kaller *et al*., 2006; Dubin *et al*., 2010) and is consistent with observations in *S. pombe*, where centromeres exhibit a similar behavior (Funabiki *et al*., 1993). In the course of our experiments, however, we frequently discovered cells whose centromeres were clearly declustered, but yet exhibited seemingly uncondensed DNA together with a fully developed microtubule cytoskeleton, which is a hallmark of interphase cells (Fig. 25 E-H and 32 E-H). Concomitantly, in all cases when GFP-Mad1 expressing cells were imaged, GFP-Mad1 was associated with the declustered centromeres in above mentioned cells, while it was usually not found to decorate the centromeres of interphase cells forming the typical tight cluster (Fig. 32 A-D). This suggests that the recruitment of *Dictyostelium* Mad1 to centromeres/kinetochores coincides with centromere declustering, which appears to take place in late G2 cells that are on the verge of entering prophase. It has to be mentioned, however, that following Mad1 recruitment to kinetochores by live cell imaging repeatedly failed. Future experiments using a suitable marker for cell cycle positions, such as fluorescently labeled α-tubulin or histone, will allow to determine the point of centromere declustering and kinetochore assembly in *Dictyostelium* more precisely.

4.3.4 CP103 might function in dynein targeting

CP103 displays weak homology to ZW10 proteins, but it remains unclear whether it represents a functional *Dictyostelium* homologue of ZW10. During mitosis, the animal representatives of this family were shown to play a crucial role in targeting SAC components and the dynein/dynactin complex to kinetochores (Karess, 2005). However, in contrast to ZW10 proteins of higher eukaryotes, GFP-CP103 was not found at kinetochores at any time, suggesting CP103 not to be involved in a similar process. Instead, GFP-CP103 colocalized with CP224 at the centrosomal corona in whole cell preparations and at isolated centrosomes that are free of microtubules (Fig. 33). Its function at the centrosomes remains unclear, since CP103 overexpressing cells did not display any obvious phenotype and the generation of knockout mutants failed. It is noteworthy to mention, however, that during interphase, ZW10 proteins were shown to interact with the dynactin subunit p50-dynamitin and were furthermore suggested to be involved in anchoring cytoplasmic dynein to the Golgi apparatus via dynactin (Starr *et al*., 1998; Vallee *et al*., 2006; Varma *et al*., 2006). As GFP-CP103, *Dictyostelium* dynein was observed to concentrate at the centrosomal corona (Rehberg *et al*., 2005). Therefore, it is tempting to speculate that CP103 fulfills a function in dynein/dynactin

targeting to the centrosome, similar to the one of ZW10 proteins in targeting dynein/dynacting to kinetochores or the Golgi apparatus. First steps to investigate such CP103 function might include the comparison of centrosomal dynein levels in wild type cells with those of CP103 overexpressing cells. Moreover, it will be necessary to figure out whether CP103 interacts with dynein/dynactin or, in particular, with dynamitin (DDB0220488) as reported for human ZW10 (Starr *et al*., 1998).

Conclusions

Taken together, this work provides a detailed analysis of *Dictyostelium* TACC localization and reveals novel aspects regarding TACC protein function. The collected data demonstrate that TACC is involved in microtubule growth during interphase. Moreover, although TACC is absent from astral microtubules, the protein was found to be crucial for their formation. TACC proteins have previously been suggested to be involved in targeting XMAP215 proteins to nascent microtubule plus ends. However, this was never demonstrated in whole cells. This study shows for the first time *in vivo* that presence of a TACC protein is in fact essential for the association of an XMAP215 protein with microtubule tips. To further investigate TACC-CP224 function in *Dictyostelium*, future experiments might aim to examine whether the two proteins are involved in antagonizing a microtubule depolymerizing factor as reported for some of their homologues. Kif9 might be a first candidate protein to test in this respect. For instance, this could be achieved by observing potential rescue effects caused by knockout of Kif9 in TACC-RNAi mutants.

Of the three centrosomal candidate proteins tested, only CP103 was confirmed as genuine centrosomal resident. Nonetheless, although Cenp68 and Mad1 do no associate with the centrosome, both proteins were found to exhibit very interesting localization and behavior. In *Dictyostelium*, Cenp68 is only the fifth constitutive centromere-associated protein known. Furthermore, GFP-Cenp68 and the anti-Cenp68 antibody have proven to be a useful tool for the investigation of centromere dynamics in *Dictyostelium*. Absence of obvious phenotypes in Cenp68 null cells made assessing Cenp68 function difficult. Albeit costly, information on Cenp68 function might, for instance, be derived from a microarray-based screen for genes being upregulated in Cenp68 knockout cells. Finally, the observed localization and behavior of GFP-Mad1 at kinetochores suggests the existence of a spindle assembly checkpoint in *Dictyostelium* and might turn out as a suitable marker for kinetochore assembly in the amoebae.

References

Akhmanova, A. and Hoogenraad, C. C. (2005). "Microtubule plus-end-tracking proteins: mechanisms and functions." Curr Opin Cell Biol **17**(1): 47-54.

Akhmanova, A. and Steinmetz, M. O. (2008). "Tracking the ends: a dynamic protein network controls the fate of microtubule tips." Nat Rev Mol Cell Biol **9**(4): 309-22.

Albee, A. J. and Wiese, C. (2008). "Xenopus TACC3/maskin is not required for microtubule stability but is required for anchoring microtubules at the centrosome." Mol Biol Cell **19**(8): 3347-56.

Andersen, J. S., Wilkinson, C. J., Mayor, T., Mortensen, P., Nigg, E. A. and Mann, M. (2003). "Proteomic characterization of the human centrosome by protein correlation profiling." Nature **426**(6966): 570-4.

Barr, A. R. and Gergely, F. (2007). "Aurora-A: the maker and breaker of spindle poles." J Cell Sci **120**(Pt 17): 2987-96.

Barros, T. P., Kinoshita, K., Hyman, A. A. and Raff, J. W. (2005). "Aurora A activates D-TACC-Msps complexes exclusively at centrosomes to stabilize centrosomal microtubules." J Cell Biol **170**(7): 1039-46.

Basto, R., Scaerou, F., Mische, S., Wojcik, E., Lefebvre, C., Gomes, R., Hays, T. and Karess, R. (2004). "In vivo dynamics of the rough deal checkpoint protein during Drosophila mitosis." Curr Biol **14**(1): 56-61.

Bellanger, J. M. and Gonczy, P. (2003). "TAC-1 and ZYG-9 form a complex that promotes microtubule assembly in C. elegans embryos." Curr Biol **13**(17): 1488-98.

Bellanger, J. M., Carter, J. C., Phillips, J. B., Canard, C., Bowerman, B. and Gonczy, P. (2007). "ZYG-9, TAC-1 and ZYG-8 together ensure correct microtubule function throughout the cell cycle of C. elegans embryos." J Cell Sci **120**(Pt 16): 2963-73.

Bharadwaj, R., Qi, W. and Yu, H. (2004). "Identification of two novel components of the human NDC80 kinetochore complex." J Biol Chem **279**(13): 13076-85.

Bieling, P., Laan, L., Schek, H., Munteanu, E. L., Sandblad, L., Dogterom, M., Brunner, D. and Surrey, T. (2007). "Reconstitution of a microtubule plus-end tracking system in vitro." Nature **450**(7172): 1100-5.

Bieling, P., Kandels-Lewis, S., Telley, I. A., van Dijk, J., Janke, C. and Surrey, T. (2008). "CLIP-170 tracks growing microtubule ends by dynamically recognizing composite EB1/tubulin-binding sites." J Cell Biol **183**(7): 1223-33.

Bretschneider, T., Anderson, K., Ecke, M., Muller-Taubenberger, A., Schroth-Diez, B., Ishikawa-Ankerhold, H. C. and Gerisch, G. (2009). "The three-dimensional dynamics of actin waves, a model of cytoskeletal self-organization." Biophys J **96**(7): 2888-900.

Brito, D. A., Strauss, J., Magidson, V., Tikhonenko, I., Khodjakov, A. and Koonce, M. P. (2005). "Pushing forces drive the comet-like motility of microtubule arrays in Dictyostelium." Mol Biol Cell **16**(7): 3334-40.

Brouhard, G. J., Stear, J. H., Noetzel, T. L., Al-Bassam, J., Kinoshita, K., Harrison, S. C., Howard, J. and Hyman, A. A. (2008). "XMAP215 is a processive microtubule polymerase." Cell **132**(1): 79-88.

Buscaino, A., Allshire, R. and Pidoux, A. (2010). "Building centromeres: home sweet home or a nomadic existence?" Curr Opin Genet Dev **20**(2): 118-126.

Carroll, C. W. and Straight, A. F. (2006). "Centromere formation: from epigenetics to self-assembly." Trends Cell Biol **16**(2): 70-8.

Carroll, C. W., Silva, M. C., Godek, K. M., Jansen, L. E. and Straight, A. F. (2009). "Centromere assembly requires the direct recognition of CENP-A nucleosomes by CENP-N." Nat Cell Biol **11**(7): 896-902.

Carroll, C. W., Milks, K. J. and Straight, A. F. (2010). "Dual recognition of CENP-A nucleosomes is required for centromere assembly." J Cell Biol **189**(7): 1143-1155.

Cassimeris, L. and Morabito, J. (2004). "TOGp, the human homolog of XMAP215/Dis1, is required for centrosome integrity, spindle pole organization, and bipolar spindle assembly." Mol Biol Cell **15**(4): 1580-90.

Charette, S. J. and Cosson, P. (2004). "Preparation of genomic DNA from Dictyostelium discoideum for PCR analysis." Biotechniques **36**(4): 574-5.

Charrasse, S., Schroeder, M., Gauthier-Rouviere, C., Ango, F., Cassimeris, L., Gard, D. L. and Larroque, C. (1998). "The TOGp protein is a new human microtubule-associated protein homologous to the Xenopus XMAP215." J Cell Sci **111 (Pt 10)**: 1371-83.

Cheeseman, I. M., Anderson, S., Jwa, M., Green, E. M., Kang, J., Yates, J. R., 3rd, Chan, C. S., Drubin, D. G. and Barnes, G. (2002). "Phospho-regulation of kinetochore-microtubule attachments by the Aurora kinase Ipl1p." Cell **111**(2): 163-72.

Cheeseman, I. M., Hori, T., Fukagawa, T. and Desai, A. (2008). "KNL1 and the CENP-H/I/K complex coordinately direct kinetochore assembly in vertebrates." Mol Biol Cell **19**(2): 587-94.

Chen, R. H., Shevchenko, A., Mann, M. and Murray, A. W. (1998). "Spindle checkpoint protein Xmad1 recruits Xmad2 to unattached kinetochores." J Cell Biol **143**(2): 283-95.

Chretien, D., Jainosi, I., Taveau, J. C. and Flyvbjerg, H. (1999). "Microtubule's conformational cap." Cell Struct Funct **24**(5): 299-303.

Conte, N., Delaval, B., Ginestier, C., Ferrand, A., Isnardon, D., Larroque, C., Prigent, C., Seraphin, B., Jacquemier, J. and Birnbaum, D. (2003). "TACC1-chTOG-Aurora A protein complex in breast cancer." Oncogene **22**(50): 8102-16.

Cosson, P., Zulianello, L., Join-Lambert, O., Faurisson, F., Gebbie, L., Benghezal, M., Van Delden, C., Curty, L. K. and Kohler, T. (2002). "Pseudomonas aeruginosa virulence analyzed in a Dictyostelium discoideum host system." J Bacteriol **184**(11): 3027-33.

Cosson, P. and Soldati, T. (2008). "Eat, kill or die: when amoeba meets bacteria." Curr Opin Microbiol **11**(3): 271-6.

Cullen, C. F., Deak, P., Glover, D. M. and Ohkura, H. (1999). "mini spindles: A gene encoding a conserved microtubule-associated protein required for the integrity of the mitotic spindle in Drosophila." J Cell Biol **146**(5): 1005-18.

Cullen, C. F. and Ohkura, H. (2001). "Msps protein is localized to acentrosomal poles to ensure bipolarity of Drosophila meiotic spindles." Nat Cell Biol **3**(7): 637-42.

Daunderer, C. and Graf, R. O. (2002). "Molecular analysis of the cytosolic Dictyostelium gamma-tubulin complex." Eur J Cell Biol **81**(4): 175-84.

De Antoni, A., Pearson, C. G., Cimini, D., Canman, J. C., Sala, V., Nezi, L., Mapelli, M., Sironi, L., Faretta, M., Salmon, E. D., et al. (2005). "The Mad1/Mad2 complex as a template for Mad2 activation in the spindle assembly checkpoint." Curr Biol **15**(3): 214-25.

De Souza C. P., Osmani A. H., Hashmi S. B. and Osmani S. A. (2004) „Partial nuclear pore complex disassembly during closed mitosis in Aspergillus nidulans.“ Current Biology **14**: 1973–1984.

De Wulf, P., McAinsh, A. D. and Sorger, P. K. (2003). "Hierarchical assembly of the budding yeast kinetochore from multiple subcomplexes." Genes Dev **17**(23): 2902-21.

Dellaire, G., Makarov, E. M., Cowger, J. J., Longman, D., Sutherland, H. G., Luhrmann, R., Torchia, J. and Bickmore, W. A. (2002). "Mammalian PRP4 kinase copurifies and interacts with components of both the U5 snRNP and the N-CoR deacetylase complexes." Mol Cell Biol **22**(14): 5141-56.

DeLuca, J. G., Dong, Y., Hergert, P., Strauss, J., Hickey, J. M., Salmon, E. D. and McEwen, B. F. (2005). "Hec1 and nuf2 are core components of the kinetochore outer plate essential for organizing microtubule attachment sites." Mol Biol Cell **16**(2): 519-31.

Dixit, R., Barnett, B., Lazarus, J. E., Tokito, M., Goldman, Y. E. and Holzbaur, E. L. (2009). "Microtubule plus-end tracking by CLIP-170 requires EB1." Proc Natl Acad Sci U S A **106**(2): 492-7.

Dragestein, K. A., van Cappellen, W. A., van Haren, J., Tsibidis, G. D., Akhmanova, A., Knoch, T. A., Grosveld, F. and Galjart, N. (2008). "Dynamic behavior of GFP-CLIP-170 reveals fast protein turnover on microtubule plus ends." J Cell Biol **180**(4): 729-37.

Dubin, M., Fuchs, J., Graf, R., Schubert, I. and Nellen, W. (2010). "Dynamics of a novel centromeric histone variant CenH3 reveals the evolutionary ancestral timing of centromere biogenesis." Nucleic Acids Res **38**(21): 7526-7537

Eichinger, L., Pachebat, J. A., Glockner, G., Rajandream, M. A., Sucgang, R., Berriman, M., Song, J., Olsen, R., Szafranski, K., Xu, Q., et al. (2005). "The genome of the social amoeba Dictyostelium discoideum." Nature **435**(7038): 43-57.

Euteneuer, U. and Schliwa, M. (1992). "Mechanism of centrosome positioning during the wound response in BSC-1 cells." J Cell Biol **116**(5): 1157-66.

Euteneuer, U., Graf, R., Kube-Granderath, E. and Schliwa, M. (1998). "Dictyostelium gamma-tubulin: molecular characterization and ultrastructural localization." J Cell Sci **111 (Pt 3)**: 405-12.

Faix, J., Weber, I., Mintert, U., Kohler, J., Lottspeich, F. and Marriott, G. (2001). "Recruitment of cortexillin into the cleavage furrow is controlled by Rac1 and IQGAP-related proteins." Embo J **20**(14): 3705-15.

Faix, J., Kreppel, L., Shaulsky, G., Schleicher, M. and Kimmel, A. R. (2004). "A rapid and efficient method to generate multiple gene disruptions in Dictyostelium discoideum using a single selectable marker and the Cre-loxP system." Nucleic Acids Res **32**: e143.

Fukui, K.-Y. a. Y. (1987a). "Reorganization of Microtubules During Mitosis in Dictyostelium: Dissociation From MTOC and Selective Assembly/Disassembly In Situ." Cell Motility and the Cytoskeleton **8**: 106-117.

Fukui, Y., Yumura, S., and Yumura, T.K. (1987b). "Agar-overlay immunofluorescence: High resolution studies of cytoskeletal components and their changes during chemotaxis." Methods Cell Biol. **28**: 347–356.

Funabiki, H., Hagan, I., Uzawa, S. and Yanagida, M. (1993). "Cell cycle-dependent specific positioning and clustering of centromeres and telomeres in fission yeast." J Cell Biol **121**(5): 961-76.

Galjart (2010). "Plus-end-tracking proteins and their interactions at microtubule ends." Current Biology **20**(12): R528-R537.

Garcia, M. A., Vardy, L., Koonrugsa, N. and Toda, T. (2001). "Fission yeast ch-TOG/XMAP215 homologue Alp14 connects mitotic spindles with the kinetochore and is a component of the Mad2-dependent spindle checkpoint." Embo J **20**(13): 3389-401.

Gergely, F., Karlsson, C., Still, I., Cowell, J., Kilmartin, J. and Raff, J. W. (2000a). "The TACC domain identifies a family of centrosomal proteins that can interact with microtubules." Proc Natl Acad Sci U S A **97**(26): 14352-7.

Gergely, F., Kidd, D., Jeffers, K., Wakefield, J. G. and Raff, J. W. (2000b). "D-TACC: a novel centrosomal protein required for normal spindle function in the early Drosophila embryo." Embo J **19**(2): 241-52.

Gergely, F. (2002). "Centrosomal TACCtics." Bioessays **24**(10): 915-25.

Gergely, F., Draviam, V. M. and Raff, J. W. (2003). "The ch-TOG/XMAP215 protein is essential for spindle pole organization in human somatic cells." Genes Dev **17**(3): 336-41.

Ghosh, I., Hamilton, A. D. and Regan, L. (2000). "Antiparallel leucine zipper-directed protein reassembly: application to the green fluorescent protein." J Am Chem Soc **122**: 5658–5659.

Giet, R., McLean, D., Descamps, S., Lee, M. J., Raff, J. W., Prigent, C. and Glover, D. M. (2002). "Drosophila Aurora A kinase is required to localize D-TACC to centrosomes and to regulate astral microtubules." J Cell Biol **156**(3): 437-51.

Glockner, G. and Heidel, A. J. (2009). "Centromere sequence and dynamics in Dictyostelium discoideum." Nucleic Acids Res **37**(6): 1809-16.

Graf, R., Euteneuer, U., Ueda, M. and Schliwa, M. (1998). "Isolation of nucleation-competent centrosomes from Dictyostelium discoideum." Eur J Cell Biol **76**(3): 167-75.

Graf, R., Daunderer, C. and Schliwa, M. (1999). "Cell cycle-dependent localization of monoclonal antibodies raised against isolated Dictyostelium centrosomes." Biol Cell **91**(6): 471-7.

Graf, R., Brusis, N., Daunderer, C., Euteneuer, U., Hestermann, A., Schliwa, M. and Ueda, M. (2000b). "Comparative structural, molecular, and functional aspects of the Dictyostelium discoideum centrosome." Curr Top Dev Biol **49**: 161-85.

Graf, R., Daunderer, C. and Schliwa, M. (2000a). "Dictyostelium DdCP224 is a microtubule-associated protein and a permanent centrosomal resident involved in centrosome duplication." J Cell Sci **113 (Pt 10)**: 1747-58.

Graf, R. (2001). "Isolation of centrosomes from Dictyostelium." Methods Cell Biol **67**: 337-57.

Graf, R., Euteneuer, U., Ho, T. H. and Rehberg, M. (2003). "Regulated expression of the centrosomal protein DdCP224 affects microtubule dynamics and reveals mechanisms for the control of supernumerary centrosome number." Mol Biol Cell **14**(10): 4067-74.

Graf, R., Daunderer, C. and Schulz, I. (2004). "Molecular and functional analysis of the dictyostelium centrosome." Int Rev Cytol **241**: 155-202.

Grewal, S. I. and Jia, S. (2007). "Heterochromatin revisited." Nat Rev Genet **8**(1): 35-46.

Hao, Z., Stoler, M. H., Sen, B., Shore, A., Westbrook, A., Flickinger, C. J., Herr, J. C. and Coonrod, S. A. (2002). "TACC3 expression and localization in the murine egg and ovary." Mol Reprod Dev **63**(3): 291-9.

Hellwig, D., Munch, S., Orthaus, S., Hoischen, C., Hemmerich, P. and Diekmann, S. (2008). "Live-cell imaging reveals sustained centromere binding of CENP-T via CENP-A and CENP-B." J Biophotonics **1**(3): 245-54.

Hemmerich, P., Weidtkamp-Peters, S., Hoischen, C., Schmiedeberg, L., Erliandri, I. and Diekmann, S. (2008). "Dynamics of inner kinetochore assembly and maintenance in living cells." J Cell Biol **180**(6): 1101-14.

Henikoff, S. and Dalal, Y. (2005). "Centromeric chromatin: what makes it unique?" Curr Opin Genet Dev **15**(2): 177-84.

Hestermann, A., Rehberg, M. and Graf, R. (2002). "Centrosomal microtubule plus end tracking proteins and their role in Dictyostelium cell dynamics." J Muscle Res Cell Motil **23**(7-8): 621-30.

Hestermann, A. and Graf, R. (2004). "The XMAP215-family protein DdCP224 is required for cortical interactions of microtubules." BMC Cell Biol **5**: 24.

Hirose, H., Arasaki, K., Dohmae, N., Takio, K., Hatsuzawa, K., Nagahama, M., Tani, K., Yamamoto, A., Tohyama, M. and Tagaya, M. (2004). "Implication of ZW10 in membrane trafficking between the endoplasmic reticulum and Golgi." Embo J **23**(6): 1267-78.

Honnappa, S., Okhrimenko, O., Jaussi, R., Jawhari, H., Jelesarov, I., Winkler, F. K. and Steinmetz, M. O. (2006). "Key interaction modes of dynamic +TIP networks." Mol Cell **23**(5): 663-71.

Howard, J. and Hyman, A. A. (2009). "Growth, fluctuation and switching at microtubule plus ends." Nat Rev Mol Cell Biol **10**(8): 569-74.

Howell, B. J., McEwen, B. F., Canman, J. C., Hoffman, D. B., Farrar, E. M., Rieder, C. L. and Salmon, E. D. (2001). "Cytoplasmic dynein/dynactin drives kinetochore protein transport to the spindle poles and has a role in mitotic spindle checkpoint inactivation." J Cell Biol **155**(7): 1159-72.

Howell, B. J., Moree, B., Farrar, E. M., Stewart, S., Fang, G. and Salmon, E. D. (2004). "Spindle checkpoint protein dynamics at kinetochores in living cells." Curr Biol **14**(11): 953-64.

Jin, Q. W., Fuchs, J. and Loidl, J. (2000). "Centromere clustering is a major determinant of yeast interphase nuclear organization." J Cell Sci **113 (Pt 11)**: 1903-12.

Kaller, M., Euteneuer, U. and Nellen, W. (2006). "Differential effects of heterochromatin protein 1 isoforms on mitotic chromosome distribution and growth in Dictyostelium discoideum." Eukaryot Cell **5**(3): 530-43.

Kalt, A. and Schliwa, M. (1993). "Molecular components of the centrosome." Trends Cell Biol **3**(4): 118-28.

Kalt, A. and Schliwa, M. (1996). "A novel structural component of the Dictyostelium centrosome." J Cell Sci **109**(13): 3103-12.

Karess, R. (2005). "Rod-Zw10-Zwilch: a key player in the spindle checkpoint." Trends Cell Biol **15**(7): 386-92.

Kerssemakers, J. W., Munteanu, E. L., Laan, L., Noetzel, T. L., Janson, M. E. and Dogterom, M. (2006). "Assembly dynamics of microtubules at molecular resolution." Nature **442**(7103): 709-12.

Kimble, M., Kuzmiak, C., McGovern, K. N. and de Hostos, E. L. (2000). "Microtubule organization and the effects of GFP-tubulin expression in dictyostelium discoideum." Cell Motil Cytoskeleton **47**(1): 48-62.

Kinoshita, K., Noetzel, T. L., Pelletier, L., Mechtler, K., Drechsel, D. N., Schwager, A., Lee, M., Raff, J. W. and Hyman, A. A. (2005). "Aurora A phosphorylation of TACC3/maskin is required for centrosome-dependent microtubule assembly in mitosis." J Cell Biol **170**(7): 1047-55.

Kinoshita, K., Noetzel, T. L., Arnal, I., Drechsel, D. N. and Hyman, A. A. (2006). "Global and local control of microtubule destabilization promoted by a catastrophe kinesin MCAK/XKCM1." J Muscle Res Cell Motil **27**(2): 107-14.

Kitanishi, T., Shibaoka, H. and Fukui, Y. (1984). "Disruption of microtubules and retardation of development of Dictyostelium with ethyl N-phenylcarbamate and thiabendazole." Protoplasma **120**(3): 185-196.

Koch, K. V., Reinders, Y., Ho, T. H., Sickmann, A. and Graf, R. (2006). "Identification and isolation of Dictyostelium microtubule-associated protein interactors by tandem affinity purification." Eur J Cell Biol **85**(9-10): 1079-90.

Kojima, T., Zama, T., Wada, K., Onogi, H. and Hagiwara, M. (2001). "Cloning of human PRP4 reveals interaction with Clk1." J Biol Chem **276**(34): 32247-56.

Koonce, M. P., Kohler, J., Neujahr, R., Schwartz, J. M., Tikhonenko, I. and Gerisch, G. (1999). "Dynein motor regulation stabilizes interphase microtubule arrays and determines centrosome position." Embo J **18**(23): 6786-92.

Koonce, M. P. and Khodjakov, A. (2002). "Dynamic microtubules in Dictyostelium." J Muscle Res Cell Motil **23**(7-8): 613-9.

Kops, G. J., Kim, Y., Weaver, B. A., Mao, Y., McLeod, I., Yates, J. R., 3rd, Tagaya, M. and Cleveland, D. W. (2005b). "ZW10 links mitotic checkpoint signaling to the structural kinetochore." J Cell Biol **169**(1): 49-60.

Kops, G. J., Weaver, B. A. and Cleveland, D. W. (2005a). "On the road to cancer: aneuploidy and the mitotic checkpoint." Nat Rev Cancer **5**(10): 773-85.

Kuspa, A. and Loomis, W. F. (1992). "Tagging developmental genes in Dictyostelium by restriction enzyme-mediated integration of plasmid DNA." Proc Natl Acad Sci U S A **89**(18): 8803-7.

Kuspa, A., Dingermann, T. and Nellen, W. (1995). "Analysis of gene function in Dictyostelium." Experientia **51**(12): 1116-23.

Kyhse-Andersen, J. (1984). "Electroblotting of multiple gels: a simple apparatus without buffer tank for rapid transfer of proteins from polyacrylamide to nitrocellulose." J Biochem Biophys Methods **10**(3-4): 203-9.

Laemmli, U. K. (1970). "Cleavage of structural proteins during the assembly of the head of bacteriophage T4." Nature **227**(5259): 680-5.

Lansbergen, G. and Akhmanova, A. (2006). "Microtubule plus end: a hub of cellular activities." Traffic **7**(5): 499-507.

Lauffart, B., Sondarva, G. V., Gangisetty, O., Cincotta, M. and Still, I. H. (2007). "Interaction of TACC proteins with the FHL family: implications for ERK signaling." J Cell Commun Signal **1**(1): 5-15.

Le Bot, N., Tsai, M. C., Andrews, R. K. and Ahringer, J. (2003). "TAC-1, a regulator of microtubule length in the C. elegans embryo." Curr Biol **13**(17): 1499-505.

Lee, M. J., Gergely, F., Jeffers, K., Peak-Chew, S. Y. and Raff, J. W. (2001). "Msps/XMAP215 interacts with the centrosomal protein D-TACC to regulate microtubule behaviour." Nat Cell Biol **3**(7): 643-9.

Li, H., Chen, Q., Kaller, M., Nellen, W., Graf, R. and De Lozanne, A. (2008). "Dictyostelium Aurora kinase has properties of both Aurora A and Aurora B kinases." Eukaryot Cell **7**(5): 894-905.

Liu, S. T., Rattner, J. B., Jablonski, S. A. and Yen, T. J. (2006). "Mapping the assembly pathways that specify formation of the trilaminar kinetochore plates in human cells." J Cell Biol **175**(1): 41-53.

Luo, X., Tang, Z., Rizo, J. and Yu, H. (2002). "The Mad2 spindle checkpoint protein undergoes similar major conformational changes upon binding to either Mad1 or Cdc20." Mol Cell **9**(1): 59-71.

Ma, S., Fey, P. and Chisholm, R. L. (2001). "Molecular motors and membrane traffic in Dictyostelium." Biochim Biophys Acta **1525**(3): 234-44.

Malchow, D., Nagele, B., Schwarz, H. and Gerisch, G. (1972). "Membrane-bound cyclic AMP phosphodiesterase in chemotactically responding cells of Dictyostelium discoideum." Eur J Biochem **28**: 136-142.

Martens, H., Novotny, J., Oberstrass, J., Steck, T. L., Postlethwait, P. and Nellen, W. (2002). "RNAi in Dictyostelium: the role of RNA-directed RNA polymerases and double-stranded RNase." Mol Biol Cell **13**(2): 445-53.

Matthews, L. R., Carter, P., Thierry-Mieg, D. and Kemphues, K. (1998). "ZYG-9, a Caenorhabditis elegans protein required for microtubule organization and function, is a component of meiotic and mitotic spindle poles." J Cell Biol **141**(5): 1159-68.

McCleland, M. L., Kallio, M. J., Barrett-Wilt, G. A., Kestner, C. A., Shabanowitz, J., Hunt, D. F., Gorbsky, G. J. and Stukenberg, P. T. (2004). "The vertebrate Ndc80 complex contains Spc24 and Spc25 homologs, which are required to establish and maintain kinetochore-microtubule attachment." Curr Biol **14**(2): 131-7.

Mehta, G. D., Agarwal, M. P. and Ghosh, S. K. (2010). "Centromere identity: a challenge to be faced." Mol Genet Genomics **284**(2): 75-94.

Mitchison, T. and Kirschner, M. (1984a). "Dynamic instability of microtubule growth." Nature **312**(5991): 237-42.

Mitchison, T. and Kirschner, M. (1984b). "Microtubule assembly nucleated by isolated centrosomes." Nature **312**(5991): 232-7.

Moens, P. B. (1976). "Spindle and kinetochore morphology of Dictyostelium discoideum." J Cell Biol **68**(1): 113-22.

Montembault, E., Dutertre, S., Prigent, C. and Giet, R. (2007). "PRP4 is a spindle assembly checkpoint protein required for MPS1, MAD1, and MAD2 localization to the kinetochores." J Cell Biol **179**(4): 601-9.

Muller-Taubenberger, A., Vos, M. J., Bottger, A., Lasi, M., Lai, F. P., Fischer, M. and Rottner, K. (2006). "Monomeric red fluorescent protein variants used for imaging studies in different species." Eur J Cell Biol **85**(9-10): 1119-29.

Musacchio, A. and Salmon, E. D. (2007). "The spindle-assembly checkpoint in space and time." Nat Rev Mol Cell Biol **8**(5): 379-93.

Neujahr, R., Albrecht, R., Kohler, J., Matzner, M., Schwartz, J. M., Westphal, M. and Gerisch, G. (1998). "Microtubule-mediated centrosome motility and the positioning of cleavage furrows in multinucleate myosin II-null cells." J Cell Sci **111 (Pt 9)**: 1227-40.

Niethammer, P., Kronja, I., Kandels-Lewis, S., Rybina, S., Bastiaens, P. and Karsenti, E. (2007). "Discrete states of a protein interaction network govern interphase and mitotic microtubule dynamics." PLoS Biol **5**(2): e29.

O'Brien, L. L., Albee, A. J., Liu, L., Tao, W., Dobrzyn, P., Lizarraga, S. B. and Wiese, C. (2005). "The Xenopus TACC homologue, maskin, functions in mitotic spindle assembly." Mol Biol Cell **16**(6): 2836-47.

Obuse, C., Iwasaki, O., Kiyomitsu, T., Goshima, G., Toyoda, Y. and Yanagida, M. (2004). "A conserved Mis12 centromere complex is linked to heterochromatic HP1 and outer kinetochore protein Zwint-1." Nat Cell Biol **6**(11): 1135-41.

Omura, F. a. F., Y. (1985). "Dictyostelium MTOC: Structure and linkage to the nucleus." Protoplasma **127**: 212-212.

Peset, I., Seiler, J., Sardon, T., Bejarano, L. A., Rybina, S. and Vernos, I. (2005). "Function and regulation of Maskin, a TACC family protein, in microtubule growth during mitosis." J Cell Biol **170**(7): 1057-66.

Peset, I. and Vernos, I. (2008). "The TACC proteins: TACC-ling microtubule dynamics and centrosome function." Trends Cell Biol **18**(8): 379-88.

Piekorz, R. P., Hoffmeyer, A., Duntsch, C. D., McKay, C., Nakajima, H., Sexl, V., Snyder, L., Rehg, J. and Ihle, J. N. (2002). "The centrosomal protein TACC3 is essential for hematopoietic stem cell function and genetically interfaces with p53-regulated apoptosis." Embo J **21**(4): 653-64.

Pinsky, B. A. and Biggins, S. (2005). "The spindle checkpoint: tension versus attachment." Trends Cell Biol **15**(9): 486-93.

Popov, A. V., Pozniakovsky, A., Arnal, I., Antony, C., Ashford, A. J., Kinoshita, K., Tournebize, R., Hyman, A. A. and Karsenti, E. (2001). "XMAP215 regulates microtubule dynamics through two distinct domains." Embo J **20**(3): 397-410.

Popov, A. V., Severin, F. and Karsenti, E. (2002). "XMAP215 is required for the microtubule-nucleating activity of centrosomes." Curr Biol **12**(15): 1326-30.

Raper, K. B. (1935). "Dictyostelium discoideum, a new species of slime mold from decaying forest leaves." J. Agr. Res **50**: 135-147.

Raynaud-Messina, B. and Merdes, A. (2007). "Gamma-tubulin complexes and microtubule organization." Curr Opin Cell Biol **19**(1): 24-30.

Rehberg, M. and Graf, R. (2002). "Dictyostelium EB1 is a genuine centrosomal component required for proper spindle formation." Mol Biol Cell **13**(7): 2301-10.

Rehberg, M., Kleylein-Sohn, J., Faix, J., Ho, T. H., Schulz, I. and Graf, R. (2005). "Dictyostelium LIS1 is a centrosomal protein required for microtubule/cell cortex interactions, nucleus/centrosome linkage, and actin dynamics." Mol Biol Cell **16**(6): 2759-71.

Reinders, Y., Schulz, I., Graf, R. and Sickmann, A. (2006). "Identification of novel centrosomal proteins in Dictyostelium discoideum by comparative proteomic approaches." J Proteome Res **5**(3): 589-98.

Rice, L. M., Montabana, E. A. and Agard, D. A. (2008). "The lattice as allosteric effector: structural studies of alphabeta- and gamma-tubulin clarify the role of GTP in microtubule assembly." Proc Natl Acad Sci U S A **105**(14): 5378-83.

Rieder, C. L. and Maiato, H. (2004). "Stuck in division or passing through: what happens when cells cannot satisfy the spindle assembly checkpoint." Dev Cell **7**(5): 637-51.

Rothbauer, U., Zolghadr, K., Muyldermans, S., Schepers, A., Cardoso, M. C. and Leonhardt, H. (2008). "A versatile nanotrap for biochemical and functional studies with fluorescent fusion proteins." Mol Cell Proteomics **7**(2): 282-9.

Rubino, S., Unger, E., Fogu, G. and Cappuccinelli, P. (1982). "Effect of microtubule inhibitors on the tubulin system of Dictyostelium discoideum." Z Allg Mikrobiol **22**(2): 127-31.

Sambrook, J., Russel, D. W., Irwin, N. and Janssen, K. A. (2001). "Molecular cloning: A laboratory manual 3rd edition." Cold spring harbor laboratory press.

Samereier, M., Meyer, I., Koonce, M. P. and Gräf, R. (2010). "Live cell-imaging techniques for analyses of microtubules in Dictyostelium." Methods Cell Biol. **97**: 341-357.

Samereier, M., Baumann, O., Meyer, I. and Gräf, R. (2011). "Analysis of Dictyostelium TACC reveals differential interactions with CP224 and unusual dynamics of Dictyostelium microtubules." Cell Mol Life Sci. **68**(2): 275-287.

Santaguida, S. and Musacchio, A. (2009). "The life and miracles of kinetochores." Embo J **28**(17): 2511-31.

Sato, M., Vardy, L., Angel Garcia, M., Koonrugsa, N. and Toda, T. (2004). "Interdependency of fission yeast Alp14/TOG and coiled coil protein Alp7 in microtubule localization and bipolar spindle formation." Mol Biol Cell **15**(4): 1609-22.

Schatten, H. (2008). "The mammalian centrosome and its functional significance." Histochem Cell Biol **129**(6): 667-86.

Schliwa, M. and van Blerkom, J. (1981). "Structural interaction of cytoskeletal components." J Cell Biol **90**(1): 222-35.

Schramm, C., Elliott, S., Shevchenko, A. and Schiebel, E. (2000). "The Bbp1p-Mps2p complex connects the SPB to the nuclear envelope and is essential for SPB duplication." Embo J **19**(3): 421-33.

Schuendeln, M. M., Piekorz, R. P., Wichmann, C., Lee, Y., McKinnon, P. J., Boyd, K., Takahashi, Y. and Ihle, J. N. (2004). "The centrosomal, putative tumor suppressor protein TACC2 is dispensable for normal development, and deficiency does not lead to cancer." Mol Cell Biol **24**(14): 6403-9.

Schulz, I., Reinders, Y., Sickmann, A. and Graf, R. (2006). "An improved method for Dictyostelium centrosome isolation." Methods Mol Biol **346**: 479-89.

Schulz, I., Baumann, O., Samereier, M., Zoglmeier, C. and Graf, R. (2009a). "Dictyostelium Sun1 is a dynamic membrane protein of both nuclear membranes and required for centrosomal association with clustered centromeres." Eur J Cell Biol **88**(11): 621-38.

Schulz, I., Erle, A., Graf, R., Kruger, A., Lohmeier, H., Putzler, S., Samereier, M. and Weidenthaler, S. (2009b). "Identification and cell cycle-dependent localization of nine novel, genuine centrosomal components in Dictyostelium discoideum." Cell Motil Cytoskeleton **66**(11): 915-28.

Severin, F., Habermann, B., Huffaker, T. and Hyman, T. (2001). "Stu2 promotes mitotic spindle elongation in anaphase." J Cell Biol **153**(2): 435-42.

Shah, J. V., Botvinick, E., Bonday, Z., Furnari, F., Berns, M. and Cleveland, D. W. (2004). "Dynamics of centromere and kinetochore proteins; implications for checkpoint signaling and silencing." Curr Biol **14**(11): 942-52.

Slep, K. C. and Vale, R. D. (2007). "Structural basis of microtubule plus end tracking by XMAP215, CLIP-170, and EB1." Mol Cell **27**(6): 976-91.

Slep, K. C. (2009). "The role of TOG domains in microtubule plus end dynamics." Biochem Soc Trans **37**(Pt 5): 1002-6.

Srayko, M., Quintin, S., Schwager, A. and Hyman, A. A. (2003). "Caenorhabditis elegans TAC-1 and ZYG-9 form a complex that is essential for long astral and spindle microtubules." Curr Biol **13**(17): 1506-11.

Starr, D. A., Williams, B. C., Hays, T. S. and Goldberg, M. L. (1998). "ZW10 helps recruit dynactin and dynein to the kinetochore." J Cell Biol **142**(3): 763-74.

Still, I. H., Hamilton, M., Vince, P., Wolfman, A. and Cowell, J. K. (1999). "Cloning of TACC1, an embryonically expressed, potentially transforming coiled coil containing gene, from the 8p11 breast cancer amplicon." Oncogene **18**(27): 4032-8.

Thompson, S. (2010). "Mechanisms of chromosomal instability." Current Biology **20**(6): R285-R295.

Tikhonenko, I., Nag, D. K., Robinson, D. N. and Koonce, M. P. (2009). "Microtubule-nucleus interactions in Dictyostelium discoideum mediated by central motor kinesins." Eukaryot Cell **8**(5): 723-31.

Torras-Llort, M., Moreno-Moreno, O. and Azorin, F. (2009). "Focus on the centre: the role of chromatin on the regulation of centromere identity and function." Embo J **28**(16): 2337-48.

Tournebize, R., Popov, A., Kinoshita, K., Ashford, A. J., Rybina, S., Pozniakovsky, A., Mayer, T. U., Walczak, C. E., Karsenti, E. and Hyman, A. A. (2000). "Control of microtubule dynamics by the antagonistic activities of XMAP215 and XKCM1 in Xenopus egg extracts." Nat Cell Biol **2**(1): 13-9.

Ueda, M., Schliwa, M. and Euteneuer, U. (1999). "Unusual centrosome cycle in Dictyostelium: correlation of dynamic behavior and structural changes." Mol Biol Cell **10**(1): 151-60.

Vallee, R. B., Varma, D. and Dujardin, D. L. (2006). "ZW10 function in mitotic checkpoint control, dynein targeting and membrane trafficking: is dynein the unifying theme?" Cell Cycle **5**(21): 2447-51.

Van der Vaart, B., Akhmanova, A. and Straube, A. (2009). "Regulation of microtubule dynamic instability." Biochem Soc Trans **37**(Pt 5): 1007-13.

Vanrheenen, S. M., Reilly, B. A., Chamberlain, S. J. and Waters, M. G. (2001). "Dsl1p, an essential protein required for membrane traffic at the endoplasmic reticulum/Golgi interface in yeast." Traffic **2**(3): 212-31.

Varma, D., Dujardin, D. L., Stehman, S. A. and Vallee, R. B. (2006). "Role of the kinetochore/cell cycle checkpoint protein ZW10 in interphase cytoplasmic dynein function." J Cell Biol **172**(5): 655-62.

Wan, X., O'Quinn, R. P., Pierce, H. L., Joglekar, A. P., Gall, W. E., DeLuca, J. G., Carroll, C. W., Liu, S. T., Yen, T. J., McEwen, B. F., et al. (2009). "Protein architecture of the human kinetochore microtubule attachment site." Cell **137**(4): 672-84.

Wang, P. J. and Huffaker, T. C. (1997). "Stu2p: A microtubule-binding protein that is an essential component of the yeast spindle pole body." J Cell Biol **139**(5): 1271-80.

Waters, J. C., Chen, R. H., Murray, A. W. and Salmon, E. D. (1998). "Localization of Mad2 to kinetochores depends on microtubule attachment, not tension." J Cell Biol **141**(5): 1181-91.

Werner , M and Glotzer, M (2008). „Control of cortical contractility during cytokinesis“ Biochem Soc Trans **36**(3): 371-7

Westphal, M., Jungbluth, A., Heidecker, M., Mühlbauer, B., Heizer, C., Schwartz, J. M., Marriott, G. and Gerisch, G. (1997). "Microfilament dynamics during cell movement and chemotaxis monitored using a GFP–actin fusion protein." Current Biology **7**(3): 176-183.

Whittington, A. T., Vugrek, O., Wei, K. J., Hasenbein, N. G., Sugimoto, K., Rashbrooke, M. C. and Wasteneys, G. O. (2001). "MOR1 is essential for organizing cortical microtubules in plants." Nature **411**(6837): 610-3.

Williams, K. L. and Newell, P. C. (1976). "A genetic study of aggregation in the cellular slime mould Dictyostelium discoideum using complementation analysis." Genetics **82**(2): 287-307.

Wojcik, E., Basto, R., Serr, M., Scaerou, F., Karess, R. and Hays, T. (2001). "Kinetochore dynein: its dynamics and role in the transport of the Rough deal checkpoint protein." Nat Cell Biol **3**(11): 1001-7.

Wouters, F. S. and Bastiaens, P. I. (2006). "Imaging protein-protein interactions by Fluorescence Resonance Energy Transfer (FRET) microscopy." Curr Protoc Neurosci **Chapter 5**: Unit 5 22.

Zang, J. H., Cavet, G., Sabry, J. H., Wagner, P., Moores, S. L. and Spudich, J. A. (1997). "On the role of myosin-II in cytokinesis: division of Dictyostelium cells under adhesive and nonadhesive conditions." Mol Biol Cell **8**(12): 2617-29.

Zimniak, T., Stengl, K., Mechtler, K. and Westermann, S. (2009). "Phosphoregulation of the budding yeast EB1 homologue Bim1p by Aurora/Ipl1p." J Cell Biol **186**(3): 379-91.

List of abbreviations

µ	micro
aa	Amino acid
ATP	Adenosine-5'-triphosphate
BCIP	Bromo-chloro-indolyl phosphate
bp	Base pairs
BSA	Bovine serum albumin
C-	Carboxy terminal
cAMP	cyclic adenosine monophosphate
cDNA	Complementary DNA
Co-IP	Co-immunoprecipitation
D	Daltons
Dd	*Dictyostelium discoideum*
DMSO	Dimethylsulfoxide
DNA	Desoxyribonucleic acid
dNTP	Desoxyribonucleotide triphosphate
dsRNA	Double-stranded RNA
DTT	Dithiothreitol
ECL	Enhanced chemiluminescence
EDTA	Ethylene-diamine-tetraacetic acid
EGTA	Ethyleneglycol-bis-(2-aminoethylether)-N,N'-tetraacetic acid
g	gram, unit of mass
GFP	Green fluorescent protein
h	hour
H2O	Distilled water

H3K9	Lysin residue 9 of the histone 3 proteine
HEPES	4-(2-hydroxyethyl)-1-piperazineethanesulfonic acid
IPTG	Isopropyl-β-thiogalactopyranoside
kb	Kilo base pairs
kDa	Kilo Daltons
k/o	knockout
l	liter
m	milli
M	Molarity [mol/l]
Mb	Mega base pairs
min	minute
MAP	Microtubule-associated protein
MOPS	Morpholinopropanesufonic acid
mRFP	Mars red fluorescent protein
mRNA	Messenger ribonucleic acid
MT	Microtubules
MTOC	Microtubule organizing center
N-	Amino terminal
NBT	Nitroblue-tetrazolium chloride
NHS	N-hydroxysuccinimide
O.D.x	Optical density at wavelength x [nm]
PAGE	Polyacrylamide gel electrophoresis
PBS	Phosphate buffered saline
PCR	Polymerase chain reaction
PDA	Piperazine diacrylyl

pH	Negative decadic logarithm of proton concentration
PIPES	Piperazine-N,N'-bis-[2-ethanesulfonic acid]
RNAi	RNA interference
ROI	Region of interest
rpm	Revolutions per minute
RT-PCR	Reverse transcription polymerase chain reaction
SAC	Spindle assembly checkpoint
SDS	Sodium dodecyl sulfate
sec	second
siRNA	Small interfering RNA
SPB	Spindle pole body
TBS	Tris buffered saline
TBZ	Thiabendazole
TEMED	N,N,N,N' -tetramethylenediamine
Tris	Tris-hydroxymethyl-ammoniumethane
Triton-X-100	T-Octylphenoxypolyethoxethanol
Tween 20	Polyoxyethylene-sorbianemonolaureate
U	Units
UTR	Untranslated region
WT	Wild type

Curriculum Vitae

Persönliche Daten	Matthias Samereier geboren am 16.07.1978 in München Staatsangehörigkeit: Deutsch Familienstand: ledig, keine Kinder

---

Schulbildung

09/85 bis 07/89	Grundschule am Agilolfingerplatz in München
09/89 bis 06/99	Asam-Gymnasium München Allgemeine Hochschulreife

Wehrersatzdienst

07/99 bis 06/00	Deutsches Jugendherbergwerk in München

Universitätsausbildung

09/00 bis 08/06	Ludwig-Maximilians-Universität München Studium der Biologie
10/02	Vordiplom in allgemeiner Biologie, Mikrobiologie, Chemie und Physik
08/06	Diplom in den Fächern Zoologie (Hauptfach), physiologische Botanik, Pharmakologie und Toxikologie, Genetik Gesamtnote: 1,1

Promotion

11/06 bis 02/11	Doktorarbeit bei Professor Ralph Gräf (Universität Potsdam) mit dem Titel „Functional analyses of microtubule and centrosome-associated proteins in *Dictyostelium discoideum“*

Danke sagen…

Zuallererst möchte ich mich natürlich bei Prof. Dr. Ralph Gräf bedanken, der mir in den vergangen Jahren ein Doktorvater war, wie man ihn sich nicht besser wünschen kann.
Ich durfte dieses interessante Promotionsthema eigenständig bearbeiten und mir sind dabei stets alle Türen und Ohren offen gestanden. Vielen vielen Dank!

Großer Dank gilt auch Frau Dr. Irene Meyer, die mir jederzeit mit Rat und Tat beigestanden hat und mir immer eine hervorragende Betreuerin war, wenn der Weg ins Chef'sche Büro mal wieder zu weit war.

Außerdem möchte ich mich sehr herzlich bei Prof. Dr. Manfred Schliwa, Prof. Dr. Wolfgang Nellen und Prof. Dr. Reinhard Fischer für die Bereitschaft bedanken, diese Arbeit zu begutachten.

Weiterer Dank gilt natürlich auch allen Mitgliedern der AG Zellbiologie für das fantastische Arbeitsklima im Labor (Olli, Arbeitsklima, nicht für die Klimakatastrophen in unserem Büro). Vielen Dank Anita, Anne, Olli, Petros, Sascha, Tatjana und Rocky!

Schließlich möchte ich mich bei meiner Freundin Natascha Berger bedanken, die die Hochs und Tiefs des Doktorandendaseins sicher am intensivsten verfolgen konnte. Ein riesengroßes Dankeschön für Deine Geduld!

Allergrößter Dank gilt meinen Eltern, die mir durch ihre unerschütterliche Unterstützung in allen nur erdenklichen Belagen so viel mehr ermöglicht haben als diese Arbeit!

Viele weitere Menschen haben zum Gelingen dieser Arbeit beigetragen. Bei all jenen, die sich angesprochen fühlen, an dieser Stelle aber unerwähnt bleiben, möchte ich mich hiermit gerne entschuldigen und schließlich auch meinen herzlichen Dank aussprechen!